Title
The cellular and synaptic mechanisms of parkinsonism and levodopa-induced dyskinesia

Author
Ryan, Michael B.

Publication Date
2020

Peer reviewed|Thesis/dissertation

The cellular and synaptic mechanisms of parkinsonism and levodopa-induced dyskinesia

by
Michael Ryan

DISSERTATION
Submitted in partial satisfaction of the requirements for degree of
DOCTOR OF PHILOSOPHY

in

Neuroscience

in the

GRADUATE DIVISION
of the
UNIVERSITY OF CALIFORNIA, SAN FRANCISCO

Approved:

DocuSigned by:
Anatol Kreitzer
03F45B9A4CF445E...
Anatol Kreitzer
Chair

DocuSigned by:
Alexandra Nelson
Alexandra Nelson

DocuSigned by:
Joshua Berke
Joshua Berke

DocuSigned by:
Massimo Scanziani
4AF406E430B7472...
Massimo Scanziani

Committee Members

Dedication

To my dad, Daniel Ryan, who always supported me in pursuing my goals.

To all the incredible mentors I have been so fortunate to learn from – Alexandra Nelson, Anne Churchland, Craig Evinger, and Brenda Anderson.

Acknowledgements

The work described in this dissertation would not have been possible, nor would I be the scientist I am today, without the constant support and mentorship of my PhD advisor, Alexandra Nelson. Words certainly could never convey my appreciation. Be that as it may, I can say with confidence that most of my ability to convey *anything* via the written word is due in large part to the countless hours you spent editing my work. In addition to my writing, you have taught me so much about being a rigorous, thorough, creative, and curious scientist – from the importance of fluorophore controls to large behavioral cohorts to spotting p-hacking from a mile away. Your passion for science and mentorship are infectious and I hope to carry that passion with me as I embark on this next stage of my career.

So much of my scientific, and personal, growth I can also clearly attribute to the past and present members of the Nelson lab: Ally Girasole, Match McGregor, Jon Schor, Emily Twedell, Chloe Bair-Marshall, Matthew Lum, Rea Brakaj, and Jasmine Stansil. I have learned and laughed (a lot) more than I could have ever dreamed with all of you. I will always cherish our endless debates in the office, hours of staring at abnormally behaving mice together, and being supported by each of you. I would not have made it to the end of this journey without you. In particular, I need to thank Allison Elizabeth Girasole (aka Ally, Al, AEG, Age, Dr. Girasole). You were my partner-in-crime, my collaborator, my lab-mate, my mentor, and my friend. The latter half of this dissertation is work that would have never been possible without our combined efforts.

I have also had the great fortune of being supported by several mentors outside of the Nelson lab, whose guidance and instruction has proven to be invaluable during my time at UCSF. I want to extend a special thank you to Drs. Kevin Bender, Massimo Scanziani, Guy Bouvier,

Anatol Kreitzer, Dorit Ron, Joshua Berke, Evan Feinberg, and Phil Starr. To Dr. Charles Gerfen, my collaborator at the NIMH, thank you not only for your scientific contribution to the synaptic tracing experiments included in this dissertation, but for your mentorship as well.

I need to also thank my classmates (UCSF Neuroscience 2014!) for being an exceptionally great cohort of people to go through this experience with. You were my first friends in San Francisco and I'm so thankful that those friendships have carried me through graduate school. In particular, Nerissa Hoglen, thank you for always being my biggest cheerleader, while also simultaneously criticizing most of my choices – it's a rare skill to possess. You have been my rock for the past 6 years. Tess Veuthey, thank you for always being my role model. Even though we are the same age, I hope to be more like you when I grow up. Thank you for all the laughs, tarot card readings, and therapy sessions.

Last, but certainly not least, I need to thank "The New Page" for being my chosen family. Sophie McCallum, Meagan Treviño, Yon Jimenez-Macuso, and Antoine Ambert – you have taught me the true meaning of the word "family." The memories we made together are some of the happiest times of my life and you made me a better person for having known each of you. I look forward to all the memories yet to be made, especially as our family grows with our three newest additions (Alexandra and Adrien Ambert-Jimenez, and the soon-to-be Yodi Treviño).

The work in this thesis was also supported through funding from the Ruth L. Kirschstein National Research Service Award (NRSA) from the National Institute of Neurological Disorders and Stroke (NINDS) and a fellowship from the ARCS Foundation.

Contributions

All sections were primarily written by Michael Ryan, with input from Alexandra Nelson.

Chapter 1 was written, and figured prepared, by Michael Ryan.

Chapter 2 is reproduced in its entirety from the following published manuscript:

> Ryan, M.B., Bair-Marshall, C.J., and Nelson, A.B. (2018). Aberrant Striatal Activity in Parkinsonism and Levodopa-Induced Dyskinesia. Cell Reports 23(12): 3438-3446.

MBR and ABN designed the experiments. MBR conducted the electrophysiological recordings and analysis. MBR, ABN, and CBM conducted optogenetic stimulation experiments. MBR wrote the manuscript, with input from ABN.

Chapter 3 has been prepared in the following manuscript:

> Ryan, M.B.*, Girasole, A.E.*, McGregor, M.M., Brakaj, R. Paletzki, R., Gerfen, C.R., Nelson, A.B. Differential Intrinsic and Synaptic Properties of Functionally-Defined Direct Pathway Neurons Shape Their Activity in Levodopa-Induced Dyskinesia. *In preparation.*

MBR, AEG, and ABN designed the experiments. MBR and AEG conducted the in vivo electrophysiology experiments and analysis. MBR, AEG, MMM, and ABN performed the slice electrophysiology experiments. Slice data was analyzed by MBR, AEG, and ABN. MBR and AEG performed the rabies tracing experiments and the data was imaged and processed by RP and CRG. Rabies data was quantified by MBR. MBR wrote the manuscript, with input from AEG and ABN.

The cellular and synaptic mechanisms of parkinsonism and levodopa-induced dyskinesia

Michael Ryan

Abstract

Parkinson's disease (PD) is a neurodegenerative disease, in which the progressive loss of dopamine neurons is associated with prominent motor deficits, including a loss of voluntary movement. Although the mechanisms underlying PD are poorly understood, these motor deficits can be effectively treated pharmacologically through dopamine replacement therapy with the dopamine precursor, levodopa. However, while levodopa is highly effective, the majority of patients develop motor complications, including levodopa-induced dyskinesia (LID) after 5-10 years of treatment. The excessive, involuntary movements observed in LID, which are triggered by levodopa administration, limit its therapeutic use. In Chapter 1, I will discuss prominent theories and experimental evidence suggesting aberrant activity of neurons in the striatum, the primary input nucleus of the basal ganglia, plays a crucial role in the abnormal movements seen in both PD and LID. This will be focused on the two main cell-types in the striatum, whose activity is thought to underlie the generation and coordination of movement in health and disease: the direct and indirect pathway medium spiny neurons (dMSNs and iMSNs, respectively). However, the precise cellular and circuit mechanisms of striatal dysfunction in PD and LID, or how aberrant striatal activity relates to behavioral dysfunction, are poorly understood. To gain a better understanding of these circuit mechanisms, in Chapter 2, I use a mouse model of PD and LID combined with *in vivo* electrophysiological recordings of dMSNs and iMSNs. Using this approach, I identified the changes in striatal physiology that correlate with the abnormal movements seen in parkinsonism and LID. In particular, this work converges on a distinct subpopulation of dMSNs with aberrant

levodopa-evoked activity. In Chapter 3, I investigate how the differential regulation of the intrinsic and synaptic properties of these LID-associated dMSNs shape their response to levodopa, using synaptic tracing, combined with *in vivo* and *ex vivo* electrophysiology experiments. Together, these studies elucidate the cellular and circuit dysfunction that arises following chronic changes in dopamine and shed light on how the heterogeneous properties of direct pathway neurons in LID contribute to the differential therapeutic and dyskinetic effects of levodopa.

Table of Contents

List of Figures

Chapter1

Chapter 2

Chapter 3

List of Tables

Chapter 3

Chapter 1: Introduction

1.1 Clinical Overview of Parkinson's Disease and Levodopa-Induced Dyskinesia

Parkinson's disease (PD), the second most common neurodegenerative disease (Beitz, 2014), is characterized by prominent motor and non-motor symptoms (McGregor and Nelson, 2019). The core motor symptoms of PD, which include tremor, rigidity, akinesia (lack of movement), bradykinesia (slowing of movement), and postural instability (Jankovic, 2008), are thought to result from the cellular and circuit dysfunction that arise from the progressive loss of midbrain dopamine neurons. Although the specific mechanisms underlying PD motor deficits are poorly understood, the mainstay treatment since the 1960's has been dopamine replacement therapy with levodopa, the dopamine precursor (Hornykiewicz, 2015). While levodopa is highly effective at treating the motor deficits in PD, with chronic treatment the vast majority of patients (75-80%) develop motor complications by 5-10 years of treatment (Ahlskog and Muenter, 2001; Bhidayasiri and Truong, 2008), and nearly all patients develop complications by 20 years of treatment (Hely et al., 2008). These complications include motor fluctuations (rapid onset/offset or variable relief of symptoms) and levodopa-induced dyskinesia (LID). Patients with LID experience excessive, involuntary, choreiform (repetitive, purposeless, jerky) movements, which are triggered in response to each dose of levodopa. (Aquino and Fox, 2015; Vijayakumar and Jankovic, 2016). These complications from chronic dopamine replacement therapy are not only a clinical problem for managing PD motor symptoms, but highlight our lack of understanding regarding how these chronic changes in dopamine lead to aberrant activity in the brain. One brain circuit that is a likely

candidate to mediate both the normal and abnormal movements seen in PD and LID is the basal ganglia.

1.2 The Basal Ganglia

The basal ganglia are a highly interconnected group of subcortical nuclei (Figure 1) which have garnered attention for their prominent role in movement, as well as their modulation by dopamine. For these reasons, this circuit is also an attractive candidate for mediating both the loss of movement in PD and the involuntary movements in LID. The striatum, the major input nucleus of the basal ganglia, receives excitatory input from numerous cortical and thalamic areas, as well as the densest projection of midbrain dopamine neurons in the brain (Beckstead et al., 1979; Haber et al., 2000). The dorsal striatum in particular integrates signals from the motor cortex with robust dopaminergic inputs, making it well poised to regulate normal and pathological movements (Gerfen and Surmeier, 2011; Lenz and Lobo, 2013). The principal projection neurons of the striatum, medium spiny neurons (MSNs), can be divided into two types based on their projections and dopamine receptor expression: direct pathway neurons (dMSNs) and indirect pathway neurons (iMSNs). dMSNs project directly to basal ganglia output (globus pallidus pars interna, GPi; substantia nigra pars reticulata, SNr), while iMSNs polysynaptically project to basal ganglia output via the globus pallidus pars externa (GPe) and subthalamic nucleus (STN). Neurons in the GPi/SNr send direct inhibitory projections to the motor regions of the brain stem and thalamus (ventral anterior and ventral lateral portions). Thalamic neurons in turn send excitatory projections to sensorimotor cortical regions. Prevailing theories regarding the pathological movements in PD and LID point towards aberrant activity in many nodes of this basal ganglia-thalamo-cortical loop, but striatal activity may be the initial locus of aberrant activity.

1.3 The Striatal Microcircuit

The dorsal striatum plays a key role in the proper generation and coordination of movement, which is thought to arise through integration of excitatory, inhibitory, and neuromodulatory extrastriatal inputs within the dense inhibitory intrastriatal network. The main sources of excitatory inputs to the dorsal striatum are from sensorimotor cortical and intralaminar thalamic brain regions (Guo et al., 2015; McGeorge and Faull, 1987; Pan et al., 2010; Wall et al., 2013). The striatum also receives prominent neuromodulatory inputs from serotonergic neurons of the dorsal raphe nucleus (Mathur and Lovinger, 2012), as well as from cholinergic neurons of the pedunculopontine and laterodorsal tegmental areas (Dautan et al., 2014; Mena-Segovia et al., 2004). Importantly, the striatum receives dense dopaminergic input from midbrain dopamine neurons (Haber et al., 2000), which have been shown to be critical for reinforcement learning, action selection, and gross movement (Gerfen and Surmeier, 2011; Schultz, 2016) (Figure 2). Each of these extrastriatal signals converge on the primary GABAergic projection neurons of the striatum, medium spiny neurons (MSNs), which comprise approximately 90% of neurons in the striatum (Chang et al., 1982; Graveland and DiFiglia, 1985). The remaining proportion of striatal neurons include GABAergic (Tepper et al., 2010) and cholinergic interneurons (Deffains and Bergman, 2015), each of which play a distinct role in shaping the responses of MSNs and are differentially engaged in the abnormal movements seen in PD and LID. However, for the purposes of this dissertation, I will focus on the main projection neurons in the striatum: direct and indirect pathway MSNs (dMSNs and iMSNs, respectively). Functionally, dMSNs and iMSNs are thought to have opposing influences over behavior via their divergent effects on basal ganglia output (GPi/SNr). As the canonical output of the basal ganglia, these structures are tonically active and exert an inhibitory influence over thalamic neurons, thereby modulating movement. As dMSNs provide a direct inhibitory projection

to the GPi/SNr, their activation has been shown to decrease activity in the SNr and result in a facilitation of movement (Freeze et al., 2013; Kravitz et al., 2010). However, iMSNs project via several synapses to GPi/SNr, with iMSN activation leading to an increase in SNr activity and a resultant decrease in movement (Freeze et al., 2013; Kravitz et al., 2010). Importantly, MSNs also provide feedforward inhibition onto each other, via extensive collaterals, shaping their activity. The activation of these two pathways is thus thought to exert bidirectional control over movement. Accordingly, aberrant activity of dMSNs and iMSNs has long been hypothesized to underlie the loss of movement in PD and excessive movements in LID (Albin et al., 1989; DeLong, 1990).

1.4 Striatal Circuit Dysfunction and the Classical Model

Given the importance of dopaminergic input in regulating striatal activity, the loss of midbrain dopamine neurons in PD is believed to be the root cause of striatal dysfunction and eventual vulnerability to LID. Developed in the late 1980s, the "classical model" of basal ganglia function (Figure 3), founded on the idea of striatal dysfunction in PD and LID, has been influential in shaping our understanding of the basal ganglia (Albin et al., 1989; Alexander and Crutcher, 1990; DeLong, 1990). According to this theory, dopamine is hypothesized to bidirectionally modulate dMSNs and iMSNs due to differential expression of D1-like and D2-like dopamine receptors (Gerfen et al., 1990; Surmeier et al., 1996). dMSNs largely express the "excitatory" D1-like dopamine receptors ($G_{\alpha olf}$-coupled), whose activation by dopamine leads to elevated cyclic adenosine monophosphate (cAMP) and protein kinase A (PKA). iMSNs largely express the "inhibitory" D2-like dopamine receptor (G_i-coupled), whose activation by dopamine leads to reduced cAMP and PKA levels. Through multiple downstream signaling cascades, modulation of PKA can lead to intracellular changes, including transcription factors, ion channels, receptor expression, etc (Gerfen and Surmeier, 2011; Hernandez-Lopez et al., 2000; Hernández-López et

al., 1997; Surmeier et al., 2007). Therefore, dopamine is thought to excite direct pathway and inhibit indirect pathway neurons. Accordingly, the classical model predicts that dopamine loss causes birdirectional dysregulation of MSNs, with increased iMSN and decreased dMSN activity, leading to reduced movement in PD. This model also predicts that dopamine replacement with levodopa, by replenishing striatal dopamine, normalizes the activity of dMSNs and iMSNs. Via unknown mechanisms, chronic exposure to levodopa is thought to result in dysregulated dopamine release leading to excessive inhibition of iMSNs and activation of dMSNs. The classical model posits that dysregulation of these pathways propagates through the basal ganglia-thalamo-cortical loop resulting in the motor impairments in PD and involuntary movements in LID. However, at the beginning of my PhD, support for the classical model was mostly indirect, derived from recordings in downstream basal ganglia nuclei.

According to the classical model, dysregulation favoring the indirect pathway in Parkinson's disease should lead to (1) decreased GPe and (2) increased STN and GPi/SNr activity, leading to a suppression of movement. Indeed, extracellular recordings in PD patients and parkinsonian nonhuman primates (NHPs) show elevated activity in the GPi in the parkinsonian state (Boraud et al., 1998; Filion and Tremblay, 1991; Hutchinson et al., 1994). Increased firing has also been observed in the STN (Benazzouz et al., 2002; Bergman et al., 1994; Kreiss et al., 1997) and decreased firing in the GPe in patients and animal models of PD, in line with the classical model (Boraud et al., 1998; Filion and Tremblay, 1991; Mallet et al., 2008; Pan and Walters, 1988; Soares et al., 2004). A corollary of the classical model suggests that dysregulation in favor of the movement-facilitating direct pathway in LID should lead to (1) increased GPe and (2) decreased STN and GPi/SNr activity leading to a loss of movement suppression and the emergence of involuntary movements. In line with this theory, in parkinsonian NHPs levodopa

causes a near suppression of GPi activity in LID (Boraud et al., 1998; Papa et al., 1999). GPe neurons also show a modest increase in firing rate in response to apomorphine-induced dyskinesia in parkinsonian NHPs (Filion et al., 1991; Hutchinson et al., 1997), suggestive of decreased iMSN firing. However, no significant change in GPe activity was found during LID in NHPs (Boraud et al., 1998), which is one study, among others (Aristieta et al., 2012; Aristieta et al., 2016), that have failed to confirm the firing rate changes of basal ganglia nuclei predicted by the classical model. It is also important to note that other models of basal ganglia function propose a more complementary function of the direct and indirect pathways. These models posit that concurrent activation of dMSNs and iMSNs is necessary to facilitate purposeful and suppress unwanted movements (Mink, 1996, 2003), which has been shown to occur during movement in healthy mice (Cui et al., 2013). This model suggests that a relative imbalance, as opposed to absolute firing rates, may be key to understanding how striatal dysfunction shapes the behavioral deficits. Other models stress the importance of changes in firing *pattern*, in addition to firing *rate*, as a key aspect of aberrant basal ganglia activity in PD and LID. For the purposes of this dissertation, however, I will focus on addressing the "rate-based" hypotheses generated by the classical model.

Given the recurrent connections among basal ganglia nuclei, it is difficult to attribute behavioral dysfunction to striatal activity alone. In the case of LID, aberrant levodopa-evoked activity originating in the striatum is supported by intracranial administration of levodopa in rats, which elicit dyskinesia when infused into the dorsolateral striatum, but not GP (GPe equivalent in rodents) or SNr (Buck et al., 2010; Carta et al., 2006). In addition, while striatal activity is altered during LID, the respective contributions of dMSNs and iMSNs to dyskinesia are poorly understood. Causal experiments have shown optogenetic or chemogenetic activation of dMSNs in the dorsolateral striatum is sufficient to elicit dyskinesia in healthy mice (Rothwell et al., 2015),

which is potentiated by chronic levodopa administration (Alcacer et al., 2017; Ryan et al., 2018), but manipulations of iMSNs have only a modulatory effect on dyskinesia (Alcacer et al., 2017). Therefore, if the striatum is the original locus of pathological levodopa-evoked activity underlying LID, a deeper understanding of striatal direct pathway dysfunction is needed. For instance, even in late stage PD, levodopa continues to relieve parkinsonian symptoms *and* trigger LID, suggesting levodopa may normalize the firing of some striatal neurons (responsible for the therapeutic levodopa response) and trigger pathological activity in others (responsible for dyskinesia). However, this theory has been largely unexplored and is the subject of this thesis.

1.5 Striatal Cellular Dysfunction

How might the loss of dopamine or chronic dopamine replacement lead to the dysfunction of striatal MSNs? Two key theories suggest that dopamine-dependent changes in (1) synaptic plasticity and (2) intrinsic properties contribute to aberrant striatal activity in PD and LID. One prominent theory suggests that cortico-striatal inputs exhibit altered synaptic plasticity due chronic changes in dopamine. For instance, long-term depression (LTD) and long-term potentiation (LTP), key mechanisms for regulating synaptic strength in the striatum, are perturbed in PD and LID. In parkinsonian animals, striatal LTD at excitatory synapses is reduced (Calabresi et al., 1997; Kreitzer and Malenka, 2007; Shen et al., 2008). In animal models of LID, LTP induced at excitatory synapses is insensitive to depotentiation, which could contribute to the excessive activity of dMSNs in LID (Picconi et al., 2003; Shen et al., 2015). The number/distribution of excitatory synaptic inputs has also been suggested to change in PD and LID. Several studies have found an overall reduction in axospinous synapses (presumed excitatory cortical/thalamic synapses) in patients and animal models of PD (Day et al., 2006; Ingham et al., 1989; McNeill et al., 1988; Villalba and Smith, 2018; Villalba et al., 2009). Thalamo-striatal excitatory inputs are

also reduced in patients and animal models of PD (Henderson et al., 2000; Villalba et al., 2014; Xuereb et al., 1991). A reduction in axospinous synapses has also been found in LID (Fieblinger et al., 2014; Suarez et al., 2016). In addition to these presynaptic changes, another theory is that postsynaptic changes in MSNs are the key to striatal dysfunction. For instance, dopamine loss and chronic levodopa have been shown to elicit bidirectional and opposing changes in dMSN and iMSN excitability (Fieblinger et al., 2014; Suarez et al., 2018; Surmeier et al., 2007). Extensive gene expression changes have also been observed in dMSNs and iMSNs in parkinsonian and dyskinetic mice (Heiman et al., 2014). Changes in dopaminergic signaling, such as increased D1-dopamine receptor expression or enhanced downstream signaling cascades has also been suggested to play a crucial role in LID (Aubert et al., 2005; Bezard et al., 2005; Guigoni et al., 2007; Jenner, 2008). Together, these studies suggest that combined presynaptic and postsynaptic changes in MSNs are likely to contribute to striatal dysfunction.

I sought to directly address the cellular and circuit dysfunction hypothesized to occur in the striatum during parkinsonism and LID, as outlined above, using a mouse model of Parkinson's disease in conjunction with a variety of cell-type specific techniques. I first address circuit level changes by characterizing the changes in direct and indirect pathway neurons following dopamine loss and replacement with levodopa, using *in vivo* electrophysiology and optogenetically labeled recordings. To address the cellular and synaptic changes that might contribute to the development of LID, I use an activity-dependent mouse line (FosTRAP) to capture LID-associated striatal neurons, in conjunction with *in vivo* and *ex vivo* electrophysiology and synaptic tracing, to investigate the differential regulation of these properties specifically in the subpopulation of direct pathway neurons involved in dyskinesia. The remaining chapters of this dissertation will detail our findings of striatal cellular and circuit dysfunction in parkinsonian animals.

1.6 Figures

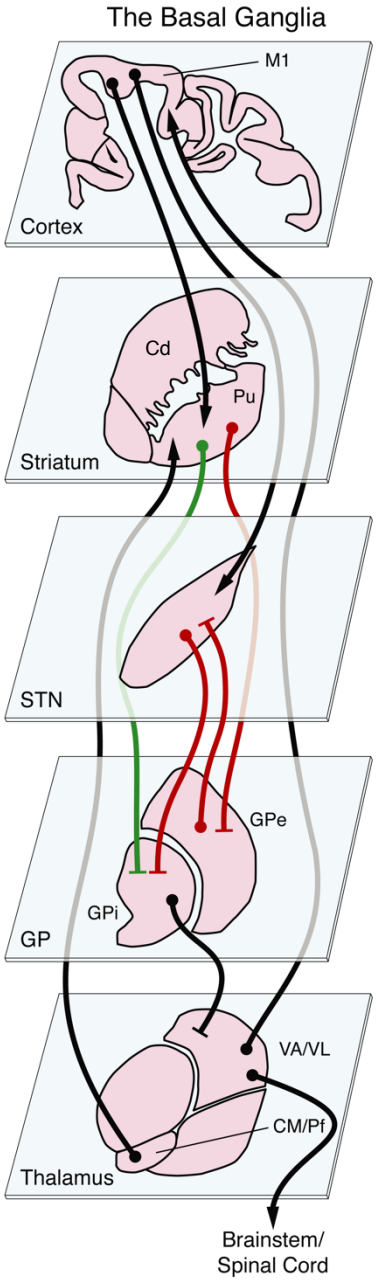

1.1 Figure 1. Circuitry of the basal ganglia

Schematic showing the major nodes of the basal ganglia. Excitatory projections are depicted with an arrow and inhibitory projections are depicted with a dash. The direct pathway is highlighted in green and the indirect pathway highlighted in red. Abbreviations: M1, primary motor cortex; Cd, caudate; Pu, putamen; STN, subthalamic nucleus; GP, globus pallidus; GPe, external globus pallidus; GPi, internal globus pallidus; VA/VL, ventral-anterior and ventral-lateral nuclei of the thalamus, CM/Pf, centromedial/parafasicular nucleus of the thalamus (also called the intralaminar thalamus).

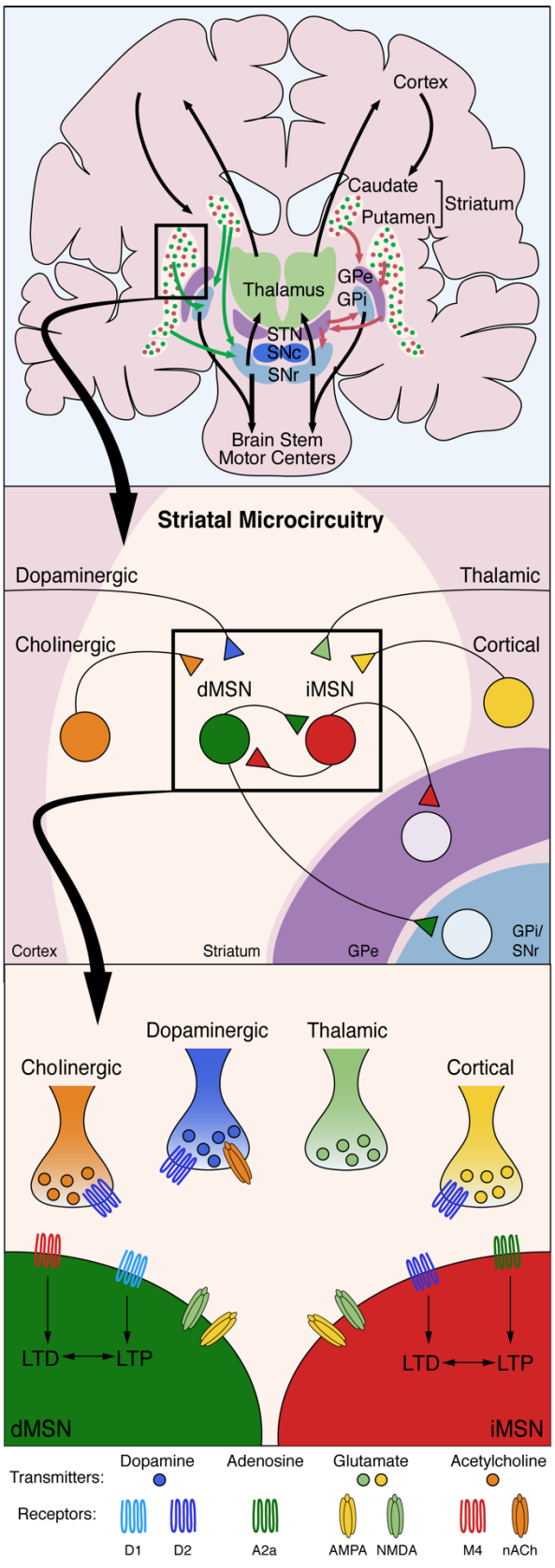
Cortex
Caudate
Putamen
Striatum
Thalamus
GPe
GPi
STN
SNc
SNr
Brain Stem
Motor Centers
Striatal Microcircuitry
Dopaminergic
Thalamic
Cholinergic
Cortical
dMSN
iMSN
Cortex
Striatum
GPe
GPi/
SNr
Dopaminergic
Thalamic
Cholinergic
Cortical
LTD
LTP
LTD
LTP
dMSN
iMSN
Transmitters:
Dopamine
Adenosine
Glutamate
Acetylcholine
Receptors:
D1
D2
A2a
AMPA
NMDA
M4
nACh

1.2 Figure 2. The striatal microcircuit

(Top) Simplified schematic of basal ganglia anatomy depicted as a coronal section from a human brain. (Middle) The striatal microcircuit (Bottom) Higher magnification of the striatal microcircuit, with important receptors and neurotransmitters represented. Abbreviations: GPe, external globus pallidus; GPi/SNr, internal globus pallidus/substantia nigra pars reticulata; STN, subthalamic nucleus, SNc, substantia nigra pars compacta; SNr, substantia nigra pars reticulate; dMSN, direct pathway medium spiny neuron; iMSN: indirect pathway medium spiny neuron; D1, D1-like dopamine receptor, D2, D2-like dopamine receptor, A2a; adenosine; AMPA, α-amino-3-hydroxy-5-methyl-4-isoxazolepropionic acid; NMDA, N-Methyl- d-aspartic acid; M4, M4-muscarinic acetylcholine receptor; nACh, nicotinic acetylcholine receptor; LTD, long-term depression; LTP, long-term potentiation.

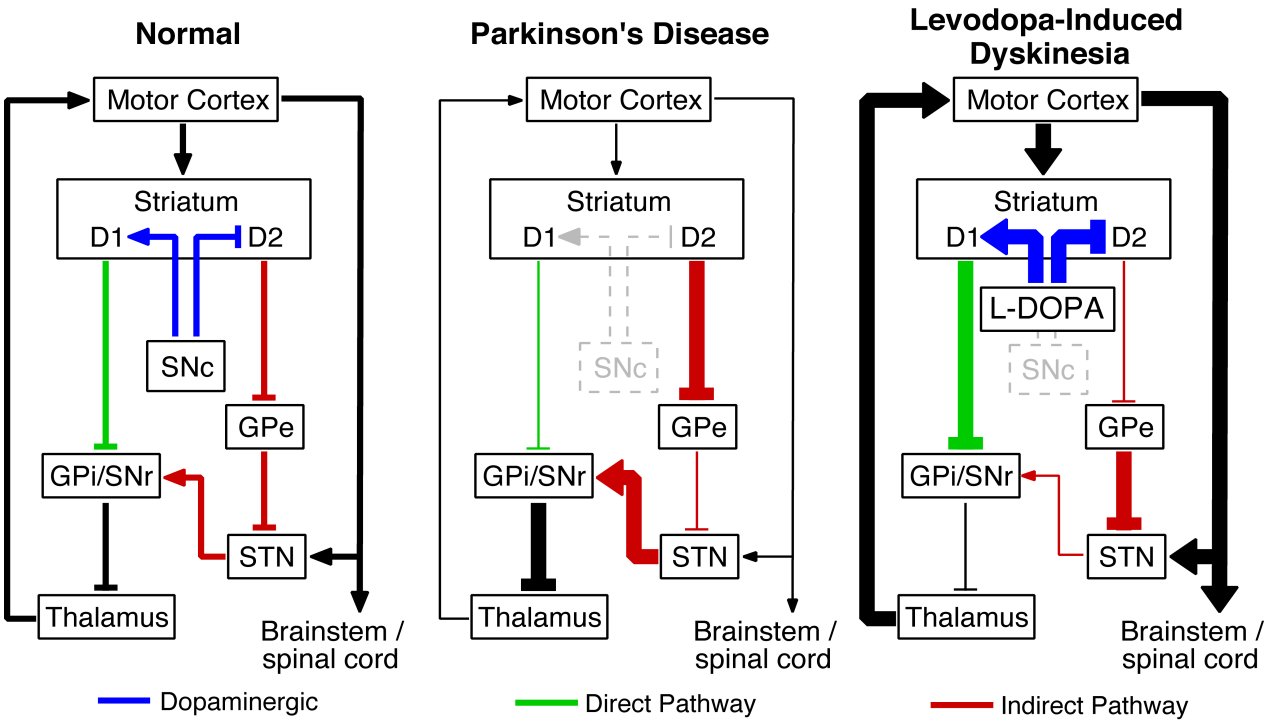

1.3 Figure 3. The classical model of basal ganglia function

Simplified schematic of the basal ganglia in healthy and disease states. Excitatory connects are depicted with an arrow and inhibitory connections are depicted with a dash. Abbreviations: D1, D1-dopamine receptor bearing direct pathway neurons; D2, D2-dopamine receptor bearing indirect pathway neurons; SNc, substantia nigra pars compacta; GPe, external globus pallidus; GPi/SNr, internal globus pallidus/substantia nigra pars reticulata; STN, subthalamic nucleus. Adapted from Delong, 1990.

1.7 References

Ahlskog, J.E., and Muenter, M.D. (2001). Frequency of levodopa-related dyskinesias and motor fluctuations as estimated from the cumulative literature. Mov. Disord. *16*, 448–458.

Albin, R.L., Young, A.B., and Penney, J.B. (1989). The functional anatomy of basal ganglia disorders. Trends Neurosci. *12*, 366–375.

Alcacer, C., Andreoli, L., Sebastianutto, I., Jakobsson, J., Fieblinger, T., and Cenci, M.A. (2017). Chemogenetic stimulation of striatal projection neurons modulates responses to Parkinson's disease therapy. Journal of Clinical Investigation *127*, 720–734.

Alexander, G.E., and Crutcher, M.D. (1990). Functional architecture of basal ganglia circuits: neural substrates of parallel processing. Trends Neurosci. *13*, 266–271.

Andersson, M., Hilbertson, A., and Cenci, M.A. (1999). Striatal fosB expression is causally linked with l-DOPA-induced abnormal involuntary movements and the associated upregulation of striatal prodynorphin mRNA in a rat model of Parkinson's disease. Neurobiol. Dis. *6*, 461–474.

Aquino, C.C., and Fox, S.H. (2015). Clinical spectrum of levodopa-induced complications. Mov. Disord. *30*, 80–89.

Aubert, I., Guigoni, C., Håkansson, K., Li, Q., Dovero, S., Barthe, N., Bioulac, B.H., Gross, C.E., Fisone, G., Bloch, B., et al. (2005). Increased D1 dopamine receptor signaling in levodopa-induced dyskinesia. Ann. Neurol. *57*, 17–26.

Bagetta, V., Sgobio, C., Pendolino, V., Del Papa, G., Tozzi, A., Ghiglieri, V., Giampà, C., Zianni, E., Gardoni, F., Calabresi, P., et al. (2012). Rebalance of striatal NMDA/AMPA receptor ratio

underlies the reduced emergence of dyskinesia during D2-like dopamine agonist treatment in experimental Parkinson's disease. J. Neurosci. *32*, 17921–17931.

Barbera, G., Liang, B., Zhang, L., Gerfen, C.R., Culurciello, E., Chen, R., Li, Y., and Lin, D.-T. (2016). Spatially Compact Neural Clusters in the Dorsal Striatum Encode Locomotion Relevant Information. Neuron *92*, 202–213.

Barnes, T.D., Kubota, Y., Hu, D., Jin, D.Z., and Graybiel, A.M. (2005). Activity of striatal neurons reflects dynamic encoding and recoding of procedural memories. Nature *437*, 1158–1161.

Bateup, H.S., Santini, E., Shen, W., Birnbaum, S., Valjent, E., Surmeier, D.J., Fisone, G., Nestler, E.J., and Greengard, P. (2010). Distinct subclasses of medium spiny neurons differentially regulate striatal motor behaviors. Proc. Natl. Acad. Sci. U.S.A. *107*, 14845–14850.

Beckstead, R.M., Domesick, V.B., and Nauta, W.J. (1979). Efferent connections of the substantia nigra and ventral tegmental area in the rat. Brain Res. *175*, 191–217.

Beier, K.T., Kim, C.K., Hoerbelt, P., Hung, L.W., Heifets, B.D., DeLoach, K.E., Mosca, T.J., Neuner, S., Deisseroth, K., Luo, L., et al. (2017). Rabies screen reveals GPe control of cocaine-triggered plasticity. Nature *549*, 345–350.

Beitz, J.M. (2014). Parkinson's disease: a review. Front Biosci (Schol Ed) *6*, 65–74.

Benazzouz, A., Breit, S., Koudsie, A., Pollak, P., Krack, P., and Benabid, A.-L. (2002). Intraoperative microrecordings of the subthalamic nucleus in Parkinson's disease. Mov. Disord. *17 Suppl 3*, S145-149.

Bergman, H., Wichmann, T., Karmon, B., and DeLong, M.R. (1994). The primate subthalamic nucleus. II. Neuronal activity in the MPTP model of parkinsonism. J. Neurophysiol. *72*, 507–520.

Berke, J.D., Okatan, M., Skurski, J., and Eichenbaum, H.B. (2004). Oscillatory entrainment of striatal neurons in freely moving rats. Neuron *43*, 883–896.

Bezard, E., Gross, C.E., Qin, L., Gurevich, V.V., Benovic, J.L., and Gurevich, E.V. (2005). l-DOPA reverses the MPTP-induced elevation of the arrestin2 and GRK6 expression and enhanced ERK activation in monkey brain. Neurobiology of Disease *18*, 323–335.

Bhidayasiri, R., and Truong, D.D. (2008). Motor complications in Parkinson disease: clinical manifestations and management. J. Neurol. Sci. *266*, 204–215.

Boraud, T., Bezard, E., Guehl, D., Bioulac, B., and Gross, C. (1998). Effects of L-DOPA on neuronal activity of the globus pallidus externalis (GPe) and globus pallidus internalis (GPi) in the MPTP-treated monkey. Brain Res. *787*, 157–160.

Borgkvist, A., Avegno, E.M., Wong, M.Y., Kheirbek, M.A., Sonders, M.S., Hen, R., and Sulzer, D. (2015). Loss of Striatonigral GABAergic Presynaptic Inhibition Enables Motor Sensitization in Parkinsonian Mice. Neuron *87*, 976–988.

Brimblecombe, K.R., and Cragg, S.J. (2017). The Striosome and Matrix Compartments of the Striatum: A Path through the Labyrinth from Neurochemistry toward Function. ACS Chem Neurosci *8*, 235–242.

Calabresi, P., Saiardi, A., Pisani, A., Baik, J.H., Centonze, D., Mercuri, N.B., Bernardi, G., and Borrelli, E. (1997). Abnormal synaptic plasticity in the striatum of mice lacking dopamine D2 receptors. J. Neurosci. *17*, 4536–4544.

Caroff, S.N., Ungvari, G.S., and Cunningham Owens, D.G. (2018). Historical perspectives on tardive dyskinesia. J. Neurol. Sci. *389*, 4–9.

Carta, M., Lindgren, H.S., Lundblad, M., Stancampiano, R., Fadda, F., and Cenci, M.A. (2006). Role of striatal L-DOPA in the production of dyskinesia in 6-hydroxydopamine lesioned rats. J. Neurochem. *96*, 1718–1727.

Cenci, M.A., and Konradi, C. (2010). Maladaptive striatal plasticity in L-DOPA-induced dyskinesia. Prog. Brain Res. *183*, 209–233.

Cenci, M.A., and Lundblad, M. (2007). Ratings of L-DOPA-induced dyskinesia in the unilateral 6-OHDA lesion model of Parkinson's disease in rats and mice. Curr Protoc Neurosci *Chapter 9*, Unit 9.25.

Chang, H.T., Wilson, C.J., and Kitai, S.T. (1982). A Golgi study of rat neostriatal neurons: light microscopic analysis. J. Comp. Neurol. *208*, 107–126.

Chen, M.-T., Morales, M., Woodward, D.J., Hoffer, B.J., and Janak, P.H. (2001). In Vivo Extracellular Recording of Striatal Neurons in the Awake Rat Following Unilateral 6-Hydroxydopamine Lesions. Experimental Neurology *171*, 72–83.

Choi, K., Holly, E., Davatolhagh, M.F., Beier, K.T., and Fuccillo, M.V. (2019). Integrated anatomical and physiological mapping of striatal afferent projections. Eur J Neurosci *49*, 623–636.

Ciriachi, C., Svane-Petersen, D., and Rickhag, M. (2019). Genetic tools to study complexity of striatal function. J. Neurosci. Res. *97*, 1181–1193.

Costa, R.M., Lin, S.-C., Sotnikova, T.D., Cyr, M., Gainetdinov, R.R., Caron, M.G., and Nicolelis, M.A.L. (2006). Rapid alterations in corticostriatal ensemble coordination during acute dopamine-dependent motor dysfunction. Neuron *52*, 359–369.

Cui, G., Jun, S.B., Jin, X., Pham, M.D., Vogel, S.S., Lovinger, D.M., and Costa, R.M. (2013). Concurrent activation of striatal direct and indirect pathways during action initiation. Nature *494*, 238–242.

Dautan, D., Huerta-Ocampo, I., Witten, I.B., Deisseroth, K., Bolam, J.P., Gerdjikov, T., and Mena-Segovia, J. (2014). A major external source of cholinergic innervation of the striatum and nucleus accumbens originates in the brainstem. J. Neurosci. *34*, 4509–4518.

Day, M., Wang, Z., Ding, J., An, X., Ingham, C.A., Shering, A.F., Wokosin, D., Ilijic, E., Sun, Z., Sampson, A.R., et al. (2006). Selective elimination of glutamatergic synapses on striatopallidal neurons in Parkinson disease models. Nat. Neurosci. *9*, 251–259.

Deffains, M., and Bergman, H. (2015). Striatal cholinergic interneurons and cortico-striatal synaptic plasticity in health and disease. Mov. Disord. *30*, 1014–1025.

Deffains, M., Iskhakova, L., Katabi, S., Haber, S.N., Israel, Z., and Bergman, H. (2016). Subthalamic, not striatal, activity correlates with basal ganglia downstream activity in normal and parkinsonian monkeys. Elife *5*.

DeLong, M.R. (1990). Primate models of movement disorders of basal ganglia origin. Trends Neurosci. *13*, 281–285.

Ding, J., Peterson, J.D., and Surmeier, D.J. (2008). Corticostriatal and Thalamostriatal Synapses Have Distinctive Properties. Journal of Neuroscience *28*, 6483–6492.

Eastwood, B.S., Hooks, B.M., Paletzki, R.F., O'Connor, N.J., Glaser, J.R., and Gerfen, C.R. (2019). Whole mouse brain reconstruction and registration to a reference atlas with standard histochemical processing of coronal sections. Journal of Comparative Neurology *527*, 2170–2178.

Fieblinger, T., Graves, S.M., Sebel, L.E., Alcacer, C., Plotkin, J.L., Gertler, T.S., Chan, C.S., Heiman, M., Greengard, P., Cenci, M.A., et al. (2014). Cell type-specific plasticity of striatal projection neurons in parkinsonism and L-DOPA-induced dyskinesia. Nat Commun *5*, 5316.

Fieblinger, T., Zanetti, L., Sebastianutto, I., Breger, L.S., Quintino, L., Lockowandt, M., Lundberg, C., and Cenci, M.A. (2018). Striatonigral neurons divide into two distinct morphological-physiological phenotypes after chronic L-DOPA treatment in parkinsonian rats. Sci Rep *8*, 10068.

Filion, M., and Tremblay, L. (1991). Abnormal spontaneous activity of globus pallidus neurons in monkeys with MPTP-induced parkinsonism. Brain Res. *547*, 142–151.

Flaherty, A.W., and Graybiel, A.M. (1991). Corticostriatal transformations in the primate somatosensory system. Projections from physiologically mapped body-part representations. J. Neurophysiol. *66*, 1249–1263.

Francardo, V., Recchia, A., Popovic, N., Andersson, D., Nissbrandt, H., and Cenci, M.A. (2011). Impact of the lesion procedure on the profiles of motor impairment and molecular responsiveness

to L-DOPA in the 6-hydroxydopamine mouse model of Parkinson's disease. Neurobiol. Dis. *42*, 327–340.

Freeze, B.S., Kravitz, A.V., Hammack, N., Berke, J.D., and Kreitzer, A.C. (2013). Control of basal ganglia output by direct and indirect pathway projection neurons. J. Neurosci. *33*, 18531–18539.

Gage, G.J., Stoetzner, C.R., Wiltschko, A.B., and Berke, J.D. (2010). Selective activation of striatal fast-spiking interneurons during choice execution. Neuron *67*, 466–479.

Galvan, A., Devergnas, A., and Wichmann, T. (2015). Alterations in neuronal activity in basal ganglia-thalamocortical circuits in the parkinsonian state. Front Neuroanat *9*, 5.

Gerfen, C.R., and Surmeier, D.J. (2011). Modulation of striatal projection systems by dopamine. Annu. Rev. Neurosci. *34*, 441–466.

Gerfen, C.R., Engber, T.M., Mahan, L.C., Susel, Z., Chase, T.N., Monsma, F.J., and Sibley, D.R. (1990). D1 and D2 dopamine receptor-regulated gene expression of striatonigral and striatopallidal neurons. Science *250*, 1429–1432.

Gerfen, C.R., Paletzki, R., and Heintz, N. (2013). GENSAT BAC cre-recombinase driver lines to study the functional organization of cerebral cortical and basal ganglia circuits. Neuron *80*, 1368–1383.

Girasole, A.E., Lum, M.Y., Nathaniel, D., Bair-Marshall, C.J., Guenthner, C.J., Luo, L., Kreitzer, A.C., and Nelson, A.B. (2018). A Subpopulation of Striatal Neurons Mediates Levodopa-Induced Dyskinesia. Neuron *97*, 787-795.e6.

Gokce, O., Stanley, G., Treutlein, B., Neff, N.F., Camp, G.J., Malenka, R.C., Rothwell, P.E., Fuccillo, M.V., Südhof, T.C., and Quake, S.R. (2016). Cellular Taxonomy of the Mouse Striatum as Revealed by Single-Cell RNA-Seq. Cell Rep *16*, 1126–1137.

Gong, S., Doughty, M., Harbaugh, C.R., Cummins, A., Hatten, M.E., Heintz, N., and Gerfen, C.R. (2007). Targeting Cre Recombinase to Specific Neuron Populations with Bacterial Artificial Chromosome Constructs. Journal of Neuroscience *27*, 9817–9823.

Graveland, G.A., and DiFiglia, M. (1985). The frequency and distribution of medium-sized neurons with indented nuclei in the primate and rodent neostriatum. Brain Res. *327*, 307–311.

Guenthner, C.J., Miyamichi, K., Yang, H.H., Heller, H.C., and Luo, L. (2013). Permanent Genetic Access to Transiently Active Neurons via TRAP: Targeted Recombination in Active Populations. Neuron *78*, 773–784.

Guigoni, C., Doudnikoff, E., Li, Q., Bloch, B., and Bezard, E. (2007). Altered D(1) dopamine receptor trafficking in parkinsonian and dyskinetic non-human primates. Neurobiol. Dis. *26*, 452–463.

Guo, Q., Wang, D., He, X., Feng, Q., Lin, R., Xu, F., Fu, L., and Luo, M. (2015). Whole-brain mapping of inputs to projection neurons and cholinergic interneurons in the dorsal striatum. PLoS ONE *10*, e0123381.

Haber, S.N., Fudge, J.L., and McFarland, N.R. (2000). Striatonigrostriatal pathways in primates form an ascending spiral from the shell to the dorsolateral striatum. J. Neurosci. *20*, 2369–2382.

Harris, K.D., Henze, D.A., Csicsvari, J., Hirase, H., and Buzsáki, G. (2000). Accuracy of tetrode spike separation as determined by simultaneous intracellular and extracellular measurements. J. Neurophysiol. *84*, 401–414.

Heiman, M., Heilbut, A., Francardo, V., Kulicke, R., Fenster, R.J., Kolaczyk, E.D., Mesirov, J.P., Surmeier, D.J., Cenci, M.A., and Greengard, P. (2014). Molecular adaptations of striatal spiny projection neurons during levodopa-induced dyskinesia. Proc. Natl. Acad. Sci. U.S.A. *111*, 4578–4583.

Hely, M.A., Reid, W.G.J., Adena, M.A., Halliday, G.M., and Morris, J.G.L. (2008). The Sydney multicenter study of Parkinson's disease: the inevitability of dementia at 20 years. Mov. Disord. *23*, 837–844.

Henderson, J.M., Carpenter, K., Cartwright, H., and Halliday, G.M. (2000). Degeneration of the centré median–parafascicular complex in Parkinson's disease. Ann Neurol. *47*, 345–352.

Hernandez, L.F., Kubota, Y., Hu, D., Howe, M.W., Lemaire, N., and Graybiel, A.M. (2013). Selective effects of dopamine depletion and L-DOPA therapy on learning-related firing dynamics of striatal neurons. J. Neurosci. *33*, 4782–4795.

Hernández-López, S., Bargas, J., Surmeier, D.J., Reyes, A., and Galarraga, E. (1997). D1 receptor activation enhances evoked discharge in neostriatal medium spiny neurons by modulating an L-type Ca2+ conductance. J. Neurosci. *17*, 3334–3342.

Hernandez-Lopez, S., Tkatch, T., Perez-Garci, E., Galarraga, E., Bargas, J., Hamm, H., and Surmeier, D.J. (2000). D2 dopamine receptors in striatal medium spiny neurons reduce L-type

Ca2+ currents and excitability via a novel PLC[beta]1-IP3-calcineurin-signaling cascade. J. Neurosci. *20*, 8987–8995.

Hornykiewicz, O. (2015). 50 years of levodopa. Mov. Disord. *30*, 1008.

Horstink, M.W., Zijlmans, J.C., Pasman, J.W., Berger, H.J., and van't Hof, M.A. (1990). Severity of Parkinson's disease is a risk factor for peak-dose dyskinesia. J. Neurol. Neurosurg. Psychiatr. *53*, 224–226.

Hutchinson, W.D., Lozano, A.M., Davis, K.D., Saint-Cyr, J.A., Lang, A.E., and Dostrovsky, J.O. (1994). Differential neuronal activity in segments of globus pallidus in Parkinson's disease patients. Neuroreport *5*, 1533–1537.

Ingham, C.A., Hood, S.H., and Arbuthnott, G.W. (1989). Spine density on neostriatal neurones changes with 6-hydroxydopamine lesions and with age. Brain Res. *503*, 334–338.

Jankovic, J. (2008). Parkinson's disease: clinical features and diagnosis. J. Neurol. Neurosurg. Psychiatr. *79*, 368–376.

Jenner, P. (2008). Molecular mechanisms of L-DOPA-induced dyskinesia. Nat. Rev. Neurosci. *9*, 665–677.

Jin, X., Tecuapetla, F., and Costa, R.M. (2014). Basal ganglia subcircuits distinctively encode the parsing and concatenation of action sequences. Nat Neurosci *17*, 423–430.

Johansson, Y., and Silberberg, G. (2020). The Functional Organization of Cortical and Thalamic Inputs onto Five Types of Striatal Neurons Is Determined by Source and Target Cell Identities. Cell Rep *30*, 1178-1194.e3.

Ketzef, M., Spigolon, G., Johansson, Y., Bonito-Oliva, A., Fisone, G., and Silberberg, G. (2017). Dopamine Depletion Impairs Bilateral Sensory Processing in the Striatum in a Pathway-Dependent Manner. Neuron *94*, 855-865.e5.

Kish, L.J., Palmer, M.R., and Gerhardt, G.A. (1999). Multiple single-unit recordings in the striatum of freely moving animals: effects of apomorphine and d-amphetamine in normal and unilateral 6-hydroxydopamine-lesioned rats. Brain Research *833*, 58–70.

Kravitz, A.V., Freeze, B.S., Parker, P.R.L., Kay, K., Thwin, M.T., Deisseroth, K., and Kreitzer, A.C. (2010). Regulation of parkinsonian motor behaviours by optogenetic control of basal ganglia circuitry. Nature *466*, 622–626.

Kravitz, A.V., Tye, L.D., and Kreitzer, A.C. (2012). Distinct roles for direct and indirect pathway striatal neurons in reinforcement. Nat Neurosci *15*, 816–818.

Kravitz, A.V., Owen, S.F., and Kreitzer, A.C. (2013). Optogenetic identification of striatal projection neuron subtypes during in vivo recordings. Brain Res. *1511*, 21–32.

Kreiss, D.S., Mastropietro, C.W., Rawji, S.S., and Walters, J.R. (1997). The response of subthalamic nucleus neurons to dopamine receptor stimulation in a rodent model of Parkinson's disease. J. Neurosci. *17*, 6807–6819.

Kreitzer, A.C., and Malenka, R.C. (2007). Endocannabinoid-mediated rescue of striatal LTD and motor deficits in Parkinson's disease models. Nature *445*, 643–647.

Lahiri, A.K., and Bevan, M.D. (2020). Dopaminergic Transmission Rapidly and Persistently Enhances Excitability of D1 Receptor-Expressing Striatal Projection Neurons. Neuron *106*, 277-290.e6.

Lenz, J.D., and Lobo, M.K. (2013). Optogenetic insights into striatal function and behavior. Behav. Brain Res. *255*, 44–54.

Levy, R., Dostrovsky, J.O., Lang, A.E., Sime, E., Hutchison, W.D., and Lozano, A.M. (2001). Effects of apomorphine on subthalamic nucleus and globus pallidus internus neurons in patients with Parkinson's disease. J. Neurophysiol. *86*, 249–260.

Liang, L., DeLong, M.R., and Papa, S.M. (2008). Inversion of dopamine responses in striatal medium spiny neurons and involuntary movements. J. Neurosci. *28*, 7537–7547.

Lozano, A.M., Lang, A.E., Levy, R., Hutchison, W., and Dostrovsky, J. (2000). Neuronal recordings in Parkinson's disease patients with dyskinesias induced by apomorphine. Ann. Neurol. *47*, S141-146.

Mallet, N., Ballion, B., Le Moine, C., and Gonon, F. (2006). Cortical inputs and GABA interneurons imbalance projection neurons in the striatum of parkinsonian rats. J. Neurosci. *26*, 3875–3884.

Mallet, N., Pogosyan, A., Sharott, A., Csicsvari, J., Bolam, J.P., Brown, P., and Magill, P.J. (2008). Disrupted dopamine transmission and the emergence of exaggerated beta oscillations in subthalamic nucleus and cerebral cortex. J. Neurosci. *28*, 4795–4806.

Mathur, B.N., and Lovinger, D.M. (2012). Serotonergic action on dorsal striatal function. Parkinsonism Relat. Disord. *18 Suppl 1*, S129-131.

McGeorge, A.J., and Faull, R.L. (1987). The organization and collateralization of corticostriate neurones in the motor and sensory cortex of the rat brain. Brain Res. *423*, 318–324.

McGregor, M.M., and Nelson, A.B. (2019). Circuit Mechanisms of Parkinson's Disease. Neuron *101*, 1042–1056.

McNeill, T.H., Brown, S.A., Rafols, J.A., and Shoulson, I. (1988). Atrophy of medium spiny I striatal dendrites in advanced Parkinson's disease. Brain Res. *455*, 148–152.

Mena-Segovia, J., Bolam, J.P., and Magill, P.J. (2004). Pedunculopontine nucleus and basal ganglia: distant relatives or part of the same family? Trends Neurosci. *27*, 585–588.

Mink, J.W. (1996). The basal ganglia: focused selection and inhibition of competing motor programs. Prog. Neurobiol. *50*, 381–425.

Mink, J.W. (2003). The Basal Ganglia and involuntary movements: impaired inhibition of competing motor patterns. Arch. Neurol. *60*, 1365–1368.

Nonomura, S., Nishizawa, K., Sakai, Y., Kawaguchi, Y., Kato, S., Uchigashima, M., Watanabe, M., Yamanaka, K., Enomoto, K., Chiken, S., et al. (2018). Monitoring and Updating of Action Selection for Goal-Directed Behavior through the Striatal Direct and Indirect Pathways. Neuron *99*, 1302-1314.e5.

Oye, C., Bouchard, R., Boucher, R., and Poirier, L.J. (1970). Spontaneous activity of the putamen after chronic interruption of the dopaminergic pathway: effect of L-dopa. J. Pharmacol. Exp. Ther. *175*, 700–708.

Pan, H.S., and Walters, J.R. (1988). Unilateral lesion of the nigrostriatal pathway decreases the firing rate and alters the firing pattern of globus pallidus neurons in the rat. Synapse *2*, 650–656.

Pan, W.X., Mao, T., and Dudman, J.T. (2010). Inputs to the dorsal striatum of the mouse reflect the parallel circuit architecture of the forebrain. Front Neuroanat *4*, 147.

Papa, S.M., Desimone, R., Fiorani, M., and Oldfield, E.H. (1999). Internal globus pallidus discharge is nearly suppressed during levodopa-induced dyskinesias. Ann. Neurol. *46*, 732–738.

Parker, J.G., Marshall, J.D., Ahanonu, B., Wu, Y.-W., Kim, T.H., Grewe, B.F., Zhang, Y., Li, J.Z., Ding, J.B., Ehlers, M.D., et al. (2018). Diametric neural ensemble dynamics in parkinsonian and dyskinetic states. Nature *557*, 177–182.

Perez, X.A., Zhang, D., Bordia, T., and Quik, M. (2017). Striatal D1 medium spiny neuron activation induces dyskinesias in parkinsonian mice. Mov. Disord.

Picconi, B., Centonze, D., Håkansson, K., Bernardi, G., Greengard, P., Fisone, G., Cenci, M.A., and Calabresi, P. (2003). Loss of bidirectional striatal synaptic plasticity in L-DOPA-induced dyskinesia. Nat. Neurosci. *6*, 501–506.

Planert, H., Berger, T.K., and Silberberg, G. (2013). Membrane properties of striatal direct and indirect pathway neurons in mouse and rat slices and their modulation by dopamine. PLoS ONE *8*, e57054.

Prager, E.M., and Plotkin, J.L. (2019). Compartmental function and modulation of the striatum. J. Neurosci. Res. *97*, 1503–1514.

Redgrave, P., Rodriguez, M., Smith, Y., Rodriguez-Oroz, M.C., Lehericy, S., Bergman, H., Agid, Y., DeLong, M.R., and Obeso, J.A. (2010). Goal-directed and habitual control in the basal ganglia: implications for Parkinson's disease. Nat. Rev. Neurosci. *11*, 760–772.

Rothwell, P.E., Hayton, S.J., Sun, G.L., Fuccillo, M.V., Lim, B.K., and Malenka, R.C. (2015). Input- and Output-Specific Regulation of Serial Order Performance by Corticostriatal Circuits. Neuron *88*, 345–356.

Ryan, M.B., Bair-Marshall, C., and Nelson, A.B. (2018). Aberrant Striatal Activity in Parkinsonism and Levodopa-Induced Dyskinesia. Cell Rep *23*, 3438-3446.e5.

Sagot, B., Li, L., and Zhou, F.-M. (2018). Hyperactive Response of Direct Pathway Striatal Projection Neurons to L-dopa and D1 Agonism in Freely Moving Parkinsonian Mice. Front Neural Circuits *12*, 57.

Schultz, W. (2016). Reward functions of the basal ganglia. J Neural Transm (Vienna) *123*, 679–693.

Shen, W., Flajolet, M., Greengard, P., and Surmeier, D.J. (2008). Dichotomous dopaminergic control of striatal synaptic plasticity. Science *321*, 848–851.

Shen, W., Plotkin, J.L., Francardo, V., Ko, W.K.D., Xie, Z., Li, Q., Fieblinger, T., Wess, J., Neubig, R.R., Lindsley, C.W., et al. (2015). M4 Muscarinic Receptor Signaling Ameliorates Striatal Plasticity Deficits in Models of L-DOPA-Induced Dyskinesia. Neuron *88*, 762–773.

Shin, J.H., Kim, D., and Jung, M.W. (2018). Differential coding of reward and movement information in the dorsomedial striatal direct and indirect pathways. Nat Commun *9*, 404.

Soares, J., Kliem, M.A., Betarbet, R., Greenamyre, J.T., Yamamoto, B., and Wichmann, T. (2004). Role of external pallidal segment in primate parkinsonism: comparison of the effects of 1-methyl-4-phenyl-1,2,3,6-tetrahydropyridine-induced parkinsonism and lesions of the external pallidal segment. J. Neurosci. *24*, 6417–6426.

Suárez, L.M., Solís, O., Caramés, J.M., Taravini, I.R., Solís, J.M., Murer, M.G., and Moratalla, R. (2014). L-DOPA Treatment Selectively Restores Spine Density in Dopamine Receptor D2–Expressing Projection Neurons in Dyskinetic Mice. Biological Psychiatry *75*, 711–722.

Suarez, L.M., Solis, O., Aguado, C., Lujan, R., and Moratalla, R. (2016). L-DOPA Oppositely Regulates Synaptic Strength and Spine Morphology in D1 and D2 Striatal Projection Neurons in Dyskinesia. Cereb. Cortex *26*, 4253–4264.

Suarez, L.M., Alberquilla, S., García-Montes, J.R., and Moratalla, R. (2018). Differential Synaptic Remodeling by Dopamine in Direct and Indirect Striatal Projection Neurons in Pitx3 $^{-/-}$ Mice, a Genetic Model of Parkinson's Disease. J. Neurosci. *38*, 3619–3630.

Surmeier, D.J., Song, W.J., and Yan, Z. (1996). Coordinated expression of dopamine receptors in neostriatal medium spiny neurons. J. Neurosci. *16*, 6579–6591.

Surmeier, D.J., Ding, J., Day, M., Wang, Z., and Shen, W. (2007). D1 and D2 dopamine-receptor modulation of striatal glutamatergic signaling in striatal medium spiny neurons. Trends Neurosci. *30*, 228–235.

Tepper, J.M., Tecuapetla, F., Koós, T., and Ibáñez-Sandoval, O. (2010). Heterogeneity and diversity of striatal GABAergic interneurons. Front Neuroanat *4*, 150.

Vijayakumar, D., and Jankovic, J. (2016). Drug-Induced Dyskinesia, Part 1: Treatment of Levodopa-Induced Dyskinesia. Drugs *76*, 759–777.

Villalba, R.M., and Smith, Y. (2018). Loss and remodeling of striatal dendritic spines in Parkinson's disease: from homeostasis to maladaptive plasticity? J Neural Transm (Vienna) *125*, 431–447.

Villalba, R.M., Lee, H., and Smith, Y. (2009). Dopaminergic denervation and spine loss in the striatum of MPTP-treated monkeys. Exp. Neurol. *215*, 220–227.

Villalba, R.M., Wichmann, T., and Smith, Y. (2014). Neuronal loss in the caudal intralaminar thalamic nuclei in a primate model of Parkinson's disease. Brain Struct Funct *219*, 381–394.

Wall, N.R., De La Parra, M., Callaway, E.M., and Kreitzer, A.C. (2013). Differential innervation of direct- and indirect-pathway striatal projection neurons. Neuron *79*, 347–360.

Wickens, J.R., and Wilson, C.J. (1998). Regulation of action-potential firing in spiny neurons of the rat neostriatum in vivo. J. Neurophysiol. *79*, 2358–2364.

Xuereb, J.H., Perry, R.H., Candy, J.M., Perry, E.K., Marshall, E., and Bonham, J.R. (1991). Nerve cell loss in the thalamus in Alzheimer's disease and Parkinson's disease. Brain *114 (Pt 3)*, 1363–1379.

Yoshida, M. (1991). The neuronal mechanism underlying parkinsonism and dyskinesia: differential roles of the putamen and caudate nucleus. Neurosci. Res. *12*, 31–40.

Zhai, S., Shen, W., Graves, S.M., and Surmeier, D.J. (2019). Dopaminergic modulation of striatal function and Parkinson's disease. J Neural Transm (Vienna) *126*, 411–422.

Chapter 2: Aberrant Striatal Activity in Parkinsonism and Levodopa-Induced Dyskinesia

2.1 Summary

Action selection relies on coordinated activity of striatal direct and indirect pathway medium spiny neurons (dMSNs and iMSNs, respectively). Loss of dopamine in Parkinson's Disease is thought to disrupt this balance. While dopamine replacement with levodopa may restore normal function, the development of involuntary movements (levodopa-induced dyskinesia, LID) limits therapy. How chronic dopamine loss and replacement with levodopa modulate firing of identified MSNs in behaving animals is currently unknown. Using optogenetically labeled striatal single-unit recordings, we assess circuit dysfunction in parkinsonism and LID. Counter to current models, we found that following dopamine depletion, iMSN firing was elevated only during periods of immobility, while dMSN firing was dramatically and persistently reduced. Most notably, we identified a subpopulation of dMSNs with abnormally high levodopa-evoked firing rates, which correlated specifically with dyskinesia. These findings provide key insights into the circuit mechanisms underlying parkinsonism and LID, with implications for developing novel, targeted therapies.

2.2 Introduction

In Parkinson's Disease (PD), progressive degeneration of midbrain dopamine neurons is associated with marked motor impairments, including bradykinesia (slowed movement), tremor, and rigidity. While the precise effect of dopamine loss on cellular and circuit function is unknown, dopamine replacement therapy with levodopa is the mainstay treatment. Levodopa is initially effective in treating PD motor deficits, but with chronic treatment the majority of patients develop drug-induced involuntary movements (Ahlskog and Muenter, 2001), known as levodopa-induced dyskinesia (LID). This clinical problem highlights the importance of identifying the circuit dysfunction resulting from dopamine loss and subsequent replacement with levodopa.

Midbrain dopamine neurons send their densest projections to the input nucleus of the basal ganglia, the striatum (Haber et al., 2000). Integrating dopaminergic inputs and glutamatergic inputs from sensorimotor cortical regions (McGeorge and Faull, 1987), the striatum is poised to control movement and decision-making (Redgrave et al., 2010). Dopamine is hypothesized to regulate movement via antagonistic control of GABAergic striatal projection neurons: direct and indirect pathway medium spiny neurons (MSNs). Direct pathway neurons (dMSNs) express the D_1-like dopamine receptor (Gerfen et al., 1990) and optical activation of dMSNs inhibits basal ganglia output and increases movement (Kravitz et al., 2010). Indirect pathway neurons (iMSNs) express the D_2-like dopamine receptor (Gerfen et al., 1990) and optical activation of iMSNs increases basal ganglia output and suppresses movement (Kravitz et al., 2010). According to the standard model of basal ganglia function, striatal dopamine release excites dMSNs and inhibits iMSNs, leading to action selection (Albin et al., 1989; DeLong, 1990). While pharmacological studies in *ex vivo* brain slices support this hypothesis (Hernández-López et al., 2000; Hernández-López et al., 1997; Planert et al., 2013), it is less clear how dopamine modulates striatal activity *in vivo*.

The standard model also predicts that dopamine loss, as occurs in PD, causes opposing changes in the activity of MSNs: persistently reduced dMSN and increased iMSN firing rates. Indirect support for this model derives from recordings in downstream basal ganglia nuclei in patients and parkinsonian primates (Bergman et al., 1994; Filion and Tremblay, 1991; Soares et al., 2004). However, direct evidence for bidirectional regulation of striatal MSN firing by dopamine in awake, behaving parkinsonian animals is lacking. As a corollary of this model, dopamine replacement with levodopa is postulated to improve motor symptoms by rebalancing striatal dMSN and iMSN activity. In addition, the prevailing hypothesis is that long-term levodopa treatment causes excessive direct pathway activity (Albin et al., 1989; DeLong, 1990), which may lead to LID. Again, some indirect evidence supports this model: altered firing in the striatum (Liang et al., 2008) and downstream basal ganglia nuclei (Boraud et al., 1998; Levy et al., 2001; Lozano et al., 2000; Papa et al., 1999), as well as pathway-specific changes in striatal gene expression in patients and animals models of LID (Heiman et al., 2014; Jenner, 2008). Crucially, once LID develops, a given dose of levodopa relieves parkinsonism *and* produces dyskinesia, suggesting that distinct mechanisms may mediate these levodopa-evoked behaviors. If these behavioral effects were indeed mediated by discrete cell types, targeted therapies could be more effective than levodopa alone.

2.3 Results

To determine how dopamine depletion and replacement with levodopa affect striatal activity, we performed optogenetically labeled single-unit recordings in the dorsolateral striatum (DLS) of freely moving parkinsonian mice (Figures 1A-1D). To render mice parkinsonian, we injected the neurotoxin 6-hydroxydopamine (6-OHDA) in the left medial forebrain bundle (Figure S1A), causing a nearly complete depletion of ipsilateral dopamine (Figure S1B). As a result, parkinsonian mice showed reduced movement velocity and predominantly ipsilesional rotations. After six weeks, mice began daily levodopa injections in conjunction with recording sessions. A typical recording session consisted of a baseline (parkinsonian) period, followed by levodopa injection (5 mg/kg; Figure S1D), which caused both dyskinesia (LID; Figures 1E and S1C) and contralesional rotations (Figure 1F). Optogenetic labeling of dMSNs and iMSNs was achieved by expressing channelrhodopsin-2 (ChR2; Figure S1B) selectively in dMSNs or iMSNs (using D1-Cre or A2a-Cre mice, respectively)(Gerfen et al., 2013; Gong et al., 2007), and recording responses to light pulses at the end of each session. Following established protocols (Kravitz et al., 2013), we identified optogenetically labeled neurons as those with short latency light-evoked firing (Figure 1D).

Dopamine Depletion Reduces the Firing Rate of dMSNs

The standard model predicts that dopamine loss causes persistent decreases in dMSN and increases in iMSN firing. To determine whether chronic dopamine depletion causes opposing changes in MSN activity, we compared the firing rate of optogenetically labeled dMSNs and iMSNs in parkinsonian mice to those in healthy mice. As predicted, labeled dMSNs from parkinsonian mice fired at dramatically lower rates than in controls (Park: 0.11 ± 0.04 Hz, n=14, N=10; Ctrl: 1.61 ±

0.19 Hz, n=64, N=5, p<0.0001, Mann-Whitney; Figures 1G and S1E). Surprisingly, the average firing rate of iMSNs was not significantly increased in parkinsonian mice (Park: 1.24 ± 0.23 Hz, n=32, N=8; Ctrl: 1.42 ± 0.28 Hz, n=34, N=5, p=0.852, Mann-Whitney; Figures 1H, middle and S1F). This imbalance in dMSN and iMSN activity was also specific to the depleted hemisphere. While activity in the contralesional striatum was lower compared to healthy controls (Contra: 0.78 ± 0.14 Hz, n=88, N=5, p<0.0001, Mann-Whitney), as previously reported (Chen et al., 2001; Kish et al., 1999; Oye et al., 1970), we found that dMSNs (0.84 ± 0.23 Hz, n=5, N=2) and iMSNs (0.73 ± 0.18, n=5, N=2) had similar rates (p=0.99, Mann-Whitney, not shown). These results demonstrate that dopamine loss produces a marked and persistent reduction in ipsilesional dMSN firing, resulting in an imbalance between dMSN and iMSN activity.

Levodopa Causes Bidirectional Dysregulation of MSN Firing Rates During LID

By increasing striatal dopamine, levodopa is hypothesized to restore the normal balance of striatal activity via bidirectional modulation of dMSNs and iMSNs. In LID, amplification of this modulation may trigger involuntary movements. To test whether levodopa increases dMSN and decreases iMSN firing rates, we recorded optogenetically identified MSNs before and after levodopa administration in parkinsonian mice. As predicted by the standard model, levodopa increased dMSN firing rates (3.44 ± 0.93 Hz, n=9, N=6, p=0.004, Wilcoxon; Figures 1G and S1E) and decreased iMSN firing rates (0.38 ± 0.22 Hz, n=16, N=6, p<0.0001 Wilcoxon; Figures 1H and S1F). Furthermore, during LID, the average firing rate of dMSNs was more than double the rate in healthy controls (p=0.035, Mann-Whitney; Figures 1G, middle and S1E). Levodopa also decreased the firing rate of iMSNs below rates in healthy mice (p<0.0001, Mann-Whitney; Figures 1H, middle and S1F). These findings confirm that MSNs are in fact bidirectionally modulated by

levodopa, and further, that LID is associated with firing rates outside the normal range for both dMSNs and iMSNs.

We also found that the directionality of neural responses was extremely consistent: no dMSN was inhibited and no iMSN was excited by levodopa. Using this reliable response of optogenetically labeled MSNs, we classified unlabeled MSNs based on levodopa-evoked firing rate change. Units with a significant levodopa-evoked increase or decrease in firing rate were classified as putative dMSNs (On, n=146, N=15) or iMSNs (Off, n=69, N=15), respectively (Figure S1G, left and middle). Units with no significant change could not be classified (No Change, n=40, N=15; Figure S1G, right). In this larger pool, we found that putative MSNs showed similar firing rates to their optogenetically labeled counterparts (Figures S1H-S1K), providing further evidence that striatal activity is dysregulated in parkinsonism and LID.

Dopamine Receptor Specific Agonists Mimic the Effects of Levodopa

While these results point toward bidirectional dysregulation of dMSNs and iMSNs as an underlying feature of LID, levodopa-evoked dopamine release might directly *or* indirectly influence dMSN and iMSN firing through activation of D_1-like (D1R) and D_2-like (D2R) dopamine receptors located on several microcircuit elements (Gerfen and Surmeier, 2011). We sought to assess how selective activation of D1R or D2R compared to combined activation with levodopa. Remarkably, we found that administration of the selective D1R agonist SKF-81297 (SKF) also produced bidirectional regulation of striatal neurons, much like levodopa (On MSN: 0.10 ± 0.05 Hz (Park) vs 2.20 ± 0.39 Hz (SKF), n=23, N=5, $p<0.0001$, Wilcoxon; Off MSN: 0.93 ± 0.33 Hz (Park) vs 0.19 ± 0.08 Hz (SKF), n=9, N=5, $p=0.004$, Wilcoxon), while evoking robust dyskinesia and contralesional rotations (Figures S2A-S2E). Administration of the selective D2R

agonist Quinpirole (Quin) also produced bidirectional regulation of striatal neurons, albeit with more modest firing rate changes in activated neurons (On MSN: 0.18 ± 0.05 Hz (Park) vs 0.76 ± 0.10 Hz (Quin), n=19, N=6, p<0.0001, Wilcoxon; Off MSN: 1.22 ± 0.39 Hz (Park) vs 0.18 ± 0.05 Hz (Quin), n=12, N=6, p<0.0001, Wilcoxon), while evoking contralesional rotations and more modest dyskinesia (Figures S2F-S2J). Interestingly, each of these agonists modulated a similar proportion of striatal neurons compared to levodopa (Figure S2K), highlighting the effects of dopamine receptor activation on striatal microcircuitry through both direct regulation of MSNs *and* indirect modulation of synaptic (local inhibitory and/or excitatory extra-striatal) inputs.

Locomotor Modulation of dMSN and iMSN Firing Is Impaired in Parkinsonism and LID

As movement robustly modulates striatal activity (Barbera et al., 2016; Cui et al., 2013; Jin et al., 2014), we next sought to determine how locomotion affected the firing rate of MSNs in control and parkinsonian mice. In healthy controls, we found a positive correlation between velocity and firing rate for both dMSNs and iMSNs (Figures S1L-S1N, bottom). We quantified this locomotor modulation by averaging the firing rate of MSNs during mobile (velocity > 3 cm/s) and immobile (velocity < 0.5 cm/s) epochs. As expected, we observed higher firing rates during locomotion for both dMSNs and iMSNs in healthy controls (dMSNs (n=41, N=5), iMSNs (n=25, N=5), and all MSNs (n=67, N=10), p<0.0001, Wilcoxon; Figures S1L-S1N, top). MSNs recorded in the contralesional striatum of parkinsonian mice also retained this modulation, with higher firing rates during locomotion (n=88, N=5, p<0.0001, Wilcoxon; Figure S1L). However, in the ipsilesional striatum the firing rate of dMSNs was not modulated by locomotion (n=144, N=12, p=0.624, Wilcoxon), and iMSN firing rates were *lower* during locomotion (n=68, N=12, p=0.005, Wilcoxon; Figures S1M-S1N). Interestingly, though overall iMSN firing rates in parkinsonian

mice were not significantly different than in healthy controls (Figure 1H), iMSN firing rates were significantly higher specifically during epochs of immobility (Park: 1.71 ± 0.21 Hz vs Ctrl: 0.69 ± 0.15 Hz, $p<0.0001$, Mann-Whitney), but not locomotion (Park: 1.37 ± 0.23 Hz vs Ctrl: 1.55 ± 0.28 Hz, $p=0.313$, Mann-Whitney, Figure S1N). Levodopa administration caused robust changes in overall firing rate (Figure 1), but did not restore locomotor modulation: dMSNs showed no significant modulation ($p=0.181$, Wilcoxon) and iMSNs showed lower firing during locomotion ($p<0.0001$, Wilcoxon; Figures S1L-S1N). These data indicate that dopamine depletion persistently decreases dMSN firing, increases iMSN firing specifically during immobility, and further, that both dMSNs and iMSNs show reduced locomotor modulation, which is not restored by levodopa.

Activation of dMSNs Is Sufficient to Cause Dyskinesia, Which Is Potentiated by Chronic Levodopa Treatment

While the preceding experiments demonstrate that dMSNs exhibit high firing rates during LID, they do not prove whether dMSN activity is *sufficient* to cause dyskinesia. Using optogenetic stimulation of dMSNs in the DLS of healthy and parkinsonian mice, we tested whether dMSN activation causes dyskinesia (Figures 2A-2B). In parkinsonian D1-Cre mice injected with ChR2, we calibrated laser power to evoke firing rates similar to those seen during LID. Blue light at 1 mW elicited dMSN firing rates (3.98 ± 1.37 Hz, n=9, N=7) comparable to those seen in dMSNs during LID (4.61 ± 1.23 Hz; Figure 1G). Stimulation produced both dyskinesia and contralateral rotations, in the absence of levodopa (Figures 1D-1E and Movie S1). Light-evoked dyskinesia was time-locked to light and increased in severity at higher powers (Figures S3A-S3B). Interestingly, we observed similar dyskinesia and contralateral rotations when stimulating the non-depleted hemisphere (Figures S3C-S3D). Bilateral stimulation also produced dyskinesia and increased

movement velocity (Figures S3E-S3F). These results suggest that dopamine depletion may not be necessary for dMSN-mediated dyskinesia.

Indeed, it is widely debated how progressive dopamine depletion and chronic levodopa treatment independently influence the development of LID (Ahlskog and Muenter, 2001; Horstink et al., 1990). Dyskinesia is observed in advanced PD patients chronically treated with levodopa, making it difficult to disentangle their individual contributions. To determine how dopamine depletion and chronic levodopa treatment modulate dMSN-mediated movements, we compared the severity of dyskinesia and number of contralateral rotations with dMSN stimulation between three groups: levodopa-naïve and chronically levodopa-treated parkinsonian mice, and healthy mice. First, to look at whether dopamine depletion itself increased severity of dMSN-mediated dyskinesia, we compared parkinsonian and healthy mice, and found no significant difference in dyskinesia during optical stimulation (Park (N=8) vs Ctrl (N=12), p=0.881, Mann-Whitney; Figures 2D-2E, top). Second, to determine how chronic levodopa treatment altered dMSN-mediated dyskinesia, we compared parkinsonian mice (N=8) before (levodopa-naïve) and after chronic levodopa treatment to healthy mice (N=12). Chronically treated mice showed significantly more optically-evoked dyskinesia than both levodopa-naïve parkinsonian (p=0.001, Wilcoxon) and healthy (p=0.014, Mann-Whitney) mice (Figures 2D-2F, top). Contralateral rotations were not significantly different between groups (Figures 2D-2F, bottom), suggesting that levodopa exposure may enhance vulnerability to dyskinesia, as opposed to other motor effects. Together, these findings support the idea that chronic levodopa treatment, perhaps more than dopamine loss itself, primes basal ganglia circuitry for dMSN-mediated dyskinesia.

A Subpopulation of dMSNs Exhibit High Firing Rates Correlated to Dyskinesia

One prominent hypothesis in the field posits that over-activation of dMSNs underlies LID. Indeed, we observed heterogeneity in dMSN responses to levodopa, with only a subset of dMSNs exhibiting high firing rates (Figure 1G). To identify dMSNs with abnormally high levodopa-evoked firing rates, we compared the rates of putative dMSNs from parkinsonian mice to labeled MSNs from healthy mice. Putative dMSNs with levodopa-evoked firing rates within the 99% confidence interval of MSN firing rates from healthy mice were classified as Moderate FR (58%), while those exceeding this threshold were classified as High FR units (42%; Figure S4A). Moderate and High FR units were commonly observed on nearby electrodes and in the same session (Figures 3B and 3D). Moreover, High FR units were rarely observed in the subset of sessions in which levodopa did not elicit dyskinesia (3%, n=30, N=4). These results indicate dMSNs have a heterogeneous response to levodopa, with only a subset of dMSNs showing excessive activity.

If high firing dMSNs are causally involved in dyskinesia, their firing may be closely correlated to the severity or onset of dyskinesia. We tested this hypothesis by calculating the correlation between individual unit firing rates and dyskinesia, as well as levodopa-evoked rotations. Some dMSNs displayed strong correlations to dyskinesia but minimal correlation to rotations (DYSK, n=47, N=15; Figures 3A-3B), while others correlated to rotational behavior, and not dyskinesia (ROT, n=14, N=15; Figures 3C-3E). Other cells did not show a strong correlation to either behavior (ON, n=74, N=15; Figures 3E-3F). Remarkably, the activity of most High FR units correlated with dyskinesia (Figures 3B and 3G), while the activity of Moderate FR units rarely correlated with dyskinesia (Figures 3D, 3F, 3G and Movie S2). Conversely, we categorized units by their behavioral correlation and examined their parkinsonian and levodopa-evoked firing

rates. We found that all dMSN subpopulations showed similar firing rates following dopamine loss, which were all significantly lower than healthy controls (One-Way ANOVA $F(3,229)=27.33$, $p<0.0001$, Tukey post-hoc, Ctrl vs Park: $p<0.01$; Figure 3H). Interestingly, levodopa-evoked ON and ROT unit firing rates were not significantly different than those seen in healthy mice, while DYSK unit firing rates were significantly higher (One-Way ANOVA $F(3,229)=43.63$, $p<0.0001$, Tukey post-hoc, Ctrl vs LID: ON ($p>0.05$), ROT ($p>0.05$), and DYSK ($p<0.01$); Figure 3H). Additionally, we compared the relative onset of firing rate changes and dyskinesia in these dMSN subpopulations. We found that average DYSK unit firing significantly increased 31.6 ± 13.2 seconds prior to the onset and decreased 38.1 ± 18.4 seconds prior to end of LID (Figure 2I), with most DYSK units showing a firing change before the start (72%) and end (65%) of dyskinesia. In contrast, the firing rate of ROT and ON units showed no clear relationship to the start or end of dyskinesia (Figures S4B-S4C). Therefore, as their firing tends to precede dyskinesia onset and correlate with dyskinesia severity on a fine timescale, DYSK units are poised to influence the development of dyskinesia.

To determine if DYSK unit firing was *specific* to LID, we injected mice with two doses of levodopa in a single session: a moderate (dyskinetic) dose and a lower (sub-dyskinetic) dose of levodopa, which produced contralesional rotations, but no dyskinesia. We found that ROT and ON units were activated by levodopa in the absence of dyskinesia, showing a graded response to levodopa dosage (Figures 4A and 4C). Interestingly, we found that DYSK units were not modulated by lower (sub-dyskinetic) doses of levodopa (Park: 0.07 ± 0.05 Hz vs sub-dyskinetic: 0.35 ± 0.16 Hz, $n=8$, $N=3$, $p=0.078$, Wilcoxon), but robustly activated at moderate (dyskinetic) doses (LID: 5.03 ± 2.1 Hz, $p=0.008$, Wilcoxon; Figures 4B-4C and Movie S3). In addition, DYSK units showed little to no modulation during grooming, a qualitatively similar behavior which

involves many of the same body regions (0.24 ± 0.14 Hz vs LID: 6.27 ± 0.67 Hz, n=44, N=5, $p<0.0001$, Wilcoxon), while a subset of ON units was modulated by grooming (Figure 4D and Movie S4). In fact, as compared to ON units (n=30, N=4), DYSK units showed much lower firing rates during grooming (ON: 0.99 ± 0.34 Hz vs DYSK 0.24 ± 0.14 Hz, $p=0.003$, Mann-Whitney, Figure 4D), suggesting their firing properties are not solely the result of sensorimotor feedback. Together, these results demonstrate that DYSK unit firing is specific to the dyskinetic state, suggesting these dMSNs represent a distinct and stable subpopulation in parkinsonian animals.

2.4 Discussion

Here, we directly tested fundamental tenets of the standard model: (1) loss of dopamine reduces dMSN and increases iMSN firing rates, (2) levodopa bidirectionally modulates dMSNs and iMSNs, and (3) LID is associated with excessive dMSN activity. Using optogenetically labeled single-unit recordings in parkinsonian mice, we found that dopamine depletion markedly and persistently reduced dMSN firing rates compared to healthy controls, while iMSN firing was elevated only during periods of immobility. Levodopa evoked bidirectional modulation of MSNs beyond firing rates normally observed, with dramatically elevated levodopa-evoked firing rates in a subset of dMSNs. Consistent with a dMSN-mediated mechanism of LID, optogenetic stimulation of dMSNs was sufficient to trigger dyskinesia in healthy and parkinsonian mice, and was potentiated following chronic levodopa treatment. Finally, we found functional subdivisions within the direct pathway: levodopa elicited high firing rates in a subset of dMSNs, whose firing rates strongly correlated with dyskinesia severity, suggesting a subpopulation of dMSNs which may be causally involved in LID.

Though many investigators have posited that loss of dopaminergic input results in persistent elevation of iMSN firing, we observed elevated iMSN activity only when the animal was immobile. Most evidence for increased iMSN activity in parkinsonism is indirect, based on downstream basal ganglia nuclei (Bergman et al., 1994; Filion and Tremblay, 1991; Galvan et al., 2015; Soares et al., 2004) in restrained nonhuman primates. These nuclei, however, integrate striatal *and* extrastriatal inputs; the latter perhaps more important for shaping output (Deffains et al., 2016). In anesthetized parkinsonian rodents, one recent study of identified iMSNs found no change in firing rate (Ketzef et al., 2017), while an older study of putative iMSNs showed a very modest increase (0.5 spikes/s) in the firing rate (Mallet et al., 2006). Intrinsic excitability and

synaptic inputs may drive MSN firing differently under anesthesia than in an awake, behaving animal, accounting for these differences. Another study employing acute dopamine depletion in awake mice found increased firing in a subset of unidentified striatal neurons (Costa et al., 2006). While transient reduction of striatal dopamine might increase iMSN activity, changes following chronic dopamine loss, such as reduced intrinsic excitability (Fieblinger et al., 2014), may compensate for the loss of D_2-like receptor mediated inhibition. In support of the standard model, levodopa evoked pronounced bidirectional changes in striatal activity. Studies in ex vivo brain slices showing opposing changes in striatal intrinsic excitability and corticostriatal synaptic plasticity offer potential mechanisms for these findings (Fieblinger et al., 2014; Picconi et al., 2003; Shen et al., 2015). Notably, we found similar bidirectional changes in MSN firing using a selective D1R or D2R agonist in place of levodopa. As there are no D1Rs on iMSNs, nor D2Rs on dMSNs, this observation implies dopaminergic agents produce convergent changes in striatal firing through both intrinsic and synaptic mechanisms. In fact, a recent study combining a selective D2R agonist and chemogenetic manipulations of dMSNs highlights the interactions between the two pathways in modulating dyskinesia (Alcacer et al., 2017). Taken together, these results suggest that while elevated iMSN firing is not a static feature of parkinsonism, inhibition of iMSNs may still contribute to levodopa-evoked facilitation of movement.

By optogenetically activating dMSNs in the DLS of healthy and parkinsonian mice, we evoked dyskinesia in the absence of levodopa, which was potentiated following chronic levodopa treatment. These findings are in line with recent reports of manipulating dMSNs optically (Perez et al., 2017; Rothwell et al., 2015) and chemogenetically (Alcacer et al., 2017) to evoke dyskinesia in mice. Notably, stimulation of dMSNs in the dorsomedial striatum (in contrast to the DLS) relieves parkinsonism without inducing dyskinesia (Kravitz et al., 2010). This difference

underscores the functional heterogeneity of dMSNs within dorsal striatum; thus highlighting the DLS as a candidate locus for dyskinesia, as suggested by pharmacological studies (Carta et al., 2006; Yoshida,1991). Given the increased intrinsic excitability observed in brain slices from parkinsonian mice (Fieblinger et al., 2014), we expected an increase in optically evoked dyskinesia compared to healthy controls. However, homeostatic mechanisms in striatal synaptic transmission or intrinsic excitability of downstream basal ganglia nuclei may compensate for enhanced dMSN excitability.

Our recordings of dMSNs within the DLS also showed heterogeneity in levodopa responses, which has been suggested by recordings of unidentified striatal neurons in parkinsonian primates (Liang et al., 2008). We found that levodopa evoked normal firing rates in some dMSNs and elevated rates in others. The firing rate of these latter neurons also strongly correlated with dyskinesia severity on a fine timescale and was specific for dyskinesia compared to other levodopa-evoked and spontaneous behaviors (ie. grooming). Levodopa produces both relief of parkinsonism *and* dyskinesia. Our results suggest a possible mechanism: restoration of normal firing rates in a subset of dMSNs may mediate therapeutic effects, and excessive firing in another subset may mediate dyskinesia. While additional experiments will be necessary to firmly establish causal relationships between dMSN subtypes and dyskinesia, these findings highlight the functional diversity of dMSNs in LID. If these MSN subtypes represent distinct cell populations, by virtue of molecular markers or connectivity, they offer a potential therapeutic target in LID.

2.5 Experimental Procedures

Animals

Hemizygous BAC transgenic mice expressing Cre recombinase under the control of the Drd1a (D1-Cre, GENSAT BAC transgenic EY217) or Adora2a (A2a-Cre, GENSAT BAC transgenic KG139) regulatory elements were used to restrict expression of Cre-dependent constructs to direct and indirect pathway striatal neurons, respectively. All mice were on a C57Bl/6 background and housed under a 12-h light/dark cycle with food and water *ad libitum*. Male and female mice were used. All experiments were conducted with the approval of the Institutional Animal Care and Use Committee at the University of California, San Francisco and complied with local and national ethical and legal regulations regarding the use of mice in research.

Unilateral 6-OHDA Model

Six- to ten-week-old mice were anesthetized with a combination of intraperitoneal (i.p.) ketamine/xylazine (40/10 mg/kg) for induction and inhaled isoflurane (1%) for maintenance of anesthesia. In the stereotaxic frame (Kopf Instruments), the scalp was opened and a hole drilled through the skull over the medial forebrain bundle (MFB). After puncturing the dura, 1 μL of 6-hydroxydopamine (6-OHDA; Sigma-Aldrich, 5 μg/μL in normal saline) was injected unilaterally into the left MFB at the following coordinates relative to bregma and cortical surface: AP -1.0, ML -1.0, DV -4.9, through a 33 gauge cannula (Plastics One) and syringe pump (Harvard Apparatus). To minimize uptake of the toxin by noradrenergic and serotonergic axons, desipramine (Sigman-Aldrich, 25 mg/kg i.p.) was administered immediately prior to surgery. Post-operatively, mice were monitored daily and supplemented with saline injections and high-fat diet as needed (Francardo et al., 2011). Ipsilesional rotations were quantified in open-field using video

tracking (Noldus Ethovision) periodically over two weeks to verify dopaminergic lesion and hemiparkinsonism.

Virus Injections and Implants

DIO constructs were used to express ChR2-eYFP or eYFP alone specifically in Cre-positive cells. For *in vivo* electrophysiology experiments, 6-OHDA-treated D1-Cre and A2a-Cre mice were anesthetized, the scalp reopened, and a large craniectomy (1.5 x 1 mm) made over the left dorsolateral striatum (DLS). 1.5 μL of AAV5-EF1a-DIO-hChR2(H134R)-eYFP-wpre-hGH (UPenn Vector Core, 1:1 dilution in normal saline) was injected into the ipsilesional DLS (AP +0.8, ML -2.3, DV -2.5 from cortical surface), using a 33 gauge cannula and syringe pump. Three additional holes were drilled for two skull screws (FST) and a ground wire. A fixed multichannel optrode (32-channel microwire (35 μm tungsten) array (Innovative Neurophysiology) coupled to a 200 μm optical fiber (Thorlabs)) was slowly inserted through the craniectomy into the DLS to a final depth 100-200 μm above the viral injection. A thin layer of dental cement (Metabond, Parkell) was applied to the surface of the skull and dental acrylic (Ortho-Jet, Lang Dental) was applied to cover all exposed hardware. The same procedures were followed for *in vivo* electrophysiology experiments in the right (contralesional) DLS (AP +0.8, ML +2.3, DV -2.5 from cortical surface) of 6-OHDA-treated D1-Cre and A2a-Cre mice.

For direct pathway stimulation experiments, D1-Cre mice were anesthetized, the scalp exposed, and small holes drilled bilaterally above the DLS. 1 μL of DIO-ChR2-eYFP virus (1:1 dilution as above) or AAV5-EF1a-DIO-eYFP (UNC Vector Core) was injected bilaterally into the DLS (AP +0.8, ML ±2.3, DV -2.5 from cortical surface) of healthy or 6-OHDA treated mice (4-6 weeks after 6-OHDA injection). Optic fiber-ferrule assemblies (200 μm, Thorlabs) were implanted

bilaterally 100-200 μm above each viral injection. Dental cement was applied to the scalp and the base of exposed ferrules was covered with dental acrylic. To allow for adequate expression, mice were housed for at least two weeks following viral injections before any electrophysiology or behavioral experiments began.

Behavior

Animals were acclimated to the open field (25 cm diameter acrylic cylinder, Tap Plastics) for 1-2 sessions prior to experiments. Gross movement (velocity, rotations) was measured using a top-mounted video camera and video tracking software (Noldus Ethovision). Ipsilesional and contralesional rotations were identified using a Noldus Ethovision analysis module, with a rotation threshold of 90° and a minimum distance traveled of 2 cm. Dyskinesia was quantified using the Abnormal Involuntary Movement score (AIMs), an established method of scoring levodopa-induced dyskinesia (Cenci and Lundblad, 2007). The start and end of dyskinesia were scored in 2 second bins and defined as the first and last observable dyskinetic movement (of any body segment), respectively. For optical stimulation experiments (described below in the Optogenetic Stimulation section), two mice were run at a time, gross movement measured using video tracking, and dyskinesia manually scored by raters blinded to the viral injection.

Pharmacology

Levodopa (Sigma Aldrich), in combination with benserazide (Sigma Aldrich), was dissolved in normal saline and administered daily (5 days per week) by i.p. injection. A dose of 2.5-5.0 mg/kg of levodopa (plus 1.25-2.5 mg/kg benzeraside) typically elicited dyskinetic movements and contralesional rotations. Lower doses of levodopa (0.5-2.5 mg/kg) were administered in some sessions to elicit therapeutic behavioral responses (defined as increased contralateral rotations)

without dyskinesia (sub-dyskinetic dose; Figure 4). The D1R-selective agonist SKF-81297 or the D2R-selective agonist Quinipriole (Tocris Bioscience) were administered in place of levodopa in interleaved sessions. SKF-81297 (3-5 mg/kg) and Quinpirole (0.5-2 mg/kg) were dissolved in normal saline and injected i.p., eliciting both dyskinesia and contralesional rotations (Figure S2).

In Vivo Electrophysiology

During each recording session, the animal was placed in the open-field while tethered via a lightweight, multiplexed headstage cable (Triangle Biosystems) attached to a low-torque electrical commutator (Dragonfly) to allow free movement. The animal's gross behavior was recorded by video tracking software (Noldus Ethovision). Fine behavior was manually scored by the experimenter (AIM score). Behavioral measurements were synchronized with simultaneous electrophysiological recordings via TTL pulses triggered by the video tracking software and recorded by the electrophysiology system (MAP system, Plexon). Animals were habituated to tethering and i.p. injections (saline) prior to pharmacological experiments.

In parkinsonian animals, a typical recording session consisted of a 30 minute baseline period during which animals displayed ipsilesional biased rotations, followed by i.p. injection of levodopa (Figure S1D). Contralesional rotations and levodopa-induced dyskinesia (LID) typically began within 10 minutes of injection, lasted between 30-120 minutes and terminated spontaneously. At the end of each session, once the animal had returned to baseline behavior, a fiber optic patch cable was connected to the animal's implant and the optogenetic labeling protocol commenced (see Optogenetic Labeling section below). Optogenetically labeled cells from healthy (control) mice were collected as part of another study, and a 30-minute baseline period from these recordings was used for comparison with parkinsonian recordings performed using the same techniques. Optogenetically labeled and unlabeled cells from the contralesional striatum of parkinsonian mice

were also collected during an equivalent 30-minute baseline period in which animals displayed ipsilesional biased rotations, performed using the same techniques.

In a subset of recordings, parkinsonian mice were administered an additional i.p. injection of levodopa at a sub-dyskinetic dose during a single session (Figure 4). In these experiments, the first injection of levodopa (dyskinetic or sub-dyskinetic dose was randomly chosen) occurred after the 30-minute baseline period as described above. After the animal had returned to baseline parkinsonian behavior, the second injection of levodopa was administered. Once the behavior again returned to baseline, the optogenetic labeling protocol was initiated.

Signal acquisition

Single unit activity from microwires was recorded using a 32-channel recording system (MAP system, Plexon). Spike waveforms were filtered at 154–8800 Hz and digitized at 40 kHz. The experimenter manually set a threshold for storage of electrical events.

Spike Sorting and Cell Classification

Single units (SUs) were identified offline by manual sorting into clusters (Offline Sorter, Plexon). Waveform features used for separating units were typically a combination of valley amplitude, the first three principal components (PCs), and/or nonlinear energy. Clusters were classified as SUs if they fulfilled the following criteria: (1) <1% of spikes occurred within the refractory period and (2) the cluster was statistically different ($p<0.05$, MANOVA using the aforementioned features) from the multi- and other single-unit clusters on the same wire. SUs were then classified as putative medium spiny neurons (MSNs) as previously described (Berke et al., 2004; Gage et al., 2010; Harris et al., 2000) using features of the spike waveform (peak to valley and peak width), as well as inter-spike interval distribution. Only putative MSNs were included in subsequent analyses.

Optogenetic Labeling

TTL-controlled blue laser (493 nm; Shanghai Laser and Optics Century) pulses were delivered to the optrode array via a fiber optic patch cable (200 μm; Thorlabs) connected to an optical commutator (Doric Lenses). A series of brief light pulses (1000 pulses, 150 sec duration, 1 Hz) were delivered at varying light intensities (0.5, 1, 2, and 4 mW light power at the tip of the fiber optic patch cable). Light intensity was measured daily with a light meter (Thorlabs) and calibrated for each light power. To determine if a putative MSN was optogenetically labeled, a peristimulus time histogram, aligned to laser onset, was constructed (Figure 1D). A SU was considered optogenetically labeled if it fulfilled the following criteria: (1) firing rate increased above the 95% confidence interval of pre-laser firing rate within 15 msec of laser onset, (2) firing rate remained above this threshold for at least 15 msec, and (3) laser-evoked waveforms were not different than spontaneous waveforms (correlation coefficient (R^2) > 0.9).

Optogenetic Stimulation

TTL-controlled blue laser light (473 nm; Shanghai Laser and Optics Century) was delivered to fiber-ferrule assembly via a fiber optic patch cable (200 μm; Thorlabs) connected to a dual-output optical commutator (Doric Lenses). Behavior (rotations and AIM score) was recorded over the course of a single session, which consisted of the following: a two minute baseline period with no laser illumination, then four trials of laser stimulation, followed by a two minute post-stimulation period (Figure 2C). Each trial consisted of a 30 sec laser on (constant illumination) and 30 sec laser off epoch (Figure 2C, Laser). Light intensity was measured daily and calibrated for 0.5, 1, 2, and 4 mW light powers at the tip of the fiber optic patch cable. Stimulation experiments were

conducted at each of the above-mentioned light powers and were fixed for a given session. 6-OHDA treated mice received optogenetic stimulation both in the levodopa-naive state and again after chronic levodopa treatment (levodopa/benzeraside (10/5 mg/kg i.p.) daily for 2 weeks). Treatment was withheld on the day of optogenetic stimulation experiments.

Tissue Processing and Immunohistochemistry

Mice were terminally anesthetized with ketamine/xylazine (200/40 mg/kg i.p.), transcardially perfused with 4% paraformaldyde (PFA), and the brain dissected from the skull. The brain was post-fixed overnight in 4% PFA and then placed in 30% sucrose at 4°C. Using a freezing microtome (Leica), the brain was sliced into 30 μm coronal sections. In 6-OHDA treated mice, the extent of dopamine depletion was confirmed by TH immunohistochemistry, using standard protocols. Briefly, after washing sections in PBS (5 x 10 minutes) and blocking in normal donkey serum (NDS)/0.1% Triton-X (1 hour at room temperature, RT), we incubated sections in primary antibody (Pel-Freez rabbit anti-TH, 1:1000 at 4°C overnight). Adequate expression of viral DIO constructs (ChR2-YFP and YFP) was also verified. Briefly, sections were washed in PBS, incubated in fluorescently labeled secondary antibody (donkey anti-rabbit 647 nm, Jackson Immunoresearch; 1:500 in NDS at RT for 2 hours), and washed in PBS prior to mounting onto glass slides (Vectashield Mounting Medium). Sections were imaged in the YFP/GFP (excitation 488 nm, emission 509 nm) and Cy5 (excitation 650 nm, emission 684 nm) channels, verifying striatal ChR2-YFP or YFP-control expression and ipsilesional TH depletion. Only animals with >90% dopamine depletion were included in this study (Figure S1B). Stitched multi-channel fluorescence images were taken on a Nikon 6D conventional wide-field microscope at 4-10X, using custom software (UCSF Nikon Imaging Center). To verify the location of the optrode array

in the DLS, under deep terminal anesthesia prior to transcardial perfusion, electrolytic lesions were made to mark electrode tips using a solid state, direct current Lesion Maker (Ugo Basile), by applying 100 μA for 5 sec per microwire. For optogenetic stimulation experiments, optic fiber placement in the DLS was verified by the location of tissue deformation made by the ferrule.

Quantification and Statistical Analysis

Behavior

Dyskinesia was quantified using the Abnormal Involuntary Movement score (AIMs) (Cenci and Lundblad, 2007). Briefly, abnormal axial, limb, and orolingual movements were scored manually by the experimenter for one minute every other minute for the total length of a dyskinetic episode (ranging from 30-120 minutes). The AIM scale ranges from 0 to 4 for each body segment, defined as follows for a given one minute observation period: a score of 0 represents normal movement, 1 represents abnormal movement for <50% of the time, 2 represents abnormal movement for >50% of the time, 3 represents abnormal movement for the entire period, but can be interrupted (for example, by tapping the chamber wall), and 4 represents uninterruptible, continuous abnormal movement. Total AIM score is the sum of AIM scores for the three body segments (axial, limb, orofacial; maximum score of 12).

Gross movement was quantified using several metrics. Rotation rate was calculated per minute by subtracting total ipsilesional from contralesional rotations. Locomotor activity was also quantified to identify discrete locomotor states, where we divided the behavioral session (using 2 second bins) into immobile (velocity < 0.5 cm/s) or mobile (velocity > 3 cm/s) epochs. For a more continuous measure, velocity was also quantified throughout the behavioral session (using 1

second bins). Grooming epochs were manually identified post-hoc from video of recorded behavioral sessions (using a 2 second minimum duration for classification).

In Vivo Electrophysiology

For the majority of experiments, firing rate was averaged in 1 minute bins. Modulation of firing rate by levodopa (or dopamine agonists) was determined by comparing single unit (SU) firing rates before and after drug administration, during the peak behavioral effects. The 30-minute baseline period was compared to a 30-minute period following drug injection (10-40 minutes post-injection). Following levodopa administration, unlabeled SUs were categorized into three broad groups as follows, based on significant changes in firing rate ($p<0.01$, Wilcoxon rank-sum test (denoted Mann-Whitney)) following levodopa treatment: putative dMSNs (increase in firing rate), putative iMSNs (decrease in firing rate), or no change units (nonsignificant change in firing rate). Following agonist administration, the same analysis was used to identify SUs with significant increases (On MSNs), decreases (Off MSNs), or no change in firing rate (NC). For levodopa sessions, putative dMSNs were further divided using rate-based and behavior-based methods.

For the rate-based method, we compared SU firing rates of putative dMSNs from parkinsonian mice after levodopa injection to the firing rates of healthy mice. We calculated the 99% confidence interval of firing rate for all SUs recorded in healthy mice and used the upper bound of this interval as our threshold. A putative dMSN was classified as High FR if the post-levodopa firing rate (10-40 minutes post-injection of levodopa) exceeded the 99% confidence interval of MSNs from healthy mice in any single bin. A putative dMSN with a post-levodopa firing rate within the 99% confidence interval of healthy mice was classified as a Mod FR unit (Figure 3G). For the behavior-based method, rotation rate and AIM score were also averaged in 1 minute bins and correlated with firing rate using linear regression. Putative dMSNs with a

significant correlation (R^2>0.4) to rotation rate were labeled rotation (ROT) units, those with a significant correlation to AIM score were labeled dyskinesia (DYSK) units, and those with no significant correlation (R^2<0.4) to either behavior were classified as on-unclassified (ON) units (Figures 3A-3F). Putative dMSNs with firing rates correlated to both dyskinesia and rotation rate were labeled MIXED (Figure 3E).

To determine the timing of firing rate change relative to dyskinesia, firing rates of putative dMSN subpopulations (ON, ROT, DYSK) were averaged in 2 second bins and aligned to the start and end of visible dyskinesia (Figures 3I and Figures S4B-S4C). The onset of levodopa-evoked firing rate change was calculated as the *first* of two consecutive bins in which the firing rate exceeded the 99% confidence interval of the pre-dyskinesia baseline period. The offset of levodopa-evoked firing rate change was calculated as the *last* of two consecutive bins in which the firing rate exceeded the 99% confidence interval of post-dyskinesia baseline period. The pre-dyskinesia baseline was defined using the firing rate 150-200 seconds prior to the onset of dyskinesia. The post-dyskinesia baseline was defined using the firing rate 150-200 seconds following the end of dyskinesia. We then calculated the time difference between onset/offset of levodopa-evoked firing rate change and the start/end of dyskinesia to identify the latency and proportion of units whose firing rate change preceded the change in dyskinesia.

Using defined locomotor and grooming epochs (see the Behavior section above), we calculated the average firing rate of putative dMSNs during immobile and mobile bouts (Figures S1L-S1N, top), as well as during grooming (Figure 4D). For a more continuous analysis of locomotion, we also correlated firing rate to instantaneous velocity (using 1 second bins) in increments of 1 cm/s. Given the differences in baseline firing rates between groups, we normalized

the firing rates of all MSNs, dMSNs, and iMSNs (Figures S1L-S1N, bottom) to their respective group average firing rate for the 0-1 cm/s velocity bin.

Firing rates recorded in the ipsilesional striatum of parkinsonian mice before (Park) or after (LID) levodopa were compared to recordings from healthy mice (Ctrl, Figures 1G-1H and S1L-S1M) and the contralesional striatum of parkinsonian mice (Contra, Figures S1L-S1M) using Mann-Whitney tests. Firing rates of parkinsonian mice before (Park) and after drug administration (levodopa (LID), Figure 1G-1H; SKF-81297 (SKF) or Quinpirole (Quin), Figure S2E, S2J) were compared using Wilcoxon signed-rank test (denoted Wilcoxon). Comparisons of firing rates between putative dMSN subtypes (ON, ROT, DYSK) and MSNs in healthy controls were made using a One-Way ANOVA with Tukey post-hoc test (Figure 3H). For experiments involving two doses of levodopa, firing rates between parkinsonian, sub-dyskinetic dose, and dyskinetic dose conditions were compared using Wilcoxon tests (Figure 4C).

Optogenetic Stimulation

Comparisons of rotation rate and AIM score (Figures 2D-2F) between healthy and parkinsonian mice (LD-naive or LD-treated) were conducted using a Mann-Whitney test. Comparisons within parkinsonian mice (between LD-naive and LD-treated conditions) were conducted using a Wilcoxon test.

2.6 Author Contributions and Acknowledgements

MBR and ABN designed the experiments. MBR conducted the electrophysiological recordings and analysis. MBR, ABN, and CBM conducted optogenetic stimulation experiments. MBR and ABN wrote the manuscript.

2.7 Figures

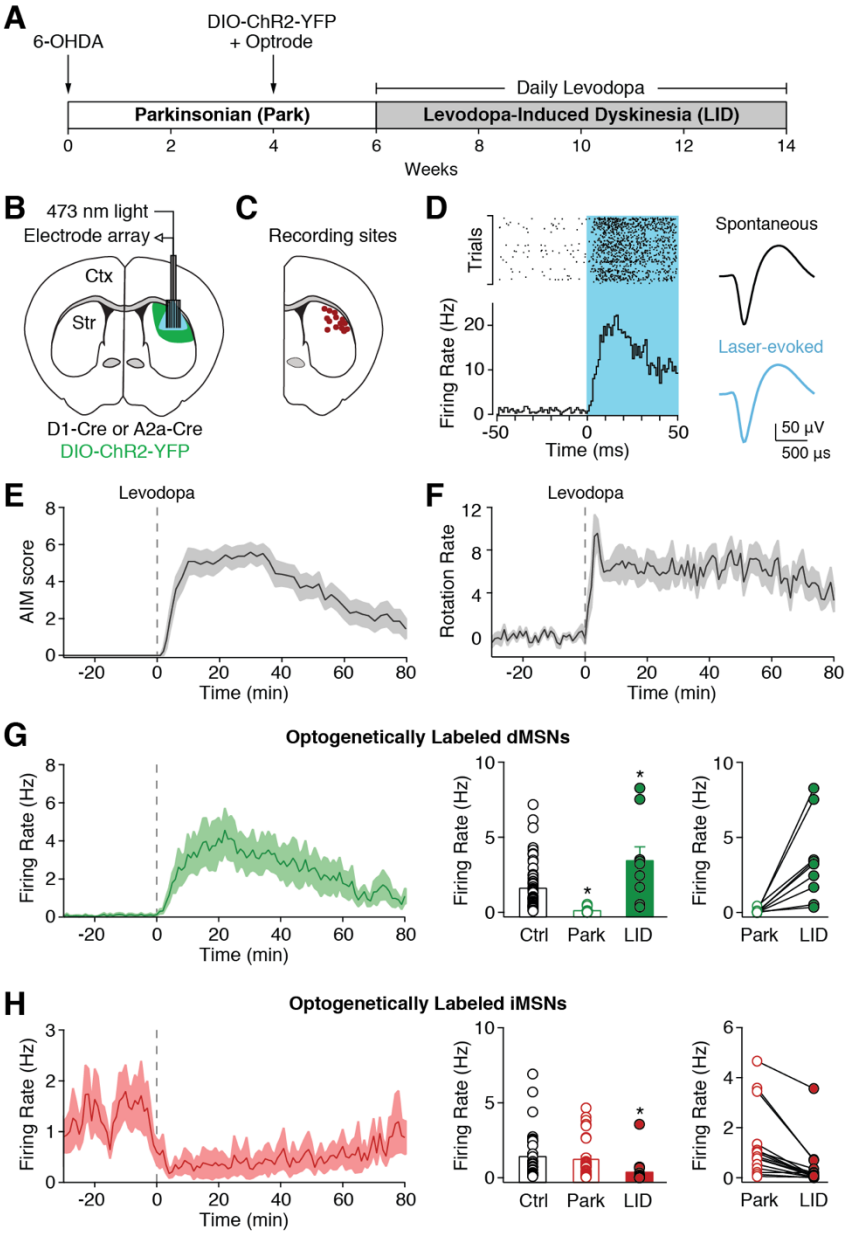
A
6-OHDA
DIO-ChR2-YFP
+ Optrode
Daily Levodopa
Parkinsonian (Park)
Levodopa-Induced Dyskinesia (LID)
0
2
4
6
8
10
12
14
Weeks
B
473 nm light
Electrode array
Ctx
Str
D1-Cre or A2a-Cre
DIO-ChR2-YFP
C
Recording sites
D
Trials
Firing Rate (Hz)
Time (ms)
Spontaneous
Laser-evoked
50 µV
500 µs
E
Levodopa
AIM score
Time (min)
F
Levodopa
Rotation Rate
Time (min)
G
Optogenetically Labeled dMSNs
Firing Rate (Hz)
Time (min)
Ctrl
Park
LID
H
Optogenetically Labeled iMSNs
Firing Rate (Hz)
Time (min)
Ctrl
Park
LID

2.1 Figure 1. Alterations in Identified Striatal Neurons Following Dopamine Depletion and Replacement with Levodopa.

(A) Experimental timeline. **(B)** Schematic of optrode in dorsolateral striatum (DLS). **(C)** Recording sites verified by electrolytic lesions. **(D)** Example of optogenetically labeled striatal direct pathway neuron (dMSN). Left: PSTH and peri-event raster aligned to laser onset. Right: average spontaneous and laser-evoked waveforms. **(E-H)** Levodopa was administered at t=0 (dotted line). **(E)** Average dyskinesia, as measured by the Abnormal Involuntary Movement (AIM) score (N=12). **(F)** Average rotations (contralesional-ipsilesional) per minute (N=12). **(G)** Left: average firing rate of optogenetically labeled dMSNs. Middle: dMSN firing rates in healthy mice (Ctrl, n=64, N=5) and parkinsonian mice before (Park, n=14, N=10) and after (LID, n=9, N=6) levodopa injection. Right: firing rate of individual dMSNs before and after levodopa. **(H)** Left: average firing rate of optogenetically labeled striatal indirect pathway neurons (iMSNs). Middle: iMSN firing rates in healthy mice (Ctrl, n=34, N=5) and parkinsonian mice before (Park, n=32, N=8) and after (LID, n=16, N=6) levodopa injection. Right: firing rate of individual iMSNs before and after levodopa. n=cells, N=animals. *$p<0.05$ vs Ctrl. All data presented as mean ± SEM. See also Figures S1 and S2.

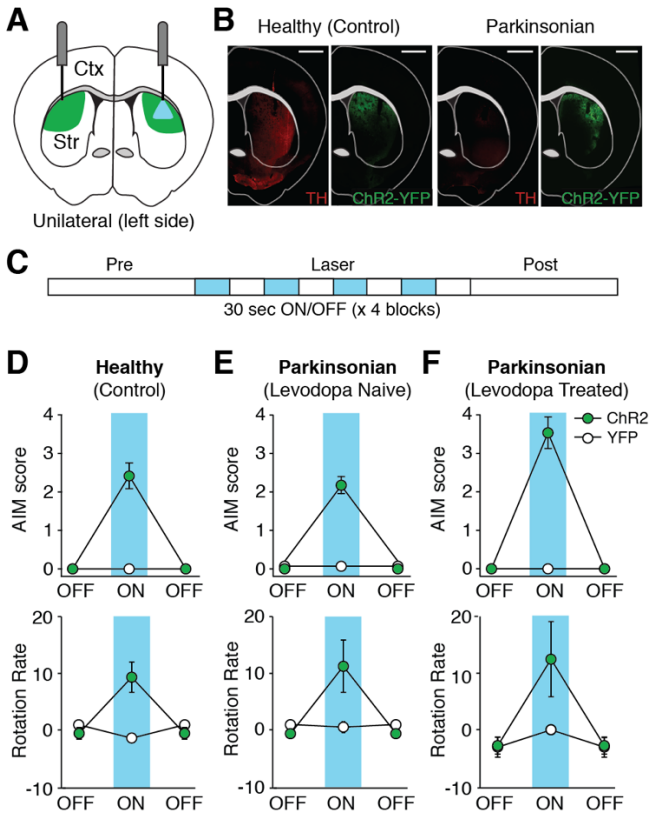

2.2 Figure 2. Optogenetic Activation of dMSNs Produces Dyskinesia in Healthy and Parkinsonian Mice

(A) Schematic showing optic fiber placement and laser stimulation in the left (ipsilesional) DLS of parkinsonian mice. Green = DIO-ChR2-YFP expression. **(B)** Representative coronal sections from healthy and parkinsonian D1-Cre mice showing tyrosine hydroxylase (TH) staining and DIO-ChR2-YFP expression. Scale bar = 1mm. **(C)** Experimental timeline. **(D-F)** Behavior before (OFF) and during (ON) dMSN stimulation. Top: average dyskinesia (AIM) score. Bottom: average rotation rate. **(D)** Healthy mice (ChR2: N=12, YFP: N=11). **(E-F)** Parkinsonian mice (ChR2: N=8, YFP: N=4) **(E)** before levodopa exposure and **(F)** after 2 weeks of chronic levodopa. N=animals. All data presented as mean ± SEM. See also Figure S3 and Movie S1.

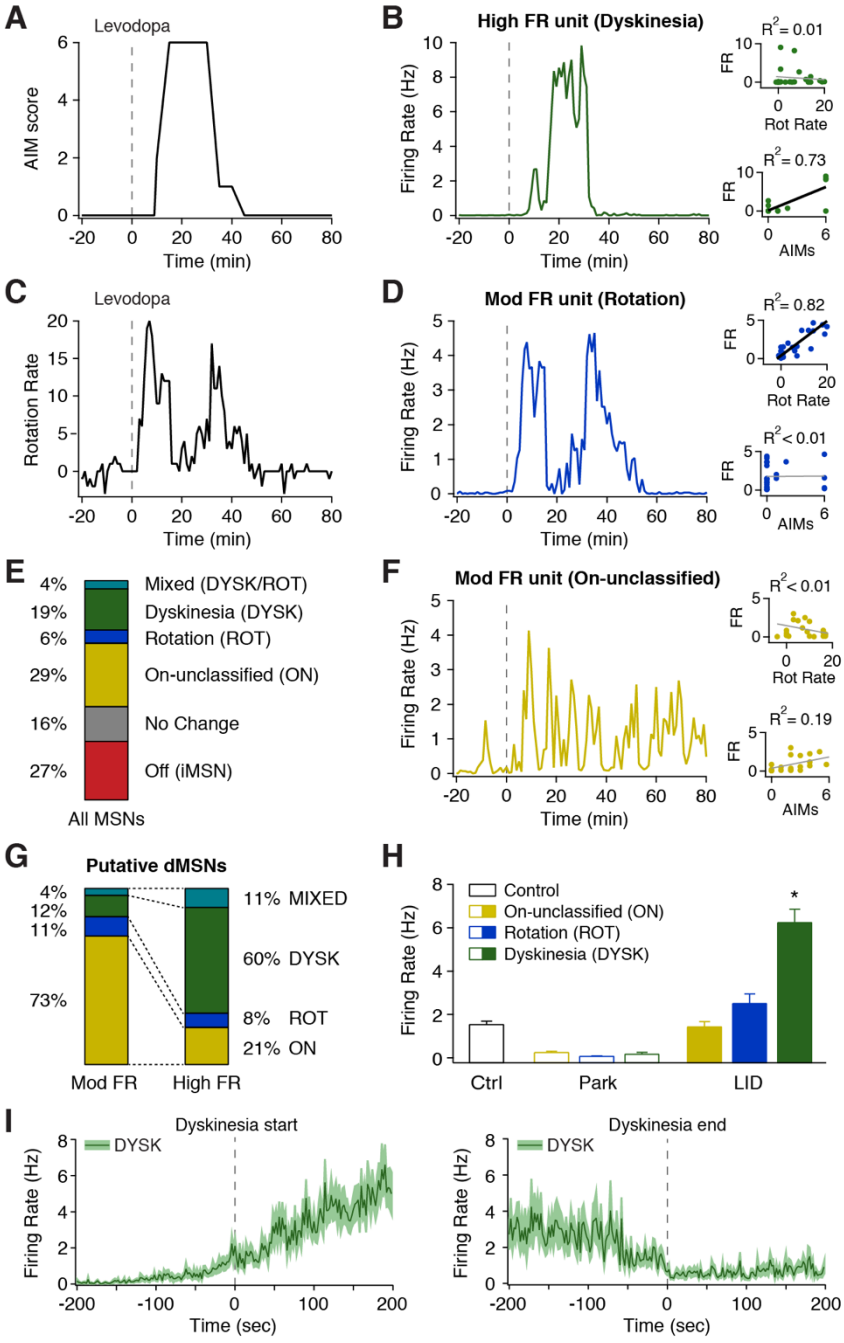
A
Levodopa
AIM score
Time (min)
B
High FR unit (Dyskinesia)
Firing Rate (Hz)
Time (min)
R2 = 0.01
FR
Rot Rate
R2 = 0.73
AIMs
C
Levodopa
Rotation Rate
Time (min)
D
Mod FR unit (Rotation)
Firing Rate (Hz)
Time (min)
R2 = 0.82
Rot Rate
R2 < 0.01
AIMs
E
4% Mixed (DYSK/ROT)
19% Dyskinesia (DYSK)
6% Rotation (ROT)
29% On-unclassified (ON)
16% No Change
27% Off (iMSN)
All MSNs
F
Mod FR unit (On-unclassified)
Firing Rate (Hz)
Time (min)
R2 < 0.01
Rot Rate
R2 = 0.19
AIMs
G
Putative dMSNs
4%
12%
11%
73%
11% MIXED
60% DYSK
8% ROT
21% ON
Mod FR
High FR
H
Control
On-unclassified (ON)
Rotation (ROT)
Dyskinesia (DYSK)
Firing Rate (Hz)
Ctrl
Park
LID
I
Dyskinesia start
DYSK
Firing Rate (Hz)
Time (sec)
Dyskinesia end
DYSK
Firing Rate (Hz)
Time (sec)

2.3 Figure 3. A Subpopulation of dMSNs Show High Firing Rates Correlated to Dyskinesia

(A-D) Behavior and single unit firing rates from a representative session. **(A)** Dyskinesia score. **(B)** Representative putative dMSN classified as High FR whose firing rate was correlated with dyskinesia score (DYSK). **(C)** Rotation rate. **(D)** Representative putative dMSN classified as Mod FR whose firing rate was correlated with rotation rate (ROT). **(E)** Fraction of all putative MSNs (n=255, N=15) classified by behavioral correlation. **(F)** Representative putative dMSN classified as Norm FR whose firing rate was uncorrelated with rotation rate or AIM score (ON). **(B,D,F)** Insets: correlation between firing rate and rotation rate (top) and dyskinesia (bottom). **(G)** Fraction of putative dMSNs classified by rate and their correlation to behavior (n=146, N=15). **(H)** Average firing rate of putative dMSNs based on correlation to behavior, before (Park) and after (LID) levodopa injection, compared to MSNs from healthy (Ctrl) mice. Ctrl: n=98, N=10; ON: n=74, ROT: n=14, DYSK: n=47, N=15. *$p<0.05$ vs Ctrl. **(I)** Average firing rate of DYSK units aligned to dyskinesia start (left, n=43) and end (right, n=37, N=15). n=cells, N=animals. All data presented as mean ± SEM. See also Figure S4 and Movie S2.

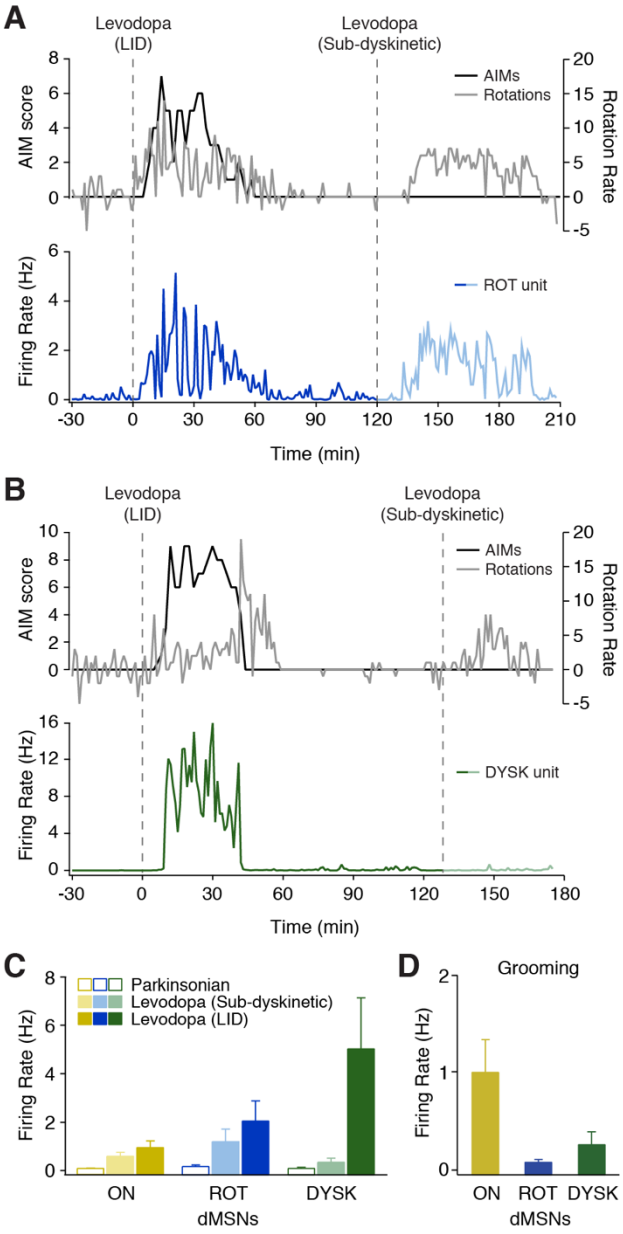

2.4 Figure 4. Dyskinesia Unit Activity is Specific to LID

(A-B) Two doses of levodopa were administered in a single session. Top: dyskinesia score (black) and rotation rate (gray). Bottom: unit firing rate, aligned to levodopa injection (dotted line). Representative **(A)** ROT unit and **(B)** DYSK unit**. (C)** Average firing rate of putative dMSN subtypes before (parkinsonian) and after dyskinetic and sub-dyskinetic doses of levodopa. ON: n=14, N=4; ROT: n=8, N=3; DYSK: n=8, N=3. **(D)** Average firing rate of putative dMSN subtypes during grooming (ON: n=30, N=4; ROT: n=5, N=2; DYSK: n=44, N=5). n=cells, N=animals. All data presented as mean ± SEM. See also Movie S3 and S4.

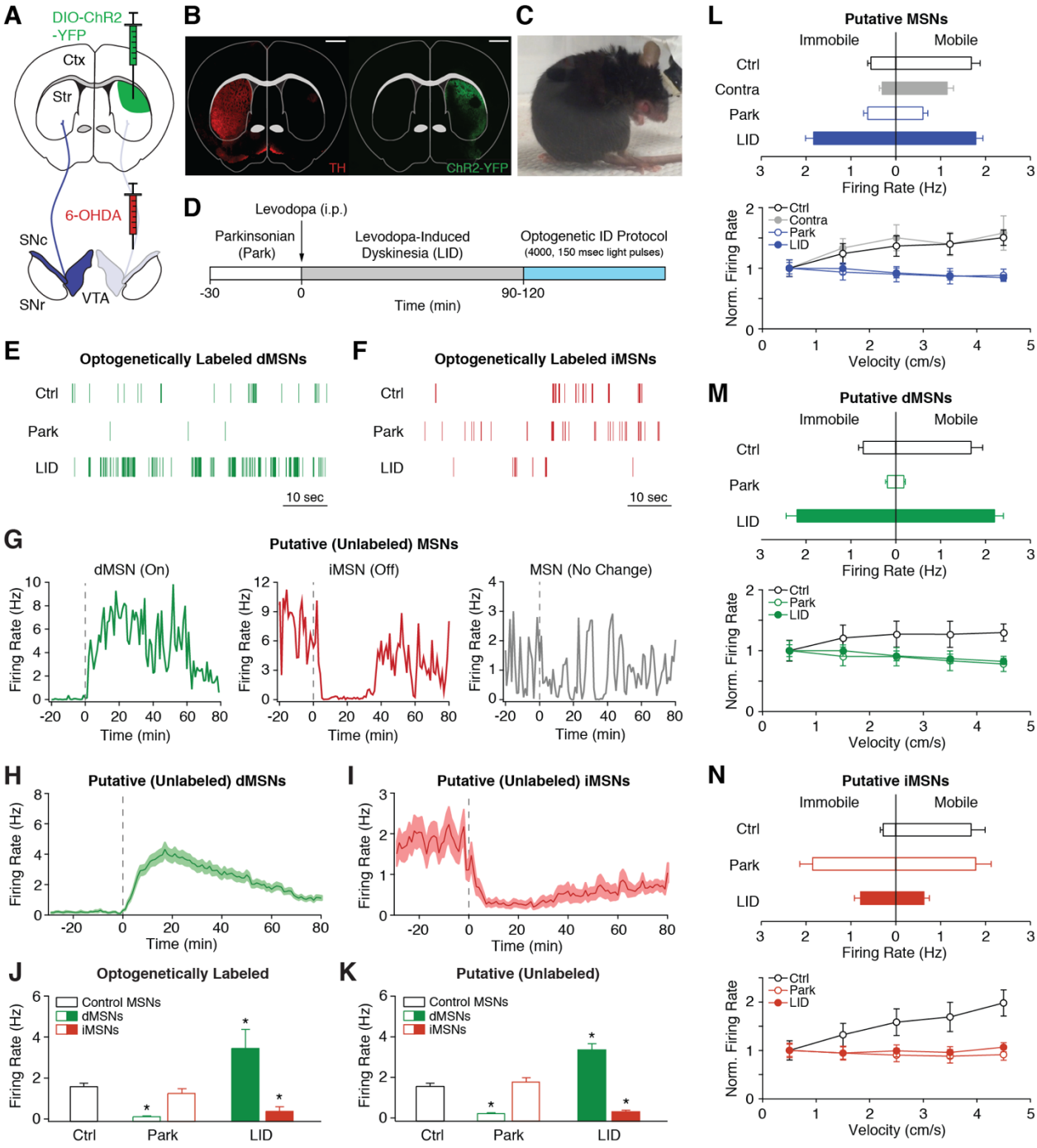
A
DIO-ChR2
-YFP
Ctx
Str
6-OHDA
SNc
SNr
VTA
B
TH
ChR2-YFP
C
D
Levodopa (i.p.)
Parkinsonian
(Park)
Levodopa-Induced
Dyskinesia (LID)
Optogenetic ID Protocol
(4000, 150 msec light pulses)
-30
0
90-120
Time (min)
E
Optogenetically Labeled dMSNs
Ctrl
Park
LID
10 sec
F
Optogenetically Labeled iMSNs
Ctrl
Park
LID
10 sec
G
Putative (Unlabeled) MSNs
dMSN (On)
iMSN (Off)
MSN (No Change)
Firing Rate (Hz)
Time (min)
H
Putative (Unlabeled) dMSNs
Firing Rate (Hz)
Time (min)
I
Putative (Unlabeled) iMSNs
Firing Rate (Hz)
Time (min)
J
Optogenetically Labeled
Control MSNs
dMSNs
iMSNs
Firing Rate (Hz)
Ctrl
Park
LID
K
Putative (Unlabeled)
Control MSNs
dMSNs
iMSNs
Firing Rate (Hz)
Ctrl
Park
LID
L
Putative MSNs
Immobile
Mobile
Ctrl
Contra
Park
LID
Firing Rate (Hz)
Norm. Firing Rate
Ctrl
Contra
Park
LID
Velocity (cm/s)
M
Putative dMSNs
Immobile
Mobile
Ctrl
Park
LID
Firing Rate (Hz)
Norm. Firing Rate
Ctrl
Park
LID
Velocity (cm/s)
N
Putative iMSNs
Immobile
Mobile
Ctrl
Park
LID
Firing Rate (Hz)
Norm. Firing Rate
Ctrl
Park
LID
Velocity (cm/s)

2.5 Figure S1. Alterations in Identified Striatal Neurons Following Dopamine Depletion and Replacement with Levodopa. Related to Figure 1.

(A) Coronal schematic showing 6-OHDA and DIO-ChR2-eYFP injection sites. **(B)** Representative coronal slices containing the striatum, showing tyrosine hydroxylase (TH) staining and viral expression of DIO-ChR2-eYFP. Scale bar = 1mm. **(C)** Photo of a dyskinetic mouse. **(D)** Single experimental session timeline. **(E)** Representative optogenetically labeled dMSN in a healthy mouse (Ctrl, top), and in a parkinsonian mouse before (Park, middle) and after (LID, bottom) levodopa injection. **(F)** Representative optogenetically labeled iMSN in a healthy mouse (Ctrl, top), and in a parkinsonian mouse before (Park, middle) and after (LID, bottom) levodopa injection. **(G)** Representative putative MSNs: dMSN (left), iMSN (middle), and unclassified MSN (right) aligned to levodopa injection (t=0, dotted line). **(H-I)** Average firing rate aligned to levodopa injection (t=0, dotted line). **(H)** Putative dMSNs (n=146, N=15). **(I)** Putative iMSNs (n=69, N=15). **(J-K)** Average firing rate of MSNs before (Park) and after (LID) levodopa administration, compared to labeled MSNs (dMSNs + iMSNs) from healthy (Ctrl) mice. *$p<0.05$ vs Ctrl. **(J)** Optogenetically labeled dMSNs and iMSNs. **(K)** Putative (unlabeled) dMSNs and iMSNs. **(L-N)** Firing rate of MSNs during movement, recorded in healthy (Ctrl) and parkinsonian mice contralateral (Contra) and ipsilateral to the depletion before (Park) and after (LID) levodopa. Top: average firing rate during immobile (velocity < 0.5 cm/s) and mobile (velocity > 3 cm/s) epochs. Bottom: normalized firing rate versus velocity. Data presented from **(L)** all putative MSNs (Ctrl: n=98, N=10; Contra: n=88, N=5; Park/LID: n=215, N=15), **(M)** putative dMSNs (Ctrl: n=64, N=5; Park/LID: n=146, N=15), and **(N)** putative iMSNs (Ctrl: n=34, N=5; Park/LID: n=69, N=15). n=cells, N=animals. All data presented as mean ± SEM.

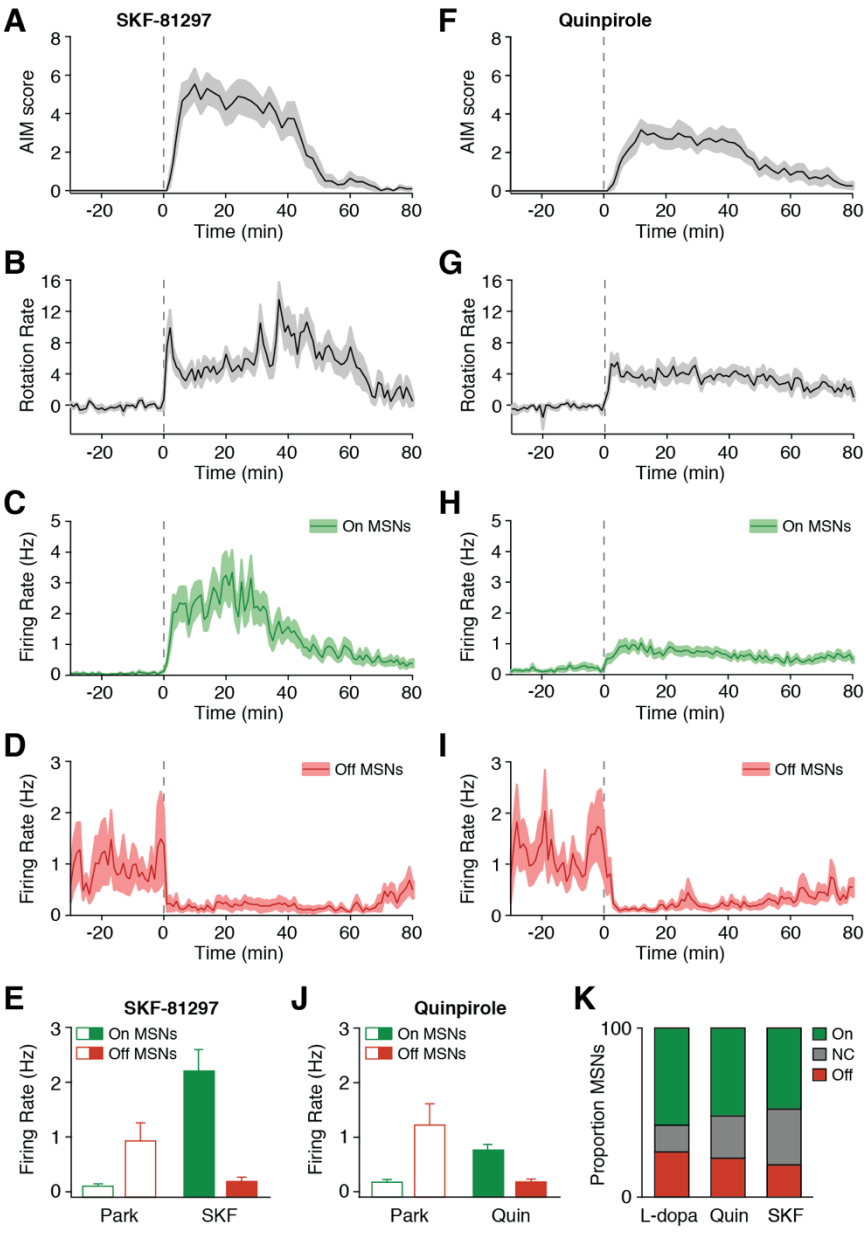
A
SKF-81297
AIM score
Time (min)
F
Quinpirole
B
Rotation Rate
G
C
On MSNs
Firing Rate (Hz)
H
D
Off MSNs
I
E
Park
SKF
J
Quin
K
Proportion MSNs
L-dopa
NC
On
Off

2.6 Figure S2. Alterations in Putative Striatal Neurons Following Dopamine Depletion and Administration of SKF-81297 or Quinpirole. Related to Figure 1.

Behavior and firing rate of putative MSNs recorded in parkinsonian mice following administration of the **(A-E)** D1R-agonist SKF-81297 (SKF, dosage 3-5 mg/kg) or **(F-J)** D2R-agonist Quinpirole (Quin, dosage 0.5-2 mg/kg). Average AIM score following **(A)** SKF (N=5) or **(F)** Quin (N=6). Average rotation rate following **(B)** SKF or **(G)** Quin. Average firing rate of putative MSNs activated (On MSNs) in response to administration of **(C)** SKF (n=23, N=5) or **(H)** Quin (n=19, N=6). Average firing rate of putative MSNs inhibited (Off MSNs) in response to administration of **(D)** SKF (n=9, N=5) or **(I)** Quin (n=12, N=6). Average behavior and firing rate aligned to i.p. drug injection at t=0 (dotted line). Average firing rate of On and Off MSNs during parkinsonian (Park) and dyskinetic states following administration of **(E)** SKF or **(J)** Quin. Proportion of all MSNs activated (On), inhibited (Off), or not changed (NC) by levodopa (L-dopa), Quinpirole (Quin) or SKF-81297 (SKF) administration. n=cells, N=animals. All data presented as mean ± SEM.

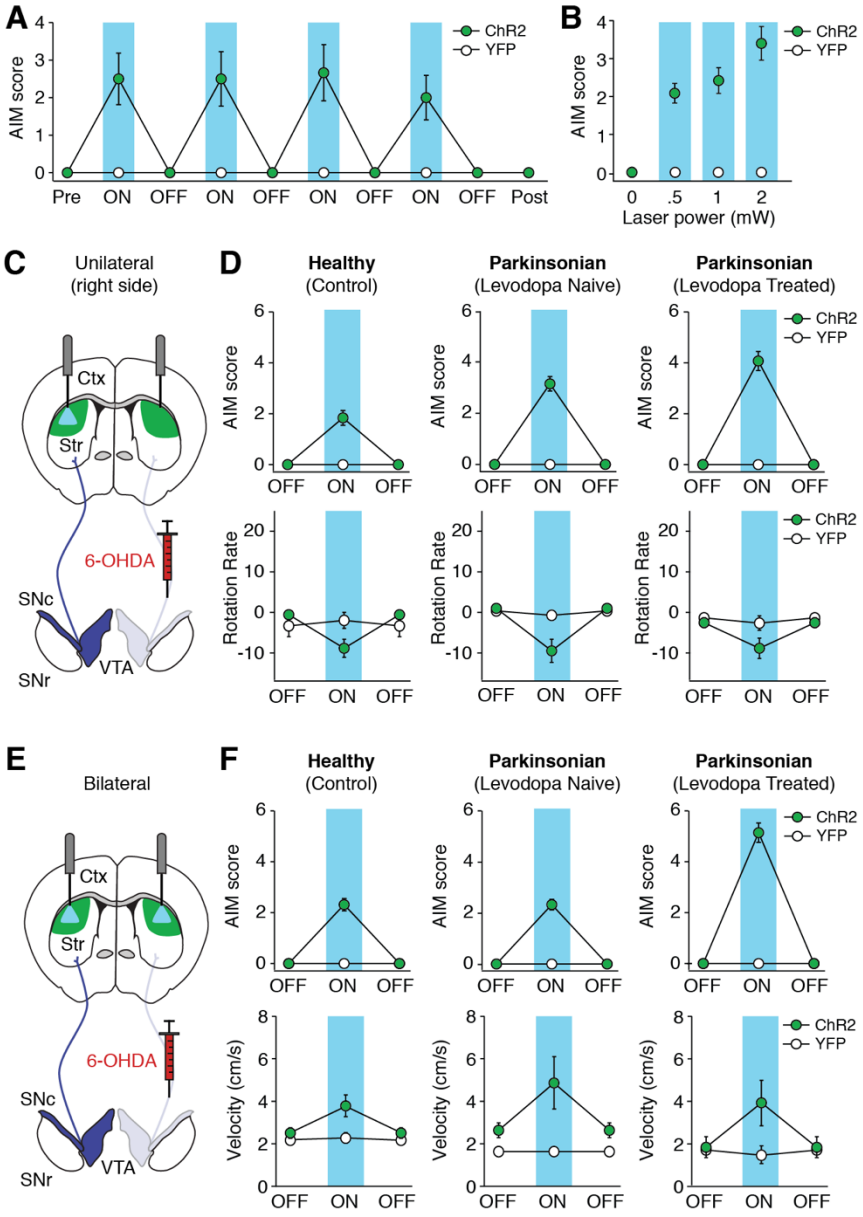

2.7 Figure S3. Optogenetic Activation of dMSNs Produces Dyskinesia in Healthy and Parkinsonian Mice. Related to Figure 2.

(A) Average dyskinesia score for healthy D1-Cre mice before (Pre), during (ON) and after (OFF) laser stimulation epochs, and post-laser stimulation (Post) period. **(B)** Average dyskinesia score for healthy mice at varying laser powers. **(C-D)** Unilateral stimulation in the right (contralesional) hemisphere. **(C)** Coronal schematic showing experimental manipulation. **(D)** Behavior before (OFF) and during (ON) dMSN stimulation in healthy (Control) and parkinsonian mice before (Levodopa Naïve) and after (Levodopa Treated) chronic levodopa treatment. Top: average dyskinesia score. Bottom: average rotation rate. **(E-F)** Bilateral stimulation. **(E)** Coronal schematic. **(D)** Behavior before (OFF) and during (ON) dMSN stimulation in healthy (Control) and parkinsonian mice before (Levodopa Naïve) and after (Levodopa Treated) chronic levodopa treatment. Top: average dyskinesia score. Bottom: average velocity. All data presented as mean ± SEM.

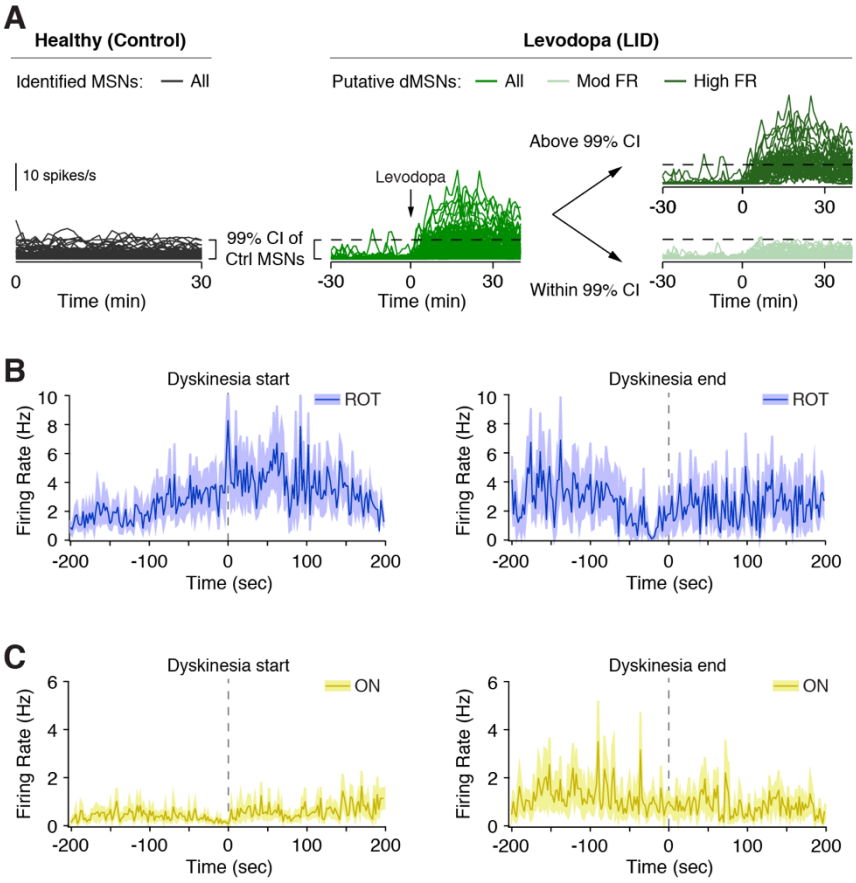

2.8 Figure S4. A Subpopulation of dMSNs Show High Firing Rates Correlated to Dyskinesia. Related to Figure 3.

(A) Rate-based classification method. 99% confidence interval (CI, dotted line) was calculated from all healthy (control) MSNs (left, black traces). Using this threshold, putative dMSNs from parkinsonian mice (middle) were classified as Mod FR units if their levodopa-evoked firing rate stayed below this threshold (right, light green) and High FR units if their levodopa-evoked firing rate exceeded this threshold (right, dark green). **(B-C)** Average firing rate of putative dMSN subtypes aligned to dyskinesia start (left, ROT: n=13, N=5; ON: n=38, N=5) and dyskinesia end (right, ROT: n=10, N=5; ON: n=26, N=5). n=cells, N=animals. All data presented as mean ± SEM.

2.8 References

Ahlskog, J.E., and Muenter, M.D. (2001). Frequency of levodopa-related dyskinesias and motor fluctuations as estimated from the cumulative literature. Mov. Disord. *16*, 448–458.

Albin, R.L., Young, A.B., and Penney, J.B. (1989). The functional anatomy of basal ganglia disorders. Trends Neurosci. *12*, 366–375.

Alcacer, C., Andreoli, L., Sebastianutto, I., Jakobsson, J., Fieblinger, T., and Cenci, M.A. (2017). Chemogenetic stimulation of striatal projection neurons modulates responses to Parkinson's disease therapy. Journal of Clinical Investigation *127*, 720–734.

Alexander, G.E., and Crutcher, M.D. (1990). Functional architecture of basal ganglia circuits: neural substrates of parallel processing. Trends Neurosci. *13*, 266–271.

Andersson, M., Hilbertson, A., and Cenci, M.A. (1999). Striatal fosB expression is causally linked with l-DOPA-induced abnormal involuntary movements and the associated upregulation of striatal prodynorphin mRNA in a rat model of Parkinson's disease. Neurobiol. Dis. *6*, 461–474.

Aquino, C.C., and Fox, S.H. (2015). Clinical spectrum of levodopa-induced complications. Mov. Disord. *30*, 80–89.

Aubert, I., Guigoni, C., Håkansson, K., Li, Q., Dovero, S., Barthe, N., Bioulac, B.H., Gross, C.E., Fisone, G., Bloch, B., et al. (2005). Increased D1 dopamine receptor signaling in levodopa-induced dyskinesia. Ann. Neurol. *57*, 17–26.

Bagetta, V., Sgobio, C., Pendolino, V., Del Papa, G., Tozzi, A., Ghiglieri, V., Giampà, C., Zianni, E., Gardoni, F., Calabresi, P., et al. (2012). Rebalance of striatal NMDA/AMPA receptor ratio

underlies the reduced emergence of dyskinesia during D2-like dopamine agonist treatment in experimental Parkinson's disease. J. Neurosci. *32*, 17921–17931.

Barbera, G., Liang, B., Zhang, L., Gerfen, C.R., Culurciello, E., Chen, R., Li, Y., and Lin, D.-T. (2016). Spatially Compact Neural Clusters in the Dorsal Striatum Encode Locomotion Relevant Information. Neuron *92*, 202–213.

Barnes, T.D., Kubota, Y., Hu, D., Jin, D.Z., and Graybiel, A.M. (2005). Activity of striatal neurons reflects dynamic encoding and recoding of procedural memories. Nature *437*, 1158–1161.

Bateup, H.S., Santini, E., Shen, W., Birnbaum, S., Valjent, E., Surmeier, D.J., Fisone, G., Nestler, E.J., and Greengard, P. (2010). Distinct subclasses of medium spiny neurons differentially regulate striatal motor behaviors. Proc. Natl. Acad. Sci. U.S.A. *107*, 14845–14850.

Beckstead, R.M., Domesick, V.B., and Nauta, W.J. (1979). Efferent connections of the substantia nigra and ventral tegmental area in the rat. Brain Res. *175*, 191–217.

Beier, K.T., Kim, C.K., Hoerbelt, P., Hung, L.W., Heifets, B.D., DeLoach, K.E., Mosca, T.J., Neuner, S., Deisseroth, K., Luo, L., et al. (2017). Rabies screen reveals GPe control of cocaine-triggered plasticity. Nature *549*, 345–350.

Beitz, J.M. (2014). Parkinson's disease: a review. Front Biosci (Schol Ed) *6*, 65–74.

Benazzouz, A., Breit, S., Koudsie, A., Pollak, P., Krack, P., and Benabid, A.-L. (2002). Intraoperative microrecordings of the subthalamic nucleus in Parkinson's disease. Mov. Disord. *17 Suppl 3*, S145-149.

Bergman, H., Wichmann, T., Karmon, B., and DeLong, M.R. (1994). The primate subthalamic nucleus. II. Neuronal activity in the MPTP model of parkinsonism. J. Neurophysiol. *72*, 507–520.

Berke, J.D., Okatan, M., Skurski, J., and Eichenbaum, H.B. (2004). Oscillatory entrainment of striatal neurons in freely moving rats. Neuron *43*, 883–896.

Bezard, E., Gross, C.E., Qin, L., Gurevich, V.V., Benovic, J.L., and Gurevich, E.V. (2005). l-DOPA reverses the MPTP-induced elevation of the arrestin2 and GRK6 expression and enhanced ERK activation in monkey brain. Neurobiology of Disease *18*, 323–335.

Bhidayasiri, R., and Truong, D.D. (2008). Motor complications in Parkinson disease: clinical manifestations and management. J. Neurol. Sci. *266*, 204–215.

Boraud, T., Bezard, E., Guehl, D., Bioulac, B., and Gross, C. (1998). Effects of L-DOPA on neuronal activity of the globus pallidus externalis (GPe) and globus pallidus internalis (GPi) in the MPTP-treated monkey. Brain Res. *787*, 157–160.

Borgkvist, A., Avegno, E.M., Wong, M.Y., Kheirbek, M.A., Sonders, M.S., Hen, R., and Sulzer, D. (2015). Loss of Striatonigral GABAergic Presynaptic Inhibition Enables Motor Sensitization in Parkinsonian Mice. Neuron *87*, 976–988.

Brimblecombe, K.R., and Cragg, S.J. (2017). The Striosome and Matrix Compartments of the Striatum: A Path through the Labyrinth from Neurochemistry toward Function. ACS Chem Neurosci *8*, 235–242.

Calabresi, P., Saiardi, A., Pisani, A., Baik, J.H., Centonze, D., Mercuri, N.B., Bernardi, G., and Borrelli, E. (1997). Abnormal synaptic plasticity in the striatum of mice lacking dopamine D2 receptors. J. Neurosci. *17*, 4536–4544.

Caroff, S.N., Ungvari, G.S., and Cunningham Owens, D.G. (2018). Historical perspectives on tardive dyskinesia. J. Neurol. Sci. *389*, 4–9.

Carta, M., Lindgren, H.S., Lundblad, M., Stancampiano, R., Fadda, F., and Cenci, M.A. (2006). Role of striatal L-DOPA in the production of dyskinesia in 6-hydroxydopamine lesioned rats. J. Neurochem. *96*, 1718–1727.

Cenci, M.A., and Konradi, C. (2010). Maladaptive striatal plasticity in L-DOPA-induced dyskinesia. Prog. Brain Res. *183*, 209–233.

Cenci, M.A., and Lundblad, M. (2007). Ratings of L-DOPA-induced dyskinesia in the unilateral 6-OHDA lesion model of Parkinson's disease in rats and mice. Curr Protoc Neurosci *Chapter 9*, Unit 9.25.

Chang, H.T., Wilson, C.J., and Kitai, S.T. (1982). A Golgi study of rat neostriatal neurons: light microscopic analysis. J. Comp. Neurol. *208*, 107–126.

Chen, M.-T., Morales, M., Woodward, D.J., Hoffer, B.J., and Janak, P.H. (2001). In Vivo Extracellular Recording of Striatal Neurons in the Awake Rat Following Unilateral 6-Hydroxydopamine Lesions. Experimental Neurology *171*, 72–83.

Choi, K., Holly, E., Davatolhagh, M.F., Beier, K.T., and Fuccillo, M.V. (2019). Integrated anatomical and physiological mapping of striatal afferent projections. Eur J Neurosci *49*, 623–636.

Ciriachi, C., Svane-Petersen, D., and Rickhag, M. (2019). Genetic tools to study complexity of striatal function. J. Neurosci. Res. *97*, 1181–1193.

Costa, R.M., Lin, S.-C., Sotnikova, T.D., Cyr, M., Gainetdinov, R.R., Caron, M.G., and Nicolelis, M.A.L. (2006). Rapid alterations in corticostriatal ensemble coordination during acute dopamine-dependent motor dysfunction. Neuron *52*, 359–369.

Cui, G., Jun, S.B., Jin, X., Pham, M.D., Vogel, S.S., Lovinger, D.M., and Costa, R.M. (2013). Concurrent activation of striatal direct and indirect pathways during action initiation. Nature *494*, 238–242.

Dautan, D., Huerta-Ocampo, I., Witten, I.B., Deisseroth, K., Bolam, J.P., Gerdjikov, T., and Mena-Segovia, J. (2014). A major external source of cholinergic innervation of the striatum and nucleus accumbens originates in the brainstem. J. Neurosci. *34*, 4509–4518.

Day, M., Wang, Z., Ding, J., An, X., Ingham, C.A., Shering, A.F., Wokosin, D., Ilijic, E., Sun, Z., Sampson, A.R., et al. (2006). Selective elimination of glutamatergic synapses on striatopallidal neurons in Parkinson disease models. Nat. Neurosci. *9*, 251–259.

Deffains, M., and Bergman, H. (2015). Striatal cholinergic interneurons and cortico-striatal synaptic plasticity in health and disease. Mov. Disord. *30*, 1014–1025.

Deffains, M., Iskhakova, L., Katabi, S., Haber, S.N., Israel, Z., and Bergman, H. (2016). Subthalamic, not striatal, activity correlates with basal ganglia downstream activity in normal and parkinsonian monkeys. Elife *5*.

DeLong, M.R. (1990). Primate models of movement disorders of basal ganglia origin. Trends Neurosci. *13*, 281–285.

Ding, J., Peterson, J.D., and Surmeier, D.J. (2008). Corticostriatal and Thalamostriatal Synapses Have Distinctive Properties. Journal of Neuroscience *28*, 6483–6492.

Eastwood, B.S., Hooks, B.M., Paletzki, R.F., O'Connor, N.J., Glaser, J.R., and Gerfen, C.R. (2019). Whole mouse brain reconstruction and registration to a reference atlas with standard histochemical processing of coronal sections. Journal of Comparative Neurology *527*, 2170–2178.

Fieblinger, T., Graves, S.M., Sebel, L.E., Alcacer, C., Plotkin, J.L., Gertler, T.S., Chan, C.S., Heiman, M., Greengard, P., Cenci, M.A., et al. (2014). Cell type-specific plasticity of striatal projection neurons in parkinsonism and L-DOPA-induced dyskinesia. Nat Commun *5*, 5316.

Fieblinger, T., Zanetti, L., Sebastianutto, I., Breger, L.S., Quintino, L., Lockowandt, M., Lundberg, C., and Cenci, M.A. (2018). Striatonigral neurons divide into two distinct morphological-physiological phenotypes after chronic L-DOPA treatment in parkinsonian rats. Sci Rep *8*, 10068.

Filion, M., and Tremblay, L. (1991). Abnormal spontaneous activity of globus pallidus neurons in monkeys with MPTP-induced parkinsonism. Brain Res. *547*, 142–151.

Flaherty, A.W., and Graybiel, A.M. (1991). Corticostriatal transformations in the primate somatosensory system. Projections from physiologically mapped body-part representations. J. Neurophysiol. *66*, 1249–1263.

Francardo, V., Recchia, A., Popovic, N., Andersson, D., Nissbrandt, H., and Cenci, M.A. (2011). Impact of the lesion procedure on the profiles of motor impairment and molecular responsiveness

to L-DOPA in the 6-hydroxydopamine mouse model of Parkinson's disease. Neurobiol. Dis. *42*, 327–340.

Freeze, B.S., Kravitz, A.V., Hammack, N., Berke, J.D., and Kreitzer, A.C. (2013). Control of basal ganglia output by direct and indirect pathway projection neurons. J. Neurosci. *33*, 18531–18539.

Gage, G.J., Stoetzner, C.R., Wiltschko, A.B., and Berke, J.D. (2010). Selective activation of striatal fast-spiking interneurons during choice execution. Neuron *67*, 466–479.

Galvan, A., Devergnas, A., and Wichmann, T. (2015). Alterations in neuronal activity in basal ganglia-thalamocortical circuits in the parkinsonian state. Front Neuroanat *9*, 5.

Gerfen, C.R., and Surmeier, D.J. (2011). Modulation of striatal projection systems by dopamine. Annu. Rev. Neurosci. *34*, 441–466.

Gerfen, C.R., Engber, T.M., Mahan, L.C., Susel, Z., Chase, T.N., Monsma, F.J., and Sibley, D.R. (1990). D1 and D2 dopamine receptor-regulated gene expression of striatonigral and striatopallidal neurons. Science *250*, 1429–1432.

Gerfen, C.R., Paletzki, R., and Heintz, N. (2013). GENSAT BAC cre-recombinase driver lines to study the functional organization of cerebral cortical and basal ganglia circuits. Neuron *80*, 1368–1383.

Girasole, A.E., Lum, M.Y., Nathaniel, D., Bair-Marshall, C.J., Guenthner, C.J., Luo, L., Kreitzer, A.C., and Nelson, A.B. (2018). A Subpopulation of Striatal Neurons Mediates Levodopa-Induced Dyskinesia. Neuron *97*, 787-795.e6.

Gokce, O., Stanley, G., Treutlein, B., Neff, N.F., Camp, G.J., Malenka, R.C., Rothwell, P.E., Fuccillo, M.V., Südhof, T.C., and Quake, S.R. (2016). Cellular Taxonomy of the Mouse Striatum as Revealed by Single-Cell RNA-Seq. Cell Rep *16*, 1126–1137.

Gong, S., Doughty, M., Harbaugh, C.R., Cummins, A., Hatten, M.E., Heintz, N., and Gerfen, C.R. (2007). Targeting Cre Recombinase to Specific Neuron Populations with Bacterial Artificial Chromosome Constructs. Journal of Neuroscience *27*, 9817–9823.

Graveland, G.A., and DiFiglia, M. (1985). The frequency and distribution of medium-sized neurons with indented nuclei in the primate and rodent neostriatum. Brain Res. *327*, 307–311.

Guenthner, C.J., Miyamichi, K., Yang, H.H., Heller, H.C., and Luo, L. (2013). Permanent Genetic Access to Transiently Active Neurons via TRAP: Targeted Recombination in Active Populations. Neuron *78*, 773–784.

Guigoni, C., Doudnikoff, E., Li, Q., Bloch, B., and Bezard, E. (2007). Altered D(1) dopamine receptor trafficking in parkinsonian and dyskinetic non-human primates. Neurobiol. Dis. *26*, 452–463.

Guo, Q., Wang, D., He, X., Feng, Q., Lin, R., Xu, F., Fu, L., and Luo, M. (2015). Whole-brain mapping of inputs to projection neurons and cholinergic interneurons in the dorsal striatum. PLoS ONE *10*, e0123381.

Haber, S.N., Fudge, J.L., and McFarland, N.R. (2000). Striatonigrostriatal pathways in primates form an ascending spiral from the shell to the dorsolateral striatum. J. Neurosci. *20*, 2369–2382.

Harris, K.D., Henze, D.A., Csicsvari, J., Hirase, H., and Buzsáki, G. (2000). Accuracy of tetrode spike separation as determined by simultaneous intracellular and extracellular measurements. J. Neurophysiol. *84*, 401–414.

Heiman, M., Heilbut, A., Francardo, V., Kulicke, R., Fenster, R.J., Kolaczyk, E.D., Mesirov, J.P., Surmeier, D.J., Cenci, M.A., and Greengard, P. (2014). Molecular adaptations of striatal spiny projection neurons during levodopa-induced dyskinesia. Proc. Natl. Acad. Sci. U.S.A. *111*, 4578–4583.

Hely, M.A., Reid, W.G.J., Adena, M.A., Halliday, G.M., and Morris, J.G.L. (2008). The Sydney multicenter study of Parkinson's disease: the inevitability of dementia at 20 years. Mov. Disord. *23*, 837–844.

Henderson, J.M., Carpenter, K., Cartwright, H., and Halliday, G.M. (2000). Degeneration of the centré median–parafascicular complex in Parkinson's disease. Ann Neurol. *47*, 345–352.

Hernandez, L.F., Kubota, Y., Hu, D., Howe, M.W., Lemaire, N., and Graybiel, A.M. (2013). Selective effects of dopamine depletion and L-DOPA therapy on learning-related firing dynamics of striatal neurons. J. Neurosci. *33*, 4782–4795.

Hernández-López, S., Bargas, J., Surmeier, D.J., Reyes, A., and Galarraga, E. (1997). D1 receptor activation enhances evoked discharge in neostriatal medium spiny neurons by modulating an L-type Ca2+ conductance. J. Neurosci. *17*, 3334–3342.

Hernandez-Lopez, S., Tkatch, T., Perez-Garci, E., Galarraga, E., Bargas, J., Hamm, H., and Surmeier, D.J. (2000). D2 dopamine receptors in striatal medium spiny neurons reduce L-type

Ca2+ currents and excitability via a novel PLC[beta]1-IP3-calcineurin-signaling cascade. J. Neurosci. *20*, 8987–8995.

Hornykiewicz, O. (2015). 50 years of levodopa. Mov. Disord. *30*, 1008.

Horstink, M.W., Zijlmans, J.C., Pasman, J.W., Berger, H.J., and van't Hof, M.A. (1990). Severity of Parkinson's disease is a risk factor for peak-dose dyskinesia. J. Neurol. Neurosurg. Psychiatr. *53*, 224–226.

Hutchinson, W.D., Lozano, A.M., Davis, K.D., Saint-Cyr, J.A., Lang, A.E., and Dostrovsky, J.O. (1994). Differential neuronal activity in segments of globus pallidus in Parkinson's disease patients. Neuroreport *5*, 1533–1537.

Ingham, C.A., Hood, S.H., and Arbuthnott, G.W. (1989). Spine density on neostriatal neurones changes with 6-hydroxydopamine lesions and with age. Brain Res. *503*, 334–338.

Jankovic, J. (2008). Parkinson's disease: clinical features and diagnosis. J. Neurol. Neurosurg. Psychiatr. *79*, 368–376.

Jenner, P. (2008). Molecular mechanisms of L-DOPA-induced dyskinesia. Nat. Rev. Neurosci. *9*, 665–677.

Jin, X., Tecuapetla, F., and Costa, R.M. (2014). Basal ganglia subcircuits distinctively encode the parsing and concatenation of action sequences. Nat Neurosci *17*, 423–430.

Johansson, Y., and Silberberg, G. (2020). The Functional Organization of Cortical and Thalamic Inputs onto Five Types of Striatal Neurons Is Determined by Source and Target Cell Identities. Cell Rep *30*, 1178-1194.e3.

Ketzef, M., Spigolon, G., Johansson, Y., Bonito-Oliva, A., Fisone, G., and Silberberg, G. (2017). Dopamine Depletion Impairs Bilateral Sensory Processing in the Striatum in a Pathway-Dependent Manner. Neuron *94*, 855-865.e5.

Kish, L.J., Palmer, M.R., and Gerhardt, G.A. (1999). Multiple single-unit recordings in the striatum of freely moving animals: effects of apomorphine and d-amphetamine in normal and unilateral 6-hydroxydopamine-lesioned rats. Brain Research *833*, 58–70.

Kravitz, A.V., Freeze, B.S., Parker, P.R.L., Kay, K., Thwin, M.T., Deisseroth, K., and Kreitzer, A.C. (2010). Regulation of parkinsonian motor behaviours by optogenetic control of basal ganglia circuitry. Nature *466*, 622–626.

Kravitz, A.V., Tye, L.D., and Kreitzer, A.C. (2012). Distinct roles for direct and indirect pathway striatal neurons in reinforcement. Nat Neurosci *15*, 816–818.

Kravitz, A.V., Owen, S.F., and Kreitzer, A.C. (2013). Optogenetic identification of striatal projection neuron subtypes during in vivo recordings. Brain Res. *1511*, 21–32.

Kreiss, D.S., Mastropietro, C.W., Rawji, S.S., and Walters, J.R. (1997). The response of subthalamic nucleus neurons to dopamine receptor stimulation in a rodent model of Parkinson's disease. J. Neurosci. *17*, 6807–6819.

Kreitzer, A.C., and Malenka, R.C. (2007). Endocannabinoid-mediated rescue of striatal LTD and motor deficits in Parkinson's disease models. Nature *445*, 643–647.

Lahiri, A.K., and Bevan, M.D. (2020). Dopaminergic Transmission Rapidly and Persistently Enhances Excitability of D1 Receptor-Expressing Striatal Projection Neurons. Neuron *106*, 277-290.e6.

Lenz, J.D., and Lobo, M.K. (2013). Optogenetic insights into striatal function and behavior. Behav. Brain Res. *255*, 44–54.

Levy, R., Dostrovsky, J.O., Lang, A.E., Sime, E., Hutchison, W.D., and Lozano, A.M. (2001). Effects of apomorphine on subthalamic nucleus and globus pallidus internus neurons in patients with Parkinson's disease. J. Neurophysiol. *86*, 249–260.

Liang, L., DeLong, M.R., and Papa, S.M. (2008). Inversion of dopamine responses in striatal medium spiny neurons and involuntary movements. J. Neurosci. *28*, 7537–7547.

Lozano, A.M., Lang, A.E., Levy, R., Hutchison, W., and Dostrovsky, J. (2000). Neuronal recordings in Parkinson's disease patients with dyskinesias induced by apomorphine. Ann. Neurol. *47*, S141-146.

Mallet, N., Ballion, B., Le Moine, C., and Gonon, F. (2006). Cortical inputs and GABA interneurons imbalance projection neurons in the striatum of parkinsonian rats. J. Neurosci. *26*, 3875–3884.

Mallet, N., Pogosyan, A., Sharott, A., Csicsvari, J., Bolam, J.P., Brown, P., and Magill, P.J. (2008). Disrupted dopamine transmission and the emergence of exaggerated beta oscillations in subthalamic nucleus and cerebral cortex. J. Neurosci. *28*, 4795–4806.

Mathur, B.N., and Lovinger, D.M. (2012). Serotonergic action on dorsal striatal function. Parkinsonism Relat. Disord. *18 Suppl 1*, S129-131.

McGeorge, A.J., and Faull, R.L. (1987). The organization and collateralization of corticostriate neurones in the motor and sensory cortex of the rat brain. Brain Res. *423*, 318–324.

McGregor, M.M., and Nelson, A.B. (2019). Circuit Mechanisms of Parkinson's Disease. Neuron *101*, 1042–1056.

McNeill, T.H., Brown, S.A., Rafols, J.A., and Shoulson, I. (1988). Atrophy of medium spiny I striatal dendrites in advanced Parkinson's disease. Brain Res. *455*, 148–152.

Mena-Segovia, J., Bolam, J.P., and Magill, P.J. (2004). Pedunculopontine nucleus and basal ganglia: distant relatives or part of the same family? Trends Neurosci. *27*, 585–588.

Mink, J.W. (1996). The basal ganglia: focused selection and inhibition of competing motor programs. Prog. Neurobiol. *50*, 381–425.

Mink, J.W. (2003). The Basal Ganglia and involuntary movements: impaired inhibition of competing motor patterns. Arch. Neurol. *60*, 1365–1368.

Nonomura, S., Nishizawa, K., Sakai, Y., Kawaguchi, Y., Kato, S., Uchigashima, M., Watanabe, M., Yamanaka, K., Enomoto, K., Chiken, S., et al. (2018). Monitoring and Updating of Action Selection for Goal-Directed Behavior through the Striatal Direct and Indirect Pathways. Neuron *99*, 1302-1314.e5.

Oye, C., Bouchard, R., Boucher, R., and Poirier, L.J. (1970). Spontaneous activity of the putamen after chronic interruption of the dopaminergic pathway: effect of L-dopa. J. Pharmacol. Exp. Ther. *175*, 700–708.

Pan, H.S., and Walters, J.R. (1988). Unilateral lesion of the nigrostriatal pathway decreases the firing rate and alters the firing pattern of globus pallidus neurons in the rat. Synapse *2*, 650–656.

Pan, W.X., Mao, T., and Dudman, J.T. (2010). Inputs to the dorsal striatum of the mouse reflect the parallel circuit architecture of the forebrain. Front Neuroanat *4*, 147.

Papa, S.M., Desimone, R., Fiorani, M., and Oldfield, E.H. (1999). Internal globus pallidus discharge is nearly suppressed during levodopa-induced dyskinesias. Ann. Neurol. *46*, 732–738.

Parker, J.G., Marshall, J.D., Ahanonu, B., Wu, Y.-W., Kim, T.H., Grewe, B.F., Zhang, Y., Li, J.Z., Ding, J.B., Ehlers, M.D., et al. (2018). Diametric neural ensemble dynamics in parkinsonian and dyskinetic states. Nature *557*, 177–182.

Perez, X.A., Zhang, D., Bordia, T., and Quik, M. (2017). Striatal D1 medium spiny neuron activation induces dyskinesias in parkinsonian mice. Mov. Disord.

Picconi, B., Centonze, D., Håkansson, K., Bernardi, G., Greengard, P., Fisone, G., Cenci, M.A., and Calabresi, P. (2003). Loss of bidirectional striatal synaptic plasticity in L-DOPA-induced dyskinesia. Nat. Neurosci. *6*, 501–506.

Planert, H., Berger, T.K., and Silberberg, G. (2013). Membrane properties of striatal direct and indirect pathway neurons in mouse and rat slices and their modulation by dopamine. PLoS ONE *8*, e57054.

Prager, E.M., and Plotkin, J.L. (2019). Compartmental function and modulation of the striatum. J. Neurosci. Res. *97*, 1503–1514.

Redgrave, P., Rodriguez, M., Smith, Y., Rodriguez-Oroz, M.C., Lehericy, S., Bergman, H., Agid, Y., DeLong, M.R., and Obeso, J.A. (2010). Goal-directed and habitual control in the basal ganglia: implications for Parkinson's disease. Nat. Rev. Neurosci. *11*, 760–772.

Rothwell, P.E., Hayton, S.J., Sun, G.L., Fuccillo, M.V., Lim, B.K., and Malenka, R.C. (2015). Input- and Output-Specific Regulation of Serial Order Performance by Corticostriatal Circuits. Neuron *88*, 345–356.

Ryan, M.B., Bair-Marshall, C., and Nelson, A.B. (2018). Aberrant Striatal Activity in Parkinsonism and Levodopa-Induced Dyskinesia. Cell Rep *23*, 3438-3446.e5.

Sagot, B., Li, L., and Zhou, F.-M. (2018). Hyperactive Response of Direct Pathway Striatal Projection Neurons to L-dopa and D1 Agonism in Freely Moving Parkinsonian Mice. Front Neural Circuits *12*, 57.

Schultz, W. (2016). Reward functions of the basal ganglia. J Neural Transm (Vienna) *123*, 679–693.

Shen, W., Flajolet, M., Greengard, P., and Surmeier, D.J. (2008). Dichotomous dopaminergic control of striatal synaptic plasticity. Science *321*, 848–851.

Shen, W., Plotkin, J.L., Francardo, V., Ko, W.K.D., Xie, Z., Li, Q., Fieblinger, T., Wess, J., Neubig, R.R., Lindsley, C.W., et al. (2015). M4 Muscarinic Receptor Signaling Ameliorates Striatal Plasticity Deficits in Models of L-DOPA-Induced Dyskinesia. Neuron *88*, 762–773.

Shin, J.H., Kim, D., and Jung, M.W. (2018). Differential coding of reward and movement information in the dorsomedial striatal direct and indirect pathways. Nat Commun *9*, 404.

Soares, J., Kliem, M.A., Betarbet, R., Greenamyre, J.T., Yamamoto, B., and Wichmann, T. (2004). Role of external pallidal segment in primate parkinsonism: comparison of the effects of 1-methyl-4-phenyl-1,2,3,6-tetrahydropyridine-induced parkinsonism and lesions of the external pallidal segment. J. Neurosci. *24*, 6417–6426.

Suárez, L.M., Solís, O., Caramés, J.M., Taravini, I.R., Solís, J.M., Murer, M.G., and Moratalla, R. (2014). L-DOPA Treatment Selectively Restores Spine Density in Dopamine Receptor D2–Expressing Projection Neurons in Dyskinetic Mice. Biological Psychiatry *75*, 711–722.

Suarez, L.M., Solis, O., Aguado, C., Lujan, R., and Moratalla, R. (2016). L-DOPA Oppositely Regulates Synaptic Strength and Spine Morphology in D1 and D2 Striatal Projection Neurons in Dyskinesia. Cereb. Cortex *26*, 4253–4264.

Suarez, L.M., Alberquilla, S., García-Montes, J.R., and Moratalla, R. (2018). Differential Synaptic Remodeling by Dopamine in Direct and Indirect Striatal Projection Neurons in Pitx3 $^{-/-}$ Mice, a Genetic Model of Parkinson's Disease. J. Neurosci. *38*, 3619–3630.

Surmeier, D.J., Song, W.J., and Yan, Z. (1996). Coordinated expression of dopamine receptors in neostriatal medium spiny neurons. J. Neurosci. *16*, 6579–6591.

Surmeier, D.J., Ding, J., Day, M., Wang, Z., and Shen, W. (2007). D1 and D2 dopamine-receptor modulation of striatal glutamatergic signaling in striatal medium spiny neurons. Trends Neurosci. *30*, 228–235.

Tepper, J.M., Tecuapetla, F., Koós, T., and Ibáñez-Sandoval, O. (2010). Heterogeneity and diversity of striatal GABAergic interneurons. Front Neuroanat *4*, 150.

Vijayakumar, D., and Jankovic, J. (2016). Drug-Induced Dyskinesia, Part 1: Treatment of Levodopa-Induced Dyskinesia. Drugs *76*, 759–777.

Villalba, R.M., and Smith, Y. (2018). Loss and remodeling of striatal dendritic spines in Parkinson's disease: from homeostasis to maladaptive plasticity? J Neural Transm (Vienna) *125*, 431–447.

Villalba, R.M., Lee, H., and Smith, Y. (2009). Dopaminergic denervation and spine loss in the striatum of MPTP-treated monkeys. Exp. Neurol. *215*, 220–227.

Villalba, R.M., Wichmann, T., and Smith, Y. (2014). Neuronal loss in the caudal intralaminar thalamic nuclei in a primate model of Parkinson's disease. Brain Struct Funct *219*, 381–394.

Wall, N.R., De La Parra, M., Callaway, E.M., and Kreitzer, A.C. (2013). Differential innervation of direct- and indirect-pathway striatal projection neurons. Neuron *79*, 347–360.

Wickens, J.R., and Wilson, C.J. (1998). Regulation of action-potential firing in spiny neurons of the rat neostriatum in vivo. J. Neurophysiol. *79*, 2358–2364.

Xuereb, J.H., Perry, R.H., Candy, J.M., Perry, E.K., Marshall, E., and Bonham, J.R. (1991). Nerve cell loss in the thalamus in Alzheimer's disease and Parkinson's disease. Brain *114 (Pt 3)*, 1363–1379.

Yoshida, M. (1991). The neuronal mechanism underlying parkinsonism and dyskinesia: differential roles of the putamen and caudate nucleus. Neurosci. Res. *12*, 31–40.

Zhai, S., Shen, W., Graves, S.M., and Surmeier, D.J. (2019). Dopaminergic modulation of striatal function and Parkinson's disease. J Neural Transm (Vienna) *126*, 411–422.

Chapter 3: Differential Intrinsic and Synaptic Properties of Functionally-Defined Direct Pathway Neurons Shape Their Activity in Levodopa-Induced Dyskinesia

3.1 Summary

Dopaminergic modulation of striatal direct and indirect pathway neurons is critical for the proper execution of movement. The important role dopamine plays in movement is most evident in the profound motor deficits that accompany the progressive degeneration of dopamine neurons, as occurs in Parkinson's disease (PD). The motor impairments in Parkinson's disease (PD) are largely attributed to the loss of midbrain dopamine neurons, resulting in dysregulated striatal activity. Dopamine replacement therapy with levodopa alleviates parkinsonian motor symptoms, however, chronic levodopa treatment also leads to the development of involuntary, excessive movements, known as levodopa-induced dyskinesia (LID). While levodopa is thought to rebalance striatal activity, and thereby restore motor function, it is also hypothesized to produce aberrant activation of direct pathway medium spiny neurons (dMSNs) in LID. One possible explanation for these differential responses to levodopa is that chronic dopamine replacement restores the activity of some striatal neurons, underlying its therapeutic effects, while causing aberrant activity in others, resulting in LID. We sought to test this theory using an activity-dependent mouse line (FosTRAP) to identify striatal neurons preferentially activated (TRAPed) during LID. Combining this approach with optically labeled single-unit recordings, cell type-specific retrograde rabies tracing, and slice electrophysiology, we compared the intrinsic, synaptic, and anatomical properties of TRAPed neurons to other (unTRAPed) striatal neurons. During LID, we found TRAPed dMSNs achieved higher firing rates, which in turn strongly correlated with dyskinesia severity, than unlabeled dMSNs. Following chronic levodopa administration, the anatomical

distribution of monosynaptic inputs did not differ between TRAPed neurons and the larger dMSN population. Functionally, however, excitatory inputs onto TRAPed dMSNs were substantially stronger than those onto unTRAPed dMSNs. Furthermore, the firing of TRAPed dMSNs was differentially enhanced by acute dopamine-receptor activation. Together, these results suggest that functionally distinct subdivisions within the canonical direct pathway may underlie the differential effects of levodopa at the behavioral level, providing a potential mechanism underlying LID.

3.2 Introduction

The striatum underlies a wide range of behaviors, from reward-based decision-making and motor skill learning to locomotion. Subdivisions within the striatum, based largely on broad anatomical divisions, are thought to represent distinct functional channels by which the striatum mediates such diverse behaviors (Alexander and Crutcher, 1990). Within these channels, the proper execution of movement is thought to be mediated by the two major striatal cell-types, direct and indirect pathway medium spiny neurons (dMSNs and iMSNs, respectively). Current models posit that dMSNs and iMSNs exert opposing control over behavior, whereby activation of dMSNs facilitates and activation of iMSNs suppresses action (Bateup et al., 2010; Kravitz et al., 2010, 2012). However, this simple model fails to address the heterogeneity amongst neurons within a pathway, which likely contributes to the complex array of striatally-mediated behaviors.

Evidence for this model of striatal function is largely derived from the behavioral *dys*function that results from disorders in which striatal activity is perturbed, such as Parkinson's Disease (PD) (Albin et al., 1989; DeLong, 1990). For instance, the progressive loss of movement seen in PD patients is thought be mediated, by an imbalance in striatal activity favoring the indirect pathway. Dopamine-replacement therapy with levodopa, the dopamine-precursor, is thought to restore movement by rebalancing striatal activity. However, chronic exposure to levodopa also often leads to excessive, involuntary movements, known as levodopa-induced dyskinesia (LID). It is unclear which striatal neurons mediate these two effects of levodopa treatment, though existing evidence implicates direct pathway neurons in both behaviors. One possibility is that distinct subsets of direct pathway neurons drive each of these behaviors.

Interestingly, heterogeneity has been observed in striatal neurons at the level of gene expression (Gokce et al., 2016), distribution of synaptic inputs (Choi et al., 2019; Flaherty and

Graybiel, 1991; Guo et al., 2015; Johansson and Silberberg, 2020; Wall et al., 2013), intrinsic electrophysiological properties (Brimblecombe and Cragg, 2017; Fieblinger et al., 2014; Planert et al., 2013), and response to neuromodulators, like dopamine (Fieblinger et al., 2014; Planert et al., 2013; Prager and Plotkin, 2019). Particularly in LID, differential regulation of the intrinsic excitability and morphology (Fieblinger et al., 2018), as well as molecular markers, such as immediate early genes, like cFos (Andersson et al., 1999; Girasole et al., 2018), have been observed across subpopulations of dMSNs. Additionally, while over-activation of the direct pathway has been observed in mouse models of LID (Parker et al., 2018; Ryan et al., 2018; Sagot et al., 2018), dMSNs show considerable heterogeneity in response to levodopa, with only a subset of dMSNs exhibiting excessive activity (Ryan et al., 2018). Whether these functional differences in dMSN responses arise at the level of their intrinsic properties, anatomical inputs, or altered synaptic plasticity is currently unknown.

To investigate the cellular and synaptic properties of striatal neurons in LID, and how these properties relate to their functional response to levodopa, we utilized the activity-dependent mouse line, FosTRAP^{CreER} (Guenthner et al., 2013). Recent work using FosTRAP^{CreER} to selectively label striatal neurons activated during LID identified a distinct and stable subset of predominantly dMSNs involved in dyskinesia (Girasole et al., 2018). Remarkably, optogenetic activation of this striatal subpopulation was sufficient to reproduce dyskinesia in the absence of levodopa. Additionally, optogenetic inhibition of TRAPed striatal neurons, unlike random dMSN inhibition, was necessary for the expression of dyskinesia, highlighting the casual contribution of TRAPed striatal neurons to LID. Here, we combined FosTRAP^{CreER} with optogenetically labeled recordings, and found that TRAPed dMSNs exhibit excessive levodopa-evoked activity in vivo. Using monosynaptic rabies tracing and slice electrophysiology, we investigated whether this

aberrant levodopa-evoked firing was related to a differential enhancement of intrinsic excitability or excitatory synaptic input onto TRAPed dMSNs. Interestingly, we found a selective dopamine-dependent increase in the excitability of TRAPed dMSNs. Excitatory motor cortical and thalamic inputs were also stronger onto TRAPed dMSNs. Together, these findings demonstrate how the synaptic and intrinsic properties of dMSNs shape their functional response to levodopa, with insights into the mechanisms underlying LID.

3.3 Results

To understand how chronic parkinsonism and levodopa administration altered the activity of functionally defined striatal subpopulations, we identify LID-associated neurons using FosTRAP^{CreER} mice (Girasole et al., 2018; Guenthner et al., 2013). First, FosTRAP;Ai14 mice were rendered parkinsonian by injecting the neurotoxin 6-hydroxydopamine (6-OHDA) into the left medial forebrain bundle (Figure 1A). Parkinsonian mice showed an almost complete loss of dopamine neurons in the ipsilesional hemisphere, as well as a reduction in movement velocity and ipsilesional rotational bias. For optogenetic labeling, mice were also injected with Cre-dependent channelrhodopsin-2 (ChR2-eYFP) into the dorsolateral striatum. After several weeks, mice began receiving daily injections of levodopa, the dopamine precursor, which caused an increase in movement velocity, contralesional rotations (Figure 1B), and robust levodopa-induced dyskinesia (LID; Figure 1C). After one week of levodopa treatment, LID-associated neurons were captured ("TRAPed") using the short-acting tamoxifen metabolite 4-hydroxytamoxifen (4-OHT), paired with a single dyskinesogenic dose of levodopa (Girasole et al., 2018). This pairing provided a transient window following an injection of levodopa, during which transcription of c-Fos could lead to Cre-dependent expression of tdTomato and ChR2-eYFP constructs in activated cells (Figure 1D) (Girasole et al., 2018; Guenthner et al., 2013). Mice were then implanted with an optrode for simultaneous recording of single-unit activity and optogenetic identification of TRAPed neurons in vivo (Figure 1E). TRAPed neurons were optogenetically identified at the end of each session by their short latency light-evoked firing (Figure 1F), as described previously (Ryan et al., 2018; Girasole et al., 2018; Kravitz et al., 2013).

TRAPed Striatal Neurons are Enriched for Direct Pathway Neurons

As the striatum is composed of diverse cell types (Ciriachi et al., 2019; Tepper et al., 2010; Zhai et al., 2019), each with heterogeneous responses to dopamine depletion and levodopa (Hernandez et al., 2013; Liang et al., 2008; Ryan et al., 2018), we first sought to determine the cellular composition of TRAPed striatal neurons in vivo. As the two main cell types in the striatum are medium spiny projection neurons (MSNs) and local interneurons (INs), including cholingeric and GABAergic neurons, we first classified striatal units (n=268 units, N=14 mice) as either medium spiny neurons (MSNs) or putative interneurons (INs) using their action potential waveform (Barnes et al., 2005; Gage et al., 2010) (Figure S1A-G). Putative MSNs were then divided into three categories based on their response to levodopa: iMSN (levodopa-evoked decrease in firing rate; Figure 1H), dMSN (levodopa-evoked increase in firing rate; Figure 1I), or no response units (NR; no significant levodopa-evoked change in firing rate; Figure S1G), as described previously (Ryan et al., 2018). Consistent with histological (Chang et al., 1982; Graveland, et al., 1985) and in vivo electrophysiological studies (Hernandez et al., 2013), MSNs constituted the vast majority of recorded units, with roughly similar proportions of dMSNs and iMSNs (Figure 1G, left). However, while the majority of TRAPed striatal neurons were also MSNs, similar to the overall striatal population, they were highly enriched for putative dMSNs, with only a small proportion of putative INs and iMSNs (Figure 1G, right). These results are consistent with previous histological characterizations (Girasole et al., 2018) and demonstrate that TRAPed, LID-associated striatal neurons are primarily dMSNs.

TRAPed Direct Pathway Neurons Show Differential Responses to Levodopa In Vivo

While striatal neurons TRAPed during LID are predominantly dMSNs, not *all* dMSNs are TRAPed (Girasole et al., 2018). With this observation in mind, we sought to test whether TRAPed dMSNs show differential sensitivity to dopamine loss or acute administration of levodopa, which might underlie their preferential capture using FosTRAP. As the activity of dMSNs has been shown to be drastically reduced in parkinsonian mice (Parker et al., 2018; Ryan et al., 2018; Sagot et al., 2018), we first investigated how dopamine loss affected TRAPed dMSN firing. However, in the absence of levodopa, we found that the firing rates of TRAPed putative dMSNs were similar to those of all recorded putative dMSNs (All: 0.14 ± 0.03 Hz, n=123, N=14; TRAP: 0.14 ± 0.07 Hz, n=8, N=6; p=0.773, RS; Figure 1K), suggesting that chronic dopamine loss has a profound, but largely uniform, effect on dMSNs.

Given the firing rates of dMSNs in the parkinsonian state were similar, we next measured the response of these striatal subpopulations to levodopa. Previous evidence has demonstrated that functionally-defined subpopulations of dMSNs, with similar parkinsonian firing rates, exhibit enormous heterogeneity in their levodopa-evoked firing rates (Ryan et al., 2018). Thus, we hypothesized that TRAPed dMSNs might exhibit higher levodopa-evoked firing rates than other dMSNs. Indeed, TRAPed putative dMSNs achieved significantly higher levodopa-evoked firing rates than all recorded putative dMSNs (All: 2.62 ± 0.32 Hz, n=123, N=14; TRAP: 5.92 ± 1.92 Hz, n=8, N=6; p=0.033, RS; Figure 1K). In fact, TRAPed putative dMSN firing in response to levodopa was ~three-fold higher than those of optogenetically labeled dMSNs from healthy controls (Ryan et al., 2018) (1.61 ± 0.19 Hz, n=64, N=5; p=0.014, RS; Figure 1K).

In addition to changes in firing *rate*, levodopa has been shown to elicit divergent firing *patterns* across dMSN subpopulations, with the firing of only a subset of dMSNs reflecting dyskinesia severity (Ryan et al., 2018). Therefore, we investigated whether the pattern of TRAPed putative dMSN firing was more coupled to dyskinetic movements compared to other putative dMSNs. While there was large variation in the correlation of firing rate to dyskinesia (Figure 1L), even amongst putative dMSNs recorded on nearby electrodes in the same recording session (Fig 1M,N), TRAPed putative dMSNs were more correlated to dyskinesia on average (All: $R^2 = 0.24 \pm 0.02$; TRAP: $R^2 = 0.39 \pm 0.06$, p=0.033, RS; Figure 1O). In fact, TRAPed putative dMSNs showed a ~two-fold higher proportion of "dyskinesia-correlated" units compared to all putative dMSNs recorded (Figure S1H). Together, these results suggest that TRAPed dMSNs are more excited by levodopa in vivo, and their activity more tightly correlated to the severity of dyskinesia.

Based on these findings, we wondered whether heterogeneous cellular and synaptic properties of dMSNs might contribute to the differential response of TRAPed neurons to levodopa. To answer this question, we focused on two potential mechanisms: (1) enhanced excitability of TRAPed dMSNs and (2) greater excitatory synaptic input.

Dopamine Receptor Activation Increases the Excitability of TRAPed, but not unTRAPed, Direct Pathway Neurons

The excitability of dMSNs in vitro has been shown to be modulated by both chronic changes in dopamine (Fieblinger et al., 2014) and acute dopamine-receptor activation (Hernandez-Lopez et al., 2000; Lahiri and Bevan, 2020; Planert et al., 2013). Thus, we investigated whether chronic dopamine loss and replacement with levodopa or acute dopamine-receptor activation differentially

modulated MSN excitability. To address this question, we prepared acute brain slices from dopamine-depleted and levodopa-treated FosTRAP;Ai14;D2-GFP (FAD) mice, which allowed us to distinguish TRAPed from unTRAPed neurons via their expression of tdTomato and dMSNs from iMSNs via their expression of GFP (Figure 2A-B). We then performed whole-cell current-clamp recordings of TRAPed dMSNs, unTRAPed dMSNs and unTRAPed iMSNs, excluding TRAPed iMSNs due to their sparse expression (Girasole 2018). Using this approach, we assessed the cell autonomous effects of chronic and acute changes in dopamine-receptor activation on intrinsic excitability.

First, we measured the excitability of MSNs in baseline conditions, in the absence of dopaminergic stimulation, to assess whether chronic dopamine depletion and dopamine replacement with levodopa *alone* differentially modulated MSN excitability. We found that unTRAPed iMSNs (Figure 2C) and dMSNs (Figure 2D) exhibited low intrinsic excitability, characterized by a low input resistance and hyperpolarized resting membrane potential (Table 1), in line with previous studies in healthy mice (Planert et al., 2013). TRAPed dMSNs (Figure 2E) showed similarly low intrinsic excitability, with no significant differences in either passive or active membrane properties compared to unTRAPed MSNs (Table 1). We also compared the number of spikes generated with increasing current injections, to determine how responsive each cell type was to the same amount of depolarization. Interestingly, the average number of spikes in response to current injection was similar between TRAPed dMSNs (T dMSN: 7.34 ±0.82), unTRAPed dMSNs (unT dMSN: 7.69 ± 0.87), and unTRAPed iMSNs (unT iMSN: 5.82 ± 0.72, $\chi^2(2)$ 1.4949, p=0.474, KW; Figure 2F). The differential levodopa-evoked firing of TRAPed dMSNs in vivo is therefore likely not due to baseline differences in excitability between TRAPed and unTRAPed dMSNs.

Given the similar baseline excitability of TRAPed and unTRAPed dMSNs, the high levodopa-evoked firing of TRAPed dMSNs is likely dependent on acute dopamine receptor activation. We directly investigated whether acute activation of D1 dopamine-receptors differentially increases the excitability of TRAPed dMSNs by bath applying the D1-receptor specific agonist, SKF-81297 (5 μM), and measuring subsequent changes in excitability. In response to D1-receptor activation, we found that unTRAPed iMSNs showed no significant modulation of membrane properties (Table 1) or average number of spikes generated by current injection (Control: 4.41 ± 0.86 vs SKF: 4.97 ± 0.96, n=9, N=7, p=0.4076, SR; Figure 2C,G). Interestingly, we also found no significant change in unTRAPed dMSN membrane properties (Table 1) or average number of spikes generated by current injection in response to activating D1-receptors (Control: 8.12 ± 1.15 vs SKF: 8.37 ± 1.07, n=11, N=9, p=0.2785, SR; Figure 2D,H). However, D1-receptor activation significantly increased the excitability of TRAPed dMSNs, with a reduction in the minimum current needed to elicit spiking (rheobase, Control: 371.4 ± 29.0 mV vs SKF: 321 ± 31.8 mV, p=0.0078, SR, Table 1) and an increase in the average number of spikes generated by current injection (Control: 8.76 ± 1.15 vs SKF: 10.06 ± 1.15, n=14, N=11, p=0.0012, SR; Figure 2E,I). This differential sensitivity to dopamine may be one explanation for the high levodopa-evoked firing rates observed in TRAPed dMSNs in vivo.

Excitatory Monosynaptic Input onto Direct Pathway and TRAPed Striatal Neurons Are Reduced in LID

Given that action potential generation in MSNs is heavily dependent on excitatory synaptic input (Wickens and Wilson, 1998), we hypothesized that neurons TRAPed during LID might receive increased excitatory synaptic input. We sought to test this hypothesis by quantifying striatal

synaptic input, using a genetically-modified rabies virus to map monosynaptic connections in a cell-type specific manner (Figure 3A). D1-Cre, A2a-Cre, and FosTRAP^{CreER} mice were used to restrict rabies infection and subsequent labeling of monosynaptic inputs onto direct pathway, indirect pathway, and TRAPed striatal neurons, respectively (Figure 3B-C). Striatal "starter" cells and presynaptic rabies-labeled cell bodies were then detected, mapped onto the Allen Brain Atlas, and quantified by brain region (Figure 3D-G, S2A-D) (Eastwood et al., 2019). Using this approach, we sought to determine whether TRAPed striatal neurons received differential excitatory synaptic input, compared to dMSNs in LID.

However, we first needed to determine the effects of dopamine depletion and/or chronic treatment with levodopa on monosynaptic striatal inputs, as these changes have not been characterized using cell-type specific retrograde tracing. To identify the effects of chronic dopamine depletion and levodopa treatment, we compared the total amount and relative distribution of synaptic inputs onto dMSNs and iMSNs across three groups: (1) healthy control, (2) untreated parkinsonian, and (3) chronically levodopa-treated parkinsonian mice. In healthy controls, we found that iMSNs and dMSNs received similar amounts of extrastriatal synaptic input (Control: iMSN vs dMSN, p=0.114, RS) (Figure S2E), with the vast majority of presynaptic inputs originating from the ipsilateral cortex (primarily motor and somatosensory cortices), thalamus, and globus pallidus (Figure S2F-H). Interestingly, following dopamine depletion, dMSNs and iMSNs showed opposing changes in their synaptic inputs. Compared to healthy mice, there was a significant increase in the relative number of cortical neurons monosynaptically connected to iMSNs in parkinsonian mice ($\chi^2(2)$ 8.881, p=0.012, KW, Control vs Park, p=0.0498, Tukey), with no change in number of thalamic or pallidal neurons (Thalamus: $\chi^2(2)$ 8.214, p=0.017, KW, Control vs Park, p=0.184; Pallidum: $\chi^2(2)$ 8.257, p=0.016, KW, Control vs Park, p=0.171, Tukey;

Figure S2F-H). This increase in inputs from excitatory brain regions onto iMSNs was seen across the majority of cerebral cortices (Figure S2I), leading to a shift in total synaptic innervation of iMSNs in favor of cortical inputs ($\chi^2(2)$ 8.2143, p=0.017, KW, Control vs Park, p=0.027, Tukey; Figure 3H). In contrast, dMSNs showed no change in the relative number of monosynaptically connected cortical or thalamic neurons (Cortex: $\chi^2(2)$ 4.185, p=0.123, KW; Thalamus: $\chi^2(2)$ 1.161, p=0.560; Figure S2F,G), but a significant increase in pallidal neurons following dopamine depletion ($\chi^2(2)$ 12.310, p=0.002, KW, Control vs Park, p=0.0497, Tukey; Figure S2H). Despite the lack of change in the number of presynaptic cortical neurons, the increase in pallidal input led to a significant reduction in total relative proportion of synaptic innervation of dMSNs from the cortex ($\chi^2(2)$ 11.079, p=0.004, KW, Control vs Park, p=0.027, Tukey; Figure 3H). Overall, these findings suggest that the relative proportion of cortical inputs are decreased onto dMSNs, but increased onto iMSNs, in parkinsonian mice.

We next investigated how chronic levodopa administration in parkinsonian mice modulated the synaptic input onto dMSNs and iMSNs. Excitatory input onto iMSNs following chronic levodopa treatment was largely similar to untreated, parkinsonian mice (Cortex: Park vs LID, p=0.970; Thalamus: Park vs LID, p=0.343, Tukey), with a persistent increase in the relative number of cortical neurons compared to healthy controls (Cortex: Healthy vs LID, p=0.024, Tukey; Figure S2F,G). Interestingly, chronic levodopa treatment did cause an increase in pallidal input onto iMSNs that was not observed in untreated parkinsonian or healthy mice (Pallidum: Healthy vs LID, p=0.019; Park vs LID, p=0.029, Tukey; Figure S2H). As a result, while the relative number of cortical neurons innervating iMSNs remained high following chronic levodopa, the concomitant increase in pallidal input lead to an overall reduction in the relative proportion of cortical input onto iMSNs, similar to healthy controls ($\chi^2(2)$ 6.424, p=0.040, KW, Control vs LID,

p=0.702, Tukey; Figure 3H). Chronic levodopa administration also had little effect on synaptic inputs from either excitatory or inhibitory brain regions onto dMSNs (Cortex: Cortex: $\chi^2(2)$ 4.185, p=0.123, KW; Thalamus: $\chi^2(2)$ 1.161, p=0.560), with levodopa-treated mice showing a persistent elevation in pallidal input compared to healthy controls (Pallidum: Healthy vs LID, p=0.002, Tukey post-hoc; Figure S2F-H). These results suggest that chronic levodopa administration does not strongly modulate the synaptic inputs onto MSNs.

Although we observed a decrease in excitatory synaptic input onto dMSNs in LID, we sought to determine if TRAPed neurons exhibited differential synaptic connectivity, as an increase in excitatory or decrease in inhibitory input might underlie their excessive levodopa-evoked firing. Initially, we found that TRAPed neurons and dMSNs in LID had a similar relative number of presynaptic inputs (TRAP vs dMSN, p=0.132, RS), suggesting there was not a global increase or decrease in their total amount of synaptic input (Fig S2E). The relative number of inhibitory pallidal neurons innervating TRAPed neurons was also similar to dMSNs in LID (TRAP vs dMSN, p=0.310, RS; Figure S2H). However, contrary to the hypothesized *increase* in excitatory input, TRAPed neurons showed an even more profound *decrease* in cortical and thalamic inputs than dMSNs from similarly levodopa-treated parkinsonian mice (Cortex: TRAP vs dMSN, p=0.009; Thalamus: TRAP vs dMSN, p=0.041, RS; Figure S2F,G). This reduction in the number of cortical neurons was observed across most motor and somatosensory cortices (Figure S2I), leading to a striking reduction in their total proportion of cortical inputs (TRAP vs dMSN, p=0.002, RS; Figure 3H). Taken together, these results suggest that dopamine loss and chronic treatment with levodopa produce opposing changes in the synaptic inputs onto iMSNs and dMSNs, with a loss of corticostriatal input onto TRAPed neurons and dMSNs in LID.

Increased Presynaptic Excitatory Transmission onto TRAPed Direct Pathway Neurons

While rabies tracing experiments revealed *structural* synaptic differences between TRAPed neurons and dMSNs, this approach fails to capture *functional* differences in synaptic transmission. Therefore, to assess the functional strength of excitatory synapses onto TRAPed dMSNs, and unTRAPed dMSNs and iMSNs, we performed whole-cell voltage-clamp recordings in acute brain slices from levodopa-treated, parkinsonian FAD mice (Figure 4A). We first recorded miniature excitatory postsynaptic currents (mEPSCs; Figure 4B), as relative changes in mEPSC frequency and amplitude are largely thought to reflect presynaptic and postsynaptic properties, respectively. Initially, we found that the amplitude of mEPSCs was higher onto unTRAPed dMSNs than iMSNs (unT iMSN: 16.86 ± 0.54 pA, unT dMSN: 19.89 ± 0.47 pA, $p<0.001$, RS; Figure 4C). However, the amplitude of mEPSCs was similar between TRAPed and unTRAPed dMSNs (T dMSN: 21.22 ± 0.67 pA, $p=0.102$, RS; Figure 4C), suggesting that the number or distribution of postsynaptic glutamate receptors is greater in dMSNs than iMSNs, but that this enhancement is similar between TRAPed and unTRAPed dMSNs. Next, we found that the frequency of mEPSCs onto unTRAPed dMSNs was higher than iMSNs in dyskinetic mice (unT iMSN: 2.80 ± 0.36 Hz, unT dMSN: 3.87 ± 0.41 Hz, $p=0.034$, RS; Figure 4D). Interestingly, TRAPed dMSNs showed an even higher mEPSC frequency than unTRAPed dMSNs (T dMSN: 5.41 ± 0.47 Hz, $p=0.021$, RS; Figure 4D). These findings suggest that either the number or probability of neurotransmitter release at excitatory synapses onto dMSNs is higher than iMSNs in LID, with a preferential increase onto TRAPed dMSNs.

To examine these synaptic properties in greater detail, we performed additional whole-cell voltage-clamp recordings while evoking synaptic release from excitatory terminals using electrical intra-striatal stimulation (Figure 4E). Given the lack of observed differences in mEPSC amplitude

between TRAPed and unTRAPed dMSNs, the postsynaptic densities of excitatory a-amino-3-hydroxy-5-methyl-4-isoxazole propionic acid (AMPA) receptors would be expected to be similar between these two cell-types. We tested this prediction by eliciting EPSCs at different holding potentials and calculating the ratio of AMPA to N-methyl-D-aspartate (NMDA) receptor-mediated currents across these striatal subpopulations (Figure 4F). Indeed, we found that the AMPA/NMDA ratio was not significantly different between TRAPed and unTRAPed dMSNs (unT dMSN: 2.92 ± 0.28, T dMSN: 4.07 ± 0.63, p=0.376, RS; Figure 4G). Next, given the increased mEPSC frequency onto TRAPed dMSNs, we hypothesized that their excitatory synapses would show a higher probability of neurotransmitter release. We tested this hypothesis by measuring the amplitude of electrically-evoked EPSCs at varying interstimulus intervals to calculate the paired-pulse ratio (PPR; Figure 4H). Compared to unTRAPed iMSNs, synapses onto unTRAPed dMSNs showed a lower PPR on average, suggesting a higher probability of release at excitatory synapses (unT iMSN: 0.97 ± 0.016, unT dMSN: 0.92 ± 0.019, p=0.002, RS; Figure 4I). This effect was even more pronounced in TRAPed dMSNs, which exhibited a markedly low average PPR compared to unTRAPed dMSNs (T dMSN: 0.82 ± 0.14, p>0.001, RS; Figure 4I). Taken together, these results provide further evidence for a preferential increase in neurotransmitter release at excitatory synapses onto TRAPed dMSNs.

Both Motor Cortical and Thalamic Inputs onto TRAPed dMSNs Are Potentiated in LID.

While the preceding findings suggest that TRAPed dMSNs receive greater presynaptic excitatory input compared to unTRAPed dMSNs, they do not indicate where these inputs come from. Although excitatory input into the dorsolateral striatum is dominated by sensorimotor cortical and

thalamic projection neurons (Figure 3), these inputs exhibits distinct presynaptic properties (Ding et al., 2008). Therefore, we assayed the relative strength of these inputs by selectively expressing ChR2-eYFP in primary motor (M1), primary somatosensory (S1), or thalamic (Thal) neurons and measuring the light-evoked postsynaptic response to terminal field stimulation in TRAPed and unTRAPed dMSNs in FAD mice (Figure 5A,B). Due to the overlapping emission spectra of D2-GFP and ChR2-eYFP constructs, positive identification of GFP+ cell bodies was markedly reduced (Figure 5C), resulting in the exclusion of iMSNs from subsequent analyses.

Armed with this approach, we tested if excitatory drive onto TRAPed dMSNs was differentially regulated between cortical and thalamic inputs, compared to unTRAPed dMSNs. Both TRAPed and unTRAPed dMSNs exhibited optically-evoked EPSCs (oEPSCs) in response to activation of cortical and thalamic terminals, with increasing amplitude as light power was increased. However, the relative strength of motor and somatosensory cortical inputs seemed to be differentially regulated between TRAPed and unTRAPed dMSNs. While activation of M1 inputs elicited oEPSCs in TRAPed dMSNs that were two-fold greater than unTRAPe dMSNs (T dMSN: 1.06 ± 0.25 nA, unT dMSN: 0.42 ± 0.14 nA, p=0.002, SR; Figure 5D-G), activation of S1 inputs resulted in similar responses between these dMSN subpopulations (T dMSN: 0.21 ± 0.05 nA, unT dMSN: 0.13 ± 0.04 nA, p=0.073, SR; Figure 5H-K). We also found that enhanced excitatory drive onto TRAPed dMSNs was not restricted to cortical inputs, as activation of Thal inputs also produced larger oEPSCs in TRAPed dMSNs (T dMSN: 0.59 ± 0.18 nA, unT dMSN: 0.32 ± 0.11 nA, p=0.013, RS; Figure 5L-O). Together, these results demonstrate that TRAPed dMSNs receive stronger motor cortical and thalamic inputs than neighboring unTRAPed dMSNs.

3.4 Discussion

Historically, the striatum has been divided into anatomical or functional channels, composed of different cortico-striatal-thalamic circuits (Alexander and Crutcher, 1990), in which intermingled direct and indirect pathway neurons are embedded. One prominent example of this functional segregation comes from causal experiments showing optogenetic activation of direct pathway neurons (dMSNs) in the dorsolateral striatum (DLS) (Perez et al., 2017; Rothwell et al., 2015; Ryan et al., 2018), but not the dorsomedial striatum (DMS) (Kravitz et al., 2010), triggers dyskinesia in mice. These findings support a decades-old model, whereby the involuntary movements observed in levodopa-induced dyskinesia (LID) are hypothesized to result from the excessive activity of dMSNs in the DLS (Albin et al., 1989; DeLong, 1990). However, as this framework treats dMSNs within the DLS as a single pathway, with shared responses to levodopa, little is known regarding how heterogeneity amongst dMSNs contributes to the behavioral effects of levodopa. For instance, while hyperactivity of the direct pathway has been observed at the population level in mouse models of LID (Parker et al., 2018; Ryan et al., 2018; Sagot et al., 2018), only a subset of dMSNs exhibit this aberrant response to levodopa (Ryan et al., 2018). These findings suggest that levodopa differentially affects neurons within the direct pathway, which might explain how levodopa continues to provide therapeutic benefit even after the development of LID. Therefore, we sought to investigate whether underlying heterogeneity in the intrinsic or synaptic properties of dMSNs relate to their functional role in LID.

Using FosTRAP mice to selectively identify LID-associated striatal neurons, combined with optogenetically labeled in vivo recordings, we first sought to test whether TRAPed dMSNs exhibited differential patterns of activity in response to levodopa. While all recorded putative dMSNs had similar firing rates in the parkinsonian state (ie in the absence of exogenous

dopaminergic stimulation), levodopa elicited much higher firing rates in TRAPed putative dMSNs (Figure 1K). The excessive levodopa-evoked firing of TRAPed putative dMSNs was also more correlated with dyskinesia severity than other putative dMSNs (Figure 1O). Together, these findings provide mechanistic insights into the causal contribution of TRAPed neurons to dyskinesia (Girasole et al., 2018), and demonstrate that FosTRAP preferentially captures dMSNs with aberrant levodopa-evoked activity. Given these results, what cellular and synaptic changes might account for the over-activation of TRAPed dMSNs to levodopa?

We first turned to intrinsic differences between TRAPed and unTRAPed dMSNs. Previous evidence has shown that chronic parkinsonism results in an increase in the excitability of dMSNs (Fieblinger et al., 2014; Suarez et al., 2016), with chronic levodopa treatment resulting in no change (Suarez et al., 2016) or only partial restoration of dMSN excitability (Fieblinger et al., 2014). Additionally, a recent study in dyskinetic mice found that subpopulations of dMSNs, defined based on projection target, exhibited differential changes in excitability (Fieblinger et al., 2018). Therefore, chronic levodopa administration could restore the excitability of unTRAPed, but not TRAPed, dMSNs accounting for their lower levodopa-evoked firing. However, we found the excitability of unTRAPed and TRAPed dMSNs was similar in dyskinetic mice. Together with our in vivo recordings of putative dMSNs from chronically levodopa-treated mice, which showed an almost uniform loss of dMSN activity in the absence of levodopa, these results suggest chronic changes in excitability are unlikely to explain the differential response of LID-associated dMSNs to levodopa.

In addition to chronic changes in dopamine, acute dopamine receptor activation is known to increase the excitability of dMSNs in healthy mice using ex vivo slice electrophysiology (Hernández-López et al., 1997; Planert et al., 2013) However, how acute dopamine receptor

activation modulates dMSNs in brain slice from parkinsonian mice is unclear. A prevailing hypothesis is that changes in dopaminergic signaling, such as increased D1-dopamine receptor expression or enhanced downstream signaling cascades play a crucial role in LID (Aubert et al., 2005; Bezard et al., 2005; Guigoni et al., 2007; Jenner, 2008). The dyskinetic movements observed in LID also only occur in response to acute levodopa-evoked dopamine release (Jankovic, 2008), unlike other long-lasting forms of drug-induced dyskinesia, such as haloperidol-induced tardive dyskinesia (Caroff et al., 2018), highlighting the importance of acute dopamine-receptor activation in LID. Accordingly, hypersensitivity to dopamine receptor stimulation could contribute to the excessive levodopa-evoked firing seen in TRAPed dMSNs. In accordance with this theory, we found that D1-dopamine receptor activation caused a selective increase in the excitability of TRAPed dMSNs, which is likely to amplify their response to excitatory cortical and thalamic inputs, driving higher firing rates.

In addition to altered intrinsic properties, changes in the synaptic plasticity and connectivity of excitatory inputs onto dMSNs has been proposed as a key mechanism underlying the motor deficits in PD and LID (Cenci and Konradi, 2010; Gerfen and Surmeier, 2011). For instance, an aberrant increase in excitatory synaptic input could contribute to the excessive levodopa-evoked firing of dMSNs in LID. However, many studies in patients (McNeill et al., 1988; Villalba and Smith, 2018) and animal models of PD (Day et al., 2006; Fieblinger et al., 2014; Ingham et al., 1989; Suárez et al., 2014; Villalba et al., 2009) have largely found a reduction, not enhancement, in postsynaptic measures of connectivity (ie. dendritic morphology or spine density) in striatal neurons. While these postsynaptic changes would suggest a reduction in excitatory input, the *presynaptic* changes in connectivity that occur in PD and LID are largely unexplored. Therefore, we investigated synaptic connectivity at the presynaptic level, by mapping the monosynaptic

inputs onto iMSNs, dMSNs, and TRAPed striatal neurons in dyskinetic mice. Interestingly, TRAPed neurons showed a significantly lower relative number of presynaptic cortical and thalamic neurons compared to dMSNs (Figure S2F,G). The relative number of presynaptic neurons innervating dMSNs, however, showed little modulation following dopamine loss and chronic levodopa administration (Figure S2E-H), despite reports of reduced dendritic arborization and spine density (Fieblinger et al., 2014; Suárez et al., 2014). These results suggest *reduced*, as opposed to the hypothetically *enhanced*, excitatory inputs onto TRAPed neurons in LID – at least at the structural level. However, it is important to note that TRAPed striatal neurons include a small proportion of iMSNs and interneurons (Figure 1G) (Girasole et al., 2018), which may contribute to these differences between dMSNs and TRAPed striatal neurons. Given the limitation of using this approach, direct comparisons between TRAPed and unTRAPed dMSNs were not possible.

In contrast to dMSNs, the relative number of presynaptic cortical neurons innervating iMSNs in parkinsonian mice were drastically *upregulated*, which persisted even in chronically levodopa-treated mice (Figure S2F). Interestingly, these presynaptic changes are largely divergent from those seen postsynaptically. The dendritic arborization and spine density observed in iMSNs is reduced in parkinsonian mice (Fieblinger et al., 2014; Suárez et al., 2014); presumed to be "homeostatic" changes to compensate for the loss of D2-dopamine receptor mediated inhibition. These contrasting pre- and postsynaptic findings may be explained by methodological differences, for instance, postsynaptic changes in dendritic properties are likely driven by changes in the distribution/number of presynaptic terminals, which may not be reflected at the level of presynaptic cell bodies. Efficiency of synaptic tracing with the rabies virus has also been shown to be regulated in an activity dependent manner (Beier et al., 2017). However, the differences

between the presynaptic changes observed in this study and the postsynaptic changes observed by others (Fieblinger et al., 2014; Suárez et al., 2014) may also reflect divergent mechanisms regulating structural synaptic plasticity at the pre- and postsynaptic level in parkinsonism and LID, which are largely unknown.

While monosynaptic rabies tracing can reveal *structural* differences, we investigated whether these changes were reflected at the *functional* level using slice electrophysiology in ex vivo brain slices. Interestingly, opposing structural and functional changes have been previously observed in striatal neurons in parkinsonian mice (Fieblinger et al., 2014). In line with these results, contrary to the reduction in structural excitatory inputs onto TRAPed striatal neurons compared to dMSNs, we found that TRAPed dMSNs received *more* functional excitatory inputs, as evidenced by the increase in their frequency of miniature EPSCs (mEPSCs) (Figure 4D). This increase in the frequency of mEPSCs could be explained by an increase in excitatory synapses and/or synaptic plasticity leading to an increase in the probability of neurotransmitter release from presynaptic terminals.

Interestingly, several studies have highlighted aberrant striatal plasticity in parkinsonism and LID. Long-term depression (LTD) is impaired in parkinsonian mice (Bagetta et al., 2012; Calabresi et al., 1997; Kreitzer and Malenka, 2007; Shen et al., 2008) and aberrant forms of long-term potentiation (LTP), resistant to depotentiation, have been observed in LID (Picconi et al., 2003; Shen et al., 2008). We tested the possibility that the presynaptic inputs onto TRAPed dMSNs were preferentially facilitated. Activity-dependent plasticity can be measured using the paired-pulse ratio (PPR), as differences in the amplitude of a second EPSC elicited from a pair of stimuli is related to the probability of neurotransmitter release. Using this approach, we found excitatory inputs onto TRAPed dMSNs showed a drastic reduction in PPR compared to unTRAPed dMSNs,

suggesting enhanced probability of release (Figure 4H,I). Interestingly, previous findings suggest that unlabeled striatal neurons from dyskinetic rats show an aberrant form of LTP that is resistant to depotentiation (Picconi et al., 2003). Excitatory synapses onto TRAPed dMSNs preferentially exhibiting this aberrant form of LTP could be one explanation for this enhancement of release probability. These results, in addition to the lack of differences observed in the postsynaptic AMPA/NMDA ratio (Figure 4F,G), suggest that functional presynaptic excitatory transmission is enhanced preferentially in TRAPed dMSNs. We further investigated *which* presynaptic inputs onto TRAPed dMSNs were potentiated in LID, by selectively activating different cortical and thalamic inputs optogenetically. Excitatory motor cortical and thalamic, but not somatosensory cortical, inputs showed greater functional connectivity onto TRAPed dMSNs (Figure 5), suggesting they receive stronger innervation from multiple motor-related brain regions.

The excessive levodopa-evoked firing of TRAPed dMSNs in vivo may be explained by the selective dopamine-dependent increase in their excitability and strengthening of their presynaptic excitatory inputs from motor-related inputs. These results contribute to the increasing evidence for cellular and synaptic heterogeneity amongst dMSNs (Fieblinger et al., 2018; Gokce et al., 2016) and relates these properties to their functional role in mediating dyskinesia. Using this approach also provides a framework for a more precise dissection of the genetic, cellular, and circuit mechanisms that contribute to the therapeutic and dyskinetic effects of levodopa, which could lead to the development of more targeted pharmacological treatments for Parkinson's disease.

3.5 Experimental Procedures

Animals

We used 3-9 month old C57Bl/6 mice of either sex. Hemizygous FosTRAP mice (Liqun Luo, Stanford) were bred to either wild-type C57Bl/6 mice (WT, Jackson Labs) or homozygous Ai14 mice (Jackson Labs) to yield FosTRAP or FosTRAP;Ai14 mice. Hemizygous D2-GFP mice (Gong et al., 2007) were bred against WT mice to produce D2-GFP animals. For slice electrophysiology experiments, hemizygous FosTRAP;Ai14 mice were bred to hemizygous D2-GFP mice to yield FosTRAP;Ai14;D2-GFP mice. Animals were housed 1-5 per cage on a 12-hour light/dark cycle with *ad libitum* access to rodent chow and water. All behavioral manipulations were performed during the light phase. We complied with local and national ethical and legal regulations regarding the use of mice in research. All experimental protocols were approved by the UC San Francisco Institutional Animal Care and Use Committee.

Surgical Procedures

All surgical procedures were performed at 3-6 months of age. Anesthesia was induced with intraperitoneal (IP) injection ketamine/xylazine and maintained with 0.5%-1.0% inhaled isoflurane. Mice were placed in a stereotaxic frame and a mounted drill was used to create holes over the left medial forebrain bundle (MFB), the left dorsolateral striatum (DLS), primary motor cortex (M1), primary somatosensory cortex (S1), or thalamus (Thal). To render mice parkinsonian, the left MFB (-1.0 AP, +1.0 ML, -4.9 mm DV) was injected using a 33-gauge needle with 1-1.5 μL per site of 6-Hydroxydopamine (6-OHDA)-bromide. In some experiments, AAV5-DIO-ChR2-eYFP (UPenn Vector Core, 1-1.5 μL) was injected in the left DLS (+0.8 AP, +2.3 ML, -2.5 mm DV). For Cre-dependent rabies tracing experiments, 300 nL helper virus, rAAV1/synp-DIO-sTbEpB-GFP (UNC Vector Core, lot AV6118CD) was injected into two left DLS sites (-0.8 AP,

-2.4 ML, -2.5 DV). Two weeks after helper virus injection, 300nL modified EnvA G-deleted Rabies-mCherry (Salk Viral Vector Core) virus was also injected into the same t DLS site at 100 nL/min. For input-specific circuit mapping onto TRAPed cells, 250-300nL of AAV5-hSyn-hChR2(H134R)-eYFP (UNC Vector Core) was injected into M1 (+1.2 AP, -1.6 ML, -0.7 mm DV), S1 (+0.95 AP, -2.9 ML, -0.75 mm DV), or thalamus (-2.3 AP, -0.6 ML, +4.0 mm DV) in FosTRAP;WT mice. 6-OHDA and virus were injected at a rate of 0.10 μL/min, after which the injection cannula was left in place for 10-15 minutes prior to being withdrawn and the scalp being sutured.

In preparation for *in vivo* single-unit recordings, FosTRAP;Ai14 mice were injected with 6-OHDA and DIO-ChR2, as described above, and optrode arrays were implanted in a second surgical procedure. After the scalp was reopened, a large craniectomy (1.5 x 1 mm) was created over the left DLS, and two small holes were drilled in the right frontal and right posterior parietal areas for placement of a skull screw (Fine Scientific Tools, FST) and ground wire, respectively. A fixed multichannel electrode array (32 Tungsten microwires, Innovative Neurophysiology) coupled to a 200 μm optical fiber (Thorlabs) was slowly lowered through the craniectomy into the DLS. The final location of the electrode tips was targeted 100-200 μm above the previous DIO-ChR2 injection (-2.3-2.4 mm DV). The array was covered and secured into place with dental cement (Metabond) and acrylic (Ortho-Jet).

All animals were given buprenorphine (IP, 0.05 mg/kg) and ketoprofen (subcutaneous injection, 5 mg/kg) for postoperative analgesia. Parkinsonian animals were monitored closely for 1 week following surgery: mouse cages were kept on a heating pad, animals received daily saline injections and were fed nutritional supplements (Diet-Gel Recovery Packs and forage/trail mix).

Behavior

Postoperatively, parkinsonian mice were monitored in the open field 1-2 times per week for 10 minutes per session. All mice were habituated to the open field (clear acrylic cylinders, 25 cm diameter) for 30 minutes 1-2 days prior to behavioral sessions. The mice were monitored via two cameras, one directly above (to capture overall movement) and one in front of the chamber (to capture fine motor behaviors). Video-tracking software (Noldus Ethovision) was used to quantify locomotor activity, including rotations (90° contralateral or ipsilateral turns), distance traveled, and velocity. After a three-week baseline period, daily injections of levodopa commenced. Levodopa-induced dyskinesia (LID) was scored during weekly sessions in which mice were injected, then placed in a clean, clear cage for visualization. For regular weekly dyskinesia scoring, 1-2 blinded experimenters rated AIMs (for details see Statistical Procedures below). For in vivo electrophysiology experiments, rotations and AIMs were quantified in one-minute bins, with dyskinesia being scored every other minute.

Pharmacology

6-OHDA (Sigma Aldrich) for MFB dopamine depletions was prepared at 5 µg/µL in normal saline solution. Levodopa (Sigma Aldrich) was administered with benserazide (Sigma Aldrich) and prepared in normal saline solution. Levodopa (5-10 mg/kg) was given via IP injection 5-7 days per week over the course of the experiment. Initially, on the 7th day of levodopa treatment for FosTRAP;WT, FosTRAP;Ai14, and FosTRAP;Ai14;D2-GFP mice were given 4-hydroxytamoxifen (4-OHT, 50 mg/kg in Chen oil, IP) exactly one hour post-levodopa injection, to capture dyskinesia-associated neurons (Figure 1A). 4-OHT was prepared as previously described (Guenthner et al., 2013). Briefly, to prepare a 20 mg/mL stock in ethanol of 4-OHT, 4-OHT was added to 200 proof ethanol, vortexed, and placed on a horizontal shaker at 37° C for 30

minutes or until the 4-OHT dissolved. The stock solution was kept covered in foil to minimize light exposure. Next, to prepare a 10 mg/mL working solution in oil, the 4-OHT/ethanol mixture was combined with Chen Oil (a mixture of 4 parts sunflower seed oil and 1 part castor oil) and placed into 1.5 mL Eppendorf tubes. The tubes were vigorously mixed, wrapped in foil, and left on a nutator for 45 min at room temperature, vortexed and shaken periodically. The tubes were then placed in a speed-vac for 2-3 hours to evaporate the ethanol. If necessary, the final volume was adjusted with Chen Oil to 1 mL to reach a final concentration of 10 mg/mL. Both levodopa and 4-OHT were injected in a quiet, familiar environment, and animals were returned to their home cages, to minimize additional stimuli. Daily levodopa injections continued for 2-6 weeks to allow expression of Cre-dependent constructs. For *in vitro* experiments, picrotoxin (Sigma) was dissolved in warm water to prepare a 5 mM stock solution, which was subsequently diluted in ACSF for a final concentration of 50 μM. Tetrodotoxin (TTX, Abcam) was dissolved in water at a stock concentration of 1 mM and added to ACSF for a final concentration of 1 μM. SKF 81298 (Tocris) was dissolved in water at a concentration of 1mM and added to ACSF for a final concentration of 5 μM. For all *in vitro* experiments, biocytin (1-2.5 mg/mL) was included in the internal solution for post-hoc confirmation of the presence or absence of Ai14 and D2-GFP.

***In Vivo* Electrophysiology**

Two weeks after optrode array implantation, mice were habituated to tethering and the recording chamber for 1-2 days. After habituation, experimental sessions occurred 3-5 times per week for 2-6 weeks. During each session, electrical signals (single-unit and LFP data from each of 32 channels) were collected using a multiplexed 32 channel headstage (Triangle Biosystems), an electrical commutator equipped with a fluid bore (Dragonfly), filtered, amplified, and recorded on a MAP system, using RASPUTIN 2.4 HLK3 acquisition software (Plexon). Spike waveforms

were filtered at 154–8800 Hz and digitized at 40 kHz. The experimenter manually set a gain and threshold for storage of electrical events.

During recording sessions, after a baseline period of 30 minutes in the parkinsonian state, levodopa (5-10 mg/kg) was injected IP. After a period of 2-3 hours of recording spontaneous activity in the open field, an optogenetic cell identification protocol was applied (Girasole et al., 2018) consisting of 100 msec blue light pulses, given at 1 Hz. At each of 4 light powers (0.5, 1, 2, and 4 mW), 1000 light pulses were delivered via a lightweight patch cable (Doric Lenses) connected to a blue laser (Shanghai Laser and Optics Century), via an optical commutator (Doric Lenses), and controlled by TTL pulses from a behavioral monitoring system (Noldus Ethovision).

Single-units were identified offline by manual sorting using Offline Sorter 3.3.5 (Plexon) and principle components analysis (PCA). Clusters were considered to represent a single unit if (1) the unit's waveforms were statistically different from multiunit activity and any other single-units on the same wire, in 3D PCA space, (2) no interspike interval <1 msec was observed. Single-units were then classified as putative medium spiny neurons (MSNs) or interneurons (INs) as previously described (Barnes et al., 2005; Berke et al., 2004; Gage et al., 2010; Harris et al., 2000) using features of the spike waveform (peak to valley and peak width), as well as inter-spike interval distribution.

After single-units had been selected for further study, their firing activity was analyzed using NeuroExplorer 4.133 (Nex Technologies). To determine if a unit was optogenetically identified, a peristimulus time histogram was constructed around the onset of laser pulses. To be considered optogenetically identified, a unit had to fulfill 3 criteria: (1) the unit had to increase firing rate above the 99% confidence interval of the baseline within 15 msec of laser onset; (2) the

unit's firing was above this threshold for at least 15 msec; (3) the unit's laser-activated waveforms were not statistically distinguishable from spontaneous waveforms.

***In Vitro* Electrophysiology**

Prior to terminal anesthesia and preparation of brain slices, animals (3-9 months) were co-injected with levodopa and benserazide (5-10 mg/kg and 2.5-5 mg/kg, respectively) to induce LID. After 30-45 minutes in the dyskinetic state, mice were deeply anesthetized with an IP ketamine-xylazine injection, transcardially perfused with ice-cold glycerol-based slicing solution, decapitated, and the brain was removed. Glycerol-based slicing solution contained (in mM): 250 glycerol, 2.5 KCl, 1.2 NaH_2PO_4, 10 HEPES, 21 $NaHCO_3$, 5 glucose, 2 $MgCl_2$, 2 $CaCl_2$. The brain was mounted on a submerged chuck, and sequential 275 μm coronal slices were cut on a vibrating microtome (Leica), transferred to a chamber of warm (34° C) carbogenated ACSF containing (in mM) 125 NaCl, 26 $NaHCO_3$, 2.5 KCl, 1 $MgCl_2$, 2 $CaCl_2$, 1.25 NaH_2PO_4, 12.5 glucose for 30-60 minutes, then stored in carbogenated ACSF at room temperature. Each slice was then submerged in a chamber superfused with carbogenated ACSF at 31-33°C for recordings.

Striatal medium spiny neurons were targeted for recordings using differential interference contrast (DIC) optics in FosTRAP;Ai14;D2GFP mice on a Olympus BX 51 WIF microscope. In FosTRAP;Ai14;D2GFP mice, TRAPed neurons were identified by their td-Tomato positive somata and D2 positive neurons were identified by GFP fluorescence. Fluorescence-negative neurons with GABAergic interneuron physiological properties (membrane tau decay <1 ms for both fast-spiking and persistent low-threshold spiking subtypes; input resistance >500 MΩ in persistent low-threshold spiking subtype) were excluded from the analysis.

Neurons were patched in whole-cell voltage-clamp configurations using borosilicate glass electrodes (3-5 MΩ) filled with cesium-based (voltage-clamp) or potassium methanesulfonate-

based (current-clamp) internal solution. Cesium based solution containing (in mM) respectively: 120 $CsMeSO_3$, 15 CsCl, 8 NaCl, 0.5 EGTA, 10 HEPES, 2 MgATP, 0.3 NaGTP, 5 QX-314, pH 7.3. Potassium based solution containing (in mM): 130 $KMeSO_3$, 10 NaCl, 2 $MgCl_2$, 0.16 $CaCl_2$, 0.5 EGTA, 10 HEPES, 2 MgATP, 0.3 NaGTP, pH 7.3. Picrotoxin (50 μM) was added to the external solution to block synaptic currents mediated by $GABA_A$ receptors. Drugs were prepared as stock solutions and added to the ACSF to yield the final concentration.

Whole-cell recordings were made using a MultiClamp 700B amplifier (Molecular Devices) and ITC-18 A/D board (HEKA). Data was acquired using Igor Pro 6.0 software (Wavemetrics) and custom acquisition routines (mafPC, courtesy of M. A. Xu-Friedman). Both voltage clamp and current-clamp recordings were filtered at 2 kHz and digitized at 10 kHz. All recorded neurons exhibited electrophysiological characteristics of medium spiny neurons. All synaptic currents were recorded with a cesium-based internal and monitored at a holding potential of -70 mV. Series resistance and leak currents were monitored continuously. Miniature EPSCs were recorded at –70 mV in 1 μM TTX and 50 μM picrotoxin. Evoked EPSCs onto medium spiny neurons were elicited in the presence of picrotoxin (50 μM) with a stimulus isolator (IsoFlex, AMPI) and a glass electrode placed dorsolateral to the recorded neuron, typically 100-200 μm away. Stimulus intensity was adjusted to yield EPSC amplitudes of approximately 400 pA with a stimulus duration was 300 μs. For evaluation of the paired pulse ratio, two stimuli were given at variable interstimulus intervals (ISIs; 25, 50, 100, 200, 500 ms) with a 20 sec intertrial interval. Paried-pulse ratio is defined as $EPSC_2/EPSC_1$. Five-eight repetitions at each ISI were averaged to yield the PPR for that ISI. For monitoring of EPSC amplitude over time, two pulses delivered with 50 ms interstimulus interval were given every 20 seconds. For AMPA/NMDA ratio experiments, one stimulus at -70 mV or +40 mV was given every 20 seconds, at 15-20 repetitions per holding

potential. AMPA/NMDA ratios were calculated as the ratio of the magnitude of the EPSC at +40 mV at 50 ms following stimulation (NMDA) to the peak of the EPSC at -70 mV (AMPA). To evoke ChR2-mediated synaptic currents from M1, S1, or thalamus, excitatory currents were optically evoked using 2 ms pulses of 473 nm light ranging in light powers of 0.5, 1, 2, and 4 mW and delivered by a TTL-controlled LED (Olympus) passed through a GFP filter (Chroma).

Current-clamp recordings were made to measure intrinsic properties of striatal neurons. The resting membrane potential (V_m) was measured as the average V_m 5-10 minutes after break-in. A series of small negative current steps were delivered from rest to calculate the input resistance of each cell. Rheobase and other input-output properties were obtained by giving a series of square-wave current steps, ranging from 100 pA to 600 pA, in 100 pA increments, with a 10 sec interstimulus interval. Application of drugs, such as SKF-81298, was applied after achieving a stable baseline 5-10 minutes after break-in. Changes in intrinsic properties due to SKF were assessed 10-15 minutes after drug wash-in.

Monosynaptic Rabies Tracing

D1-Cre and A2a-Cre mice were used to perform monosynaptic retrograde tracing onto direct and indirect pathway neurons, respectively. Groups of healthy (non-depleted), parkinsonian, and parkinsonian/levodopa-treated mice were used within each genotype. Mice were rendered parkinsonian as described above. Four weeks after dopamine depletion, animals received daily injections of levodopa. Parkinsonian mice (one week into daily levodopa injections) or untreated healthy mice, were then anesthetized and a Cre-dependent helper virus (AAV-DIO- sTpEpB-GFP) was stereotaxically injected into the left DLS (ipsilateral to the depletion in parkinsonian mice). The helper virus (AAV-DIO- sTpEpB-GFP) expresses the EnvA receptor (TVA) and rabies glycoprotein necessary for rabies infection and replication in a cell-type specific manner, termed

"starter cells," which are labeled with the green fluorophore GFP. After animals recovered for two weeks, they were anesthetized and a replication-incompetent form of the rabies virus (EnvA-G-deleted-rabies-mCherry) was stereotaxically injected into the DLS using the same coordinates. The rabies virus will then infect a subset of starter cells (co-infected) and travel retrogradely one synapse, expressing the red fluorophore mCherry in infected cells. Once the rabies virus infects a presynaptic neuron, uninfected with the helper virus, it will no longer be capable of replication and/or retrograde synaptic infection. Rabies injections were performed in an approved Biosafety Level 2 (BSL-2) surgical suite. Animals were then allowed to recover for ten days, at which point they were terminally anesthetized with ketamine/xylazine (200/40 mg/kg I.P.), transcardially perfused with 4% paraformaldyde (PFA), and the brain dissected from the skull. The brain was post-fixed overnight in 4% PFA and then placed in 30% sucrose at 4°C.

Parkinsonian, levodopa-treated FosTRAP;WT mice were prepared in a similar fashion as D1-Cre and A2a-Cre mice, with some alterations made to the experimental timeline to accommodate helper virus expression using the conditional Cre (CreER) in the FosTRAP line. In FosTRAP mice, helper virus was injected in the left DLS at the same time as the initial dopamine depletion. Three weeks after dopamine depletion, FosTRAP mice began daily levodopa injections. After one week of daily levodopa injections, as above, FosTRAP mice were injected with levodopa followed by an injection of 4-OHT, allowing for recombination and expression of the helper virus. Two weeks later, FosTRAP mice were anesthetized and the modified rabies virus was injected using the same procedures described above. The remainder of the experimental timeline was similar to that for D1-Cre and A2a-Cre mice as described above.

Fixed brains, stored in sucrose, were then sent to Charles Gerfen at the National Institutes of Mental Health (NIMH) for sectioning, mounting, imaging, and analysis using published

methods (Eastwood et al., 2019). Briefly, brains were sectioned coronally at 50 μm using a freezing microtome. Slices are then imaged using a Zeiss microscope equipped with a z axis drive, imaging each fluorophore. Cell detection and registration was done using NeuroInfo software. Custom analysis scripts were then written in MATLAB for quantification. The relative number of presynaptic neurons was quantified by dividing the total number of presynaptic neurons in the specified brain region by the total number of co-infected (sTpEpB, green and rabies, red) striatal neurons. The relative proportion of presynaptic neurons was quantified by dividing the total number of presynaptic neurons in the specified brain region by the total number of presynaptic (rabies-labeled, red) extra-striatal neurons detected in the whole brain.

Histology & Microscopy

After rabies tracing or behavioral experiments, mice were deeply anesthetized with IP ketamine-xylazine and transcardially perfused with 4% paraformaldehyde in PBS. Following *in vivo* electrophysiology experiments, prior to perfusion, electrode array location was marked by electrolytic lesioning. After deep anesthesia, the implant was connected to a solid state, direct current (DC) Lesion Maker (Ugo Basile). A current of 100 μA was passed through each microwire for 5 seconds. After perfusion, the brain was dissected from the skull and post-fixed overnight in 4% paraformaldehyde, then placed in 30% sucrose at 4°C for cryoprotection. The brain was then cut into 35 μm coronal or sagittal sections on a freezing microtome (Leica) and then mounted in Vectashield Mounting Medium onto glass slides for imaging. For immunohistochemistry, the tissue was blocked with 3% normal donkey serum (NDS) and permeabilized with 0.1% Triton X-100 for 2 hours at room temperature on a shaker. Primary antibodies were added to 3% NDS and incubated overnight at 4° C on a shaker. Primary antibodies used: Rabbit anti-TH (Pel-Freez, 1:1000), Chicken anti-TH (Sigma, 1:1000), and Chicken anti-GFP (1:500). Slices were then

incubated in secondary antibodies (donkey anti-rabbit or chicken Alexafluor 488, 593, or 647, 1:500, JacksonImmuno Research) for 2-4 hours at 4°C on a shaker, washed, and mounted onto slides for imaging. 4 or 10x images were acquired on a Nikon 6D conventional widefield microscope.

For slice electrophysiology experiments in which the internal solution contained biocytin, slices were subsectioned at 50 um and washed in PBS. Slices were blocked for 2 hours at room temperature on a shaker in a 5% NDS and 0.3% Tween-20 PBS-based solution. Primary antibodies were the same as described above. Slices were then incubated in secondary antibodies (donkey anti-rabbit or chicken Alexafluor 488, 593, or 647, 1:500, JacksonImmuno Research and Streptavidin Alexa 350, 3:500, Sigma) for 6-12 hours at 4°C on a shaker, washed, and mounted onto slides for imaging. Images were acquired on a Nikon 6D conventional widefield or Nikon Spinning Disk confocal microscope with a 40x objective microscope. Exposure times were matched between images of the same type. Post-hoc confirmation of cellular identify of a subset of recovered biocytin-filled, recorded cells revealed that online identification by experimenter using fluorescence intensity was >90% in FosTRAP;Ai14;D2-GFP mice for TRAPed dMSNs and unTRAPed dMSNs and iMSNs. The rate of positive identification of TRAPed and unTRAPed dMSNs in FosTRAP:Ai14;D2-GFP mice injected with ChR2-eYFP in M1, S1, or Thal was also > 90%, however, due to the overlap of YFP and GFP emission spectra, our positive rates of identification of unTRAPed iMSNs was reduced to ~60%, leading to the exclusion of unTRAPed iMSNs from these experiments (Figure 5).

QUANTIFICATION AND STATISTICAL ANALYSIS

Statistics

All data are presented as the mean ± SEM, with N referring to the number of animals and n to the number of cells.

Behavior

Dyskinesia was quantified using a standard scoring method (Cenci and Lundblad, 2007), which takes into account abnormal involuntary movements (AIMs) in axial, limb, and orofacial (ALO) body segments. Briefly, dyskinesia was quantified every 20 minutes, over a two-hour period, using a scale of 0-4. A score of 0 indicates no abnormal movement, and a score of 4 describes continuous and uninterruptable dyskinetic movements; 12 (4 x 3 body segments) is the maximum score possible for a given time point. Dyskinesia was quantified every other minute during in vivo electrophysiology experiments.

In Vitro Electrophysiology

Paired comparisons between TRAPed and unTRAPed dMSNs or unTRAPed dMSNs and iMSNs were made with a nonparametric Wilcoxon ranksum (RS) test. Comparisons between TRAPed dMSNs and unTRAPed dMSNs and iMSNs were made using a nonparametric Krusal-Wallis (KW) test, with a posthoc Tukey test. For mEPSC frequency and amplitude measurements, only cells with at least 500 events were included in the. Cumulative probability plots were generated from 500 randomly selected mEPSC events per cell. Changes in excitability in response to acute SKF application were analyzed by comparing a 10-minute baseline period with the value 10-15 minutes after drug application. Average amplitudes of oEPSCs were quantified manually in Igor. A nonparametric Wilcoxon sign-rank (SR) test was used to compare oEPSC amplitude from M1, S1, or thatalmus onto FosTRAP;Ai14;D2-GFP MSNs. In all

experiments involving optical stimulation, data was drawn from stimulations at 0.5, 1, 2 ,4 mW, with statistical comparisons being made at 4 mW (Figure 5G,K,O).

***In Vivo* Electrophysiology**

For the majority of analyses of single-unit firing rate and behavior, firing rate was averaged in 1 minute bins. Modulation of firing rate by levodopa was determined by comparing single-unit firing rates before and after drug administration, during the peak behavioral effects. The 30-minute baseline period was compared to a 30-minute period following drug injection (10-40 minutes post-injection). Following levodopa administration, unlabeled single-units were categorized into three broad groups as follows, based on significant changes in firing rate ($p < 0.01$, Wilcoxon rank-sum test (RS)) following levodopa treatment: putative dMSNs (On MSNs, increase in firing rate), putative iMSNs (Off MSNs, decrease in firing rate), or no change units (NC, nonsignificant change in firing rate) (Figure 1G). For levodopa sessions, putative dMSNs were further divided using behavior-based methods, as described previously (Ryan et al., 2018). For the behavior-based method, AIM scores were also averaged in 1 minute bins and correlated with firing rate using linear regression. Labeled TRAPed neurons or putative dMSNs with a significant correlation ($R^2 > 0.30$) to AIM score were labeled dyskinesia (DYSK) units and those with no significant correlation ($R^2 < 0.35$) to AIMs were classified as on-unclassified (ON) units (Figures 1L-M and Supp Figure 1H).

Firing rates of parkinsonian mice before (Park) and after drug administration (levodopa (LID), Figure 1K) were compared between optogetnetically labeled TRAPed putative dMSNs and all putative dMSNs using Wilcoxon ranksum test (RS). Comparisons of firing rates between optogenetically labeled TRAPed neurons optogenetically labeled dMSNs from healthy controls (Figure 1K; data obtained from Ryan, et al., 2018) using Wilcoxon ranksum (RS). Comparisons

between the average dyskinesia correlation of optogenetically labeled TRAPed and all putative dMSNs were made using Wilcoxon ranksum test (RS).

3.6 Author Contributions and Acknowledgements

MBR, AEG and ABN designed the experiments. MBR and AEG conducted the in vivo electrophysiological recordings and MBR did the analysis. MBR, AEG and ABN conducted the whole cell voltage- and current clamp recordings, measuring intrinsic excitability and spontaneous or electrically-evoked excitatory transmission in acute brain slices. MBR and ABN performed experiments using whole cell voltage-clamp to measure optically-evoked synaptic transmission. MBR and AEG performed the viral injections and behavior for rabies tracing experiments, which were sectioned and imaged by CP and CRG. MBR wrote the manuscript, with input from AEG and ABN.

3.7 Figures

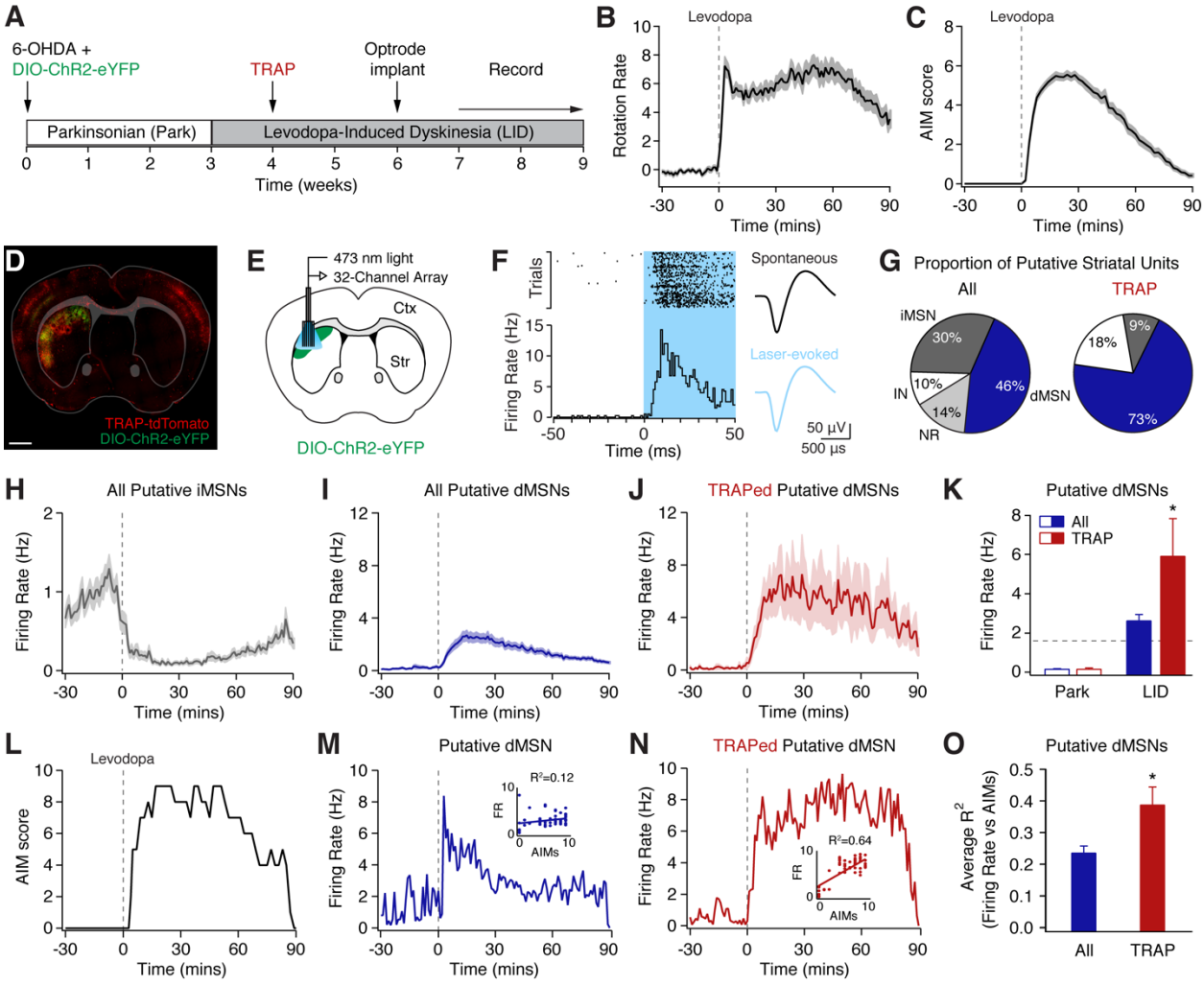
A
6-OHDA +
DIO-ChR2-eYFP
TRAP
Optrode
implant
Record
Parkinsonian (Park)
Levodopa-Induced Dyskinesia (LID)
Time (weeks)
B
Levodopa
Rotation Rate
Time (mins)
C
Levodopa
AIM score
Time (mins)
D
TRAP-tdTomato
DIO-ChR2-eYFP
E
473 nm light
32-Channel Array
Ctx
Str
DIO-ChR2-eYFP
F
Trials
Firing Rate (Hz)
Time (ms)
Spontaneous
Laser-evoked
50 µV
500 µs
G
Proportion of Putative Striatal Units
All
TRAP
iMSN
30%
46%
IN
10%
14%
NR
dMSN
18%
9%
73%
H
All Putative iMSNs
I
All Putative dMSNs
J
TRAPed Putative dMSNs
K
Putative dMSNs
All
TRAP
Park
LID
L
Levodopa
AIM score
M
Putative dMSN
R²=0.12
FR
AIMs
N
TRAPed Putative dMSN
R²=0.64
O
Putative dMSNs
Average R²
(Firing Rate vs AIMs)
All
TRAP

3.1 Figure 1. Optogenetically Identified TRAPed Striatal Neurons Show Differential Responses to Levodopa In Vivo.

(A) Experimental timeline.

(B) Average rotation rate (contralesional-ipsilesional rotations per minute) of parkinsonian mice, aligned to levodopa injection at t=0 (N=14).

(C) Average dyskinesia, measured using the Abnormal Involuntary Movement (AIM) score, of parkinsonian mice, aligned to levodopa injection at t=0 (N=14).

(D) Coronal histology from FosTRAPxAi14 mouse, showing TRAPed neurons (red) and ChR2-expressing neurons (green). Scale bar = 1 mm.

(E) Coronal schematic of viral injection (DIO-ChR2-eYFP) and optrode array implanted in the dorsolateral striatum.

(F) Representative optogenetically labeled TRAPed striatal unit. Left: perievent raster of a subset of the 4000 laser trials (top) and perievent histogram (bottom), aligned to laser at t=0. Right: average spontaneous (top) and laser-evoked (bottom) waveform.

(G) Proportion of all (left; n=268, N=14) and optically labeled TRAPed (right; n=11, N=8) putative striatal units, including putative interneurons (IN), and direct pathway (dMSN), indirect pathway (iMSN), and no response (NR) striatal units. **(H-J)** Average firing rate of putative iMSNs (n=81, N=14), dMSNs (n=117, N=14), and optically labeled TRAPed dMSNs (n=8, N=6), aligned to levodopa injection at t=0.

(K) Average firing rate of all putative dMSNs (blue) and optogenetically labeled TRAPed putative dMSNs (red) in parkinsonian mice before (Park) and after levodopa administration (LID). Dotted line represents the firing rate of optogenetically labeled dMSNs from healthy controls (Ryan, 2018).

(L-N) A representative single recording session. **(L)** Dyskinesia score **(M)** Representative putative dMSN **(N)** Representative optogenetically labeled TRAPed putative dMSN. Inset: firing rate vs dyskinesia score.

(O) Average correlation (R^2) of firing rate to dyskinesia for all (blue) and TRAPed (red) putative dMSNs. n=single units, N=mice. All data presented as mean ± SEM. See also Figure S1.

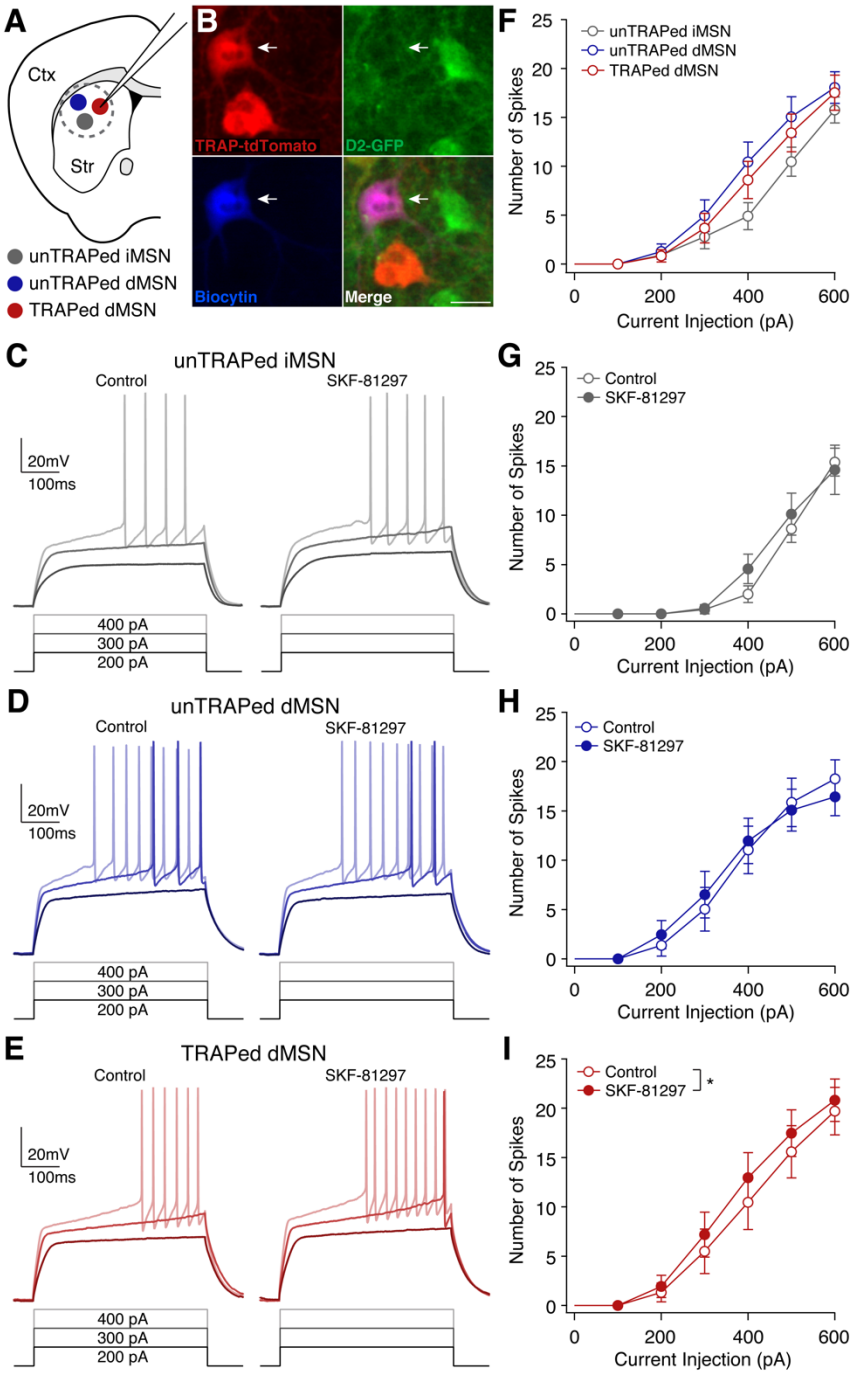
A
Ctx
Str
unTRAPed iMSN
unTRAPed dMSN
TRAPed dMSN
B
TRAP-tdTomato
D2-GFP
Biocytin
Merge
C
unTRAPed iMSN
Control
SKF-81297
20mV
100ms
400 pA
300 pA
200 pA
D
unTRAPed dMSN
Control
SKF-81297
20mV
100ms
400 pA
300 pA
200 pA
E
TRAPed dMSN
Control
SKF-81297
20mV
100ms
400 pA
300 pA
200 pA
F
unTRAPed iMSN
unTRAPed dMSN
TRAPed dMSN
Number of Spikes
Current Injection (pA)
G
Control
SKF-81297
Number of Spikes
Current Injection (pA)
H
Control
SKF-81297
Number of Spikes
Current Injection (pA)
I
Control
SKF-81297
*
Number of Spikes
Current Injection (pA)

3.2 Figure 2. Activation of D1 Dopamine Receptors Enhances the Excitability of TRAPed, but not unTRAPed, dMSNs.

(A) Coronal schematic depicting recordings of unTRAPed iMSNs (gray), unTRAPed dMSNs (blue), and TRAPed dMSNs (red) in the dorsolateral striatum of FosTRAPxAi14xD2-GFP (FAD) mice.

(B) High magnification histological image from a FAD mouse, showing TRAPed neurons (tdTomato; red), D2-expressing neurons (GFP; green), and biocytin-filled TRAPed dMSN (blue). Scale bar = 20 µm.

(C-E) Voltage traces in response to current injections before (left) and 10-15 minutes after bath application of the D1R-agonist, SKF-81297 (right) for a representative unTRAPed iMSN (C), unTRAPed dMSN (D), and TRAPed dMSN (E).

(F) Baseline current-response curves for unTRAPed iMSNs (gray, n=17, N=11), unTRAPed dMSNs (blue, n=17, N=13), and TRAPed dMSNs (red, n= 22, N=14).

(G-I) Current-response curves before (Control) and 10-15 minutes after bath application of the D1R-agonist (SKF-81297) for unTRAPed iMSNs (n=9, N=6; G), unTRAPed dMSNs (n=11, N=9; H), and TRAPed dMSNs (n=14, N=10; I).

n=cells, N=mice. Data presented as mean ± SEM. See also Tables 1-2.

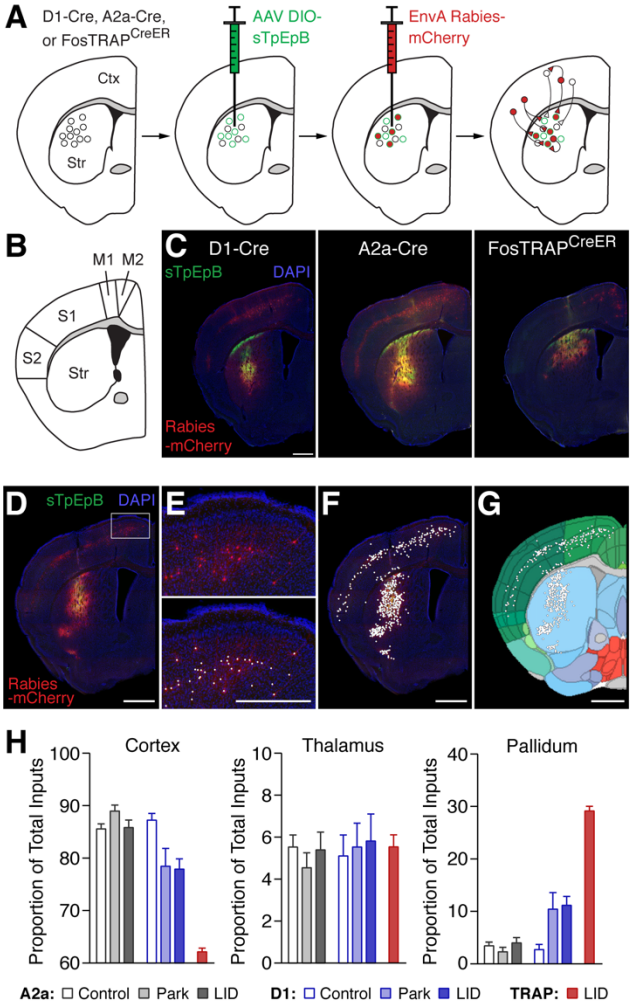

3.3 Figure 3. Monosynaptic Rabies Tracing onto Indirect Pathway, Direct Pathway, and TRAPed Striatal Neurons.

(A) Experimental approach, using a dual viral strategy, to achieve Cre-dependent, rabies tracing of monosynaptic inputs onto direct pathway (D1-Cre), indirect pathway (A2a-Cre), and TRAPed (FosTRAP^{CreER}) striatal neurons.

(B) Coronal schematic with labeled motor and somatosensory cortices.

(C) Low magnification histological sections showing helper virus expressing neurons (sTpEpB, green) and rabies-labeled neurons (Rabies-mCherry, red) in D1-Cre (left), A2a-Cre (middle), and FosTRAP^{CreER} (right) mice. DAPI = nuclear stain for visualization.

(D-G) Quantification of presynaptic rabies-labeled cell bodies. (D) Low magnification image of coronal section showing helper (green) and rabies (red) viral injection sites. (E) High magnification of the image in (D), with overlaid points denoting rabies-positive presynaptic cell bodies (bottom). (F) Low magnification image showing coronal section with overlaid cell detection. (G) Low magnification image showing the projection of detected cell bodies onto the Allen Brain Atlas for quantification by brain region.

(H) The average proportion of all extra-striatal rabies labeled cell bodies identified in the cortex (left), thalamus (middle), and globus pallidus (right). A2a: Control, N=6, Park, N=4, LID, N=4; D1: Control, N=9, Park, N=10, LID, N=6; TRAP: LID, N=6.

Data presented as mean ± SEM. N= animals. Scale bars = 1 mm. See also Figure S2.

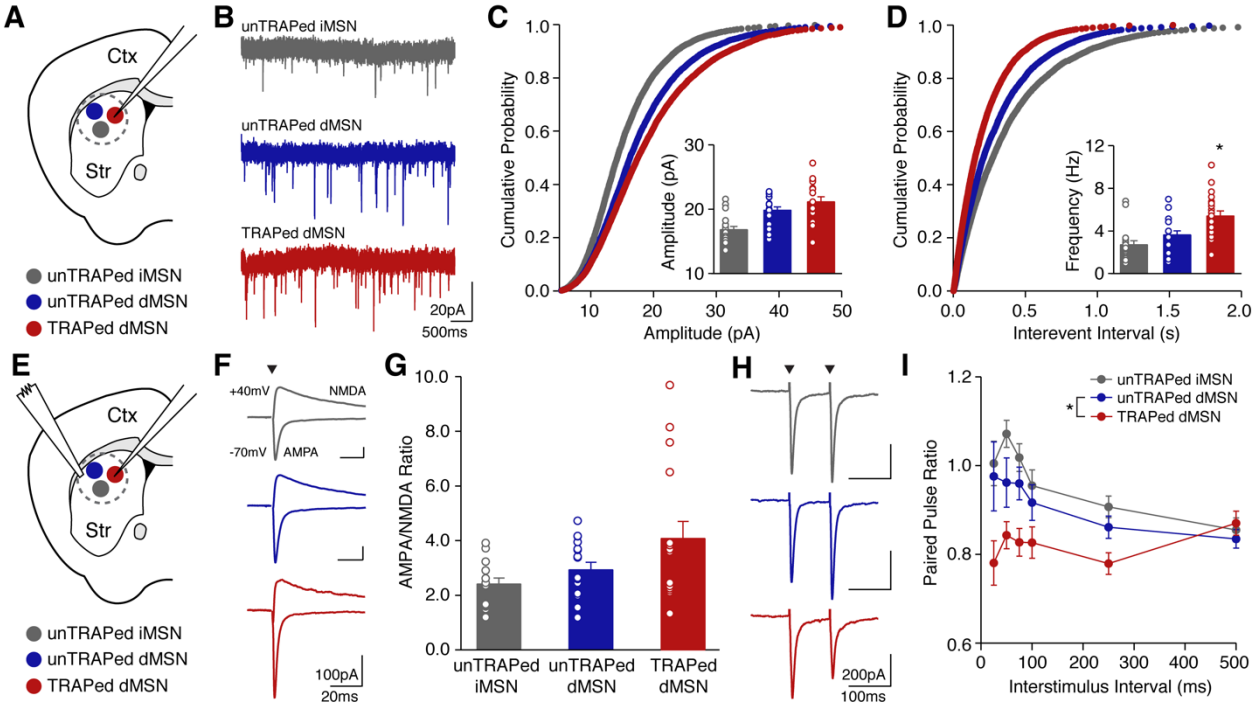

3.4 Figure 4. Increased Presynaptic Excitatory Transmission onto TRAPed dMSNs.
(A) Coronal schematic depicting recordings of unTRAPed iMSNs (gray), unTRAPed dMSNs (blue), and TRAPed dMSNs (red) in the dorsolateral striatum of FosTRAPxAi14xD2-GFP (FAD) mice.
(B) Representative miniature EPSCs (mEPSCs) recorded from an unTRAPed iMSN (top), unTRAPed dMSN (middle), and TRAPed dMSN (bottom).
(C) Cumulative probability of mEPSC amplitude. Inset: average mEPSC amplitude (unTRAPed iMSNs: n=21, N=8; unTRAPed dMSNs: n=20, N=7; TRAPed dMSNs: n=20, N=8).
(D) Cumulative probability of mEPSC interevent intervals. Inset: average mEPSC frequency (unTRAPed iMSNs: n=21, N=8; unTRAPed dMSNs: n=20, N=7; TRAPed dMSNs: n=20, N=8).
(E) Coronal schematic depicting recordings and electrical stimulation of unTRAPed iMSNs (gray), unTRAPed dMSNs (blue), and TRAPed dMSNs (red) in the dorsolateral striatum of FosTRAPxAi14xD2-GFP (FAD) mice.
(F) Representative EPSCs recorded at holding potentials of -70mV and +40mV to measure AMPA- and NMDA-mediated currents, respectively. Arrowheads denote timing of the electrical stimulus
(G) AMPA/NMDA ratio of unTRAPed iMSNs (n=14, N=7), unTRAPed dMSNs (n=16, N=9), and TRAPed dMSNs (n=16, N=8).
(H) Representative EPSCs elicited by a pair of intra-striatal electrical stimuli. Arrowheads denoting the timing of the electrical stimuli.
(I) Paired pulse ratio (2^{nd} EPSC/1^{st}EPSC) versus interstimulus interval for unTRAPed iMSNs (n=17, N=8), unTRAPed dMSNs (n=18, N=9), and TRAPed dMSNs (n=22, N=9).
n=cells, N=mice. Data presented as mean ± SEM.

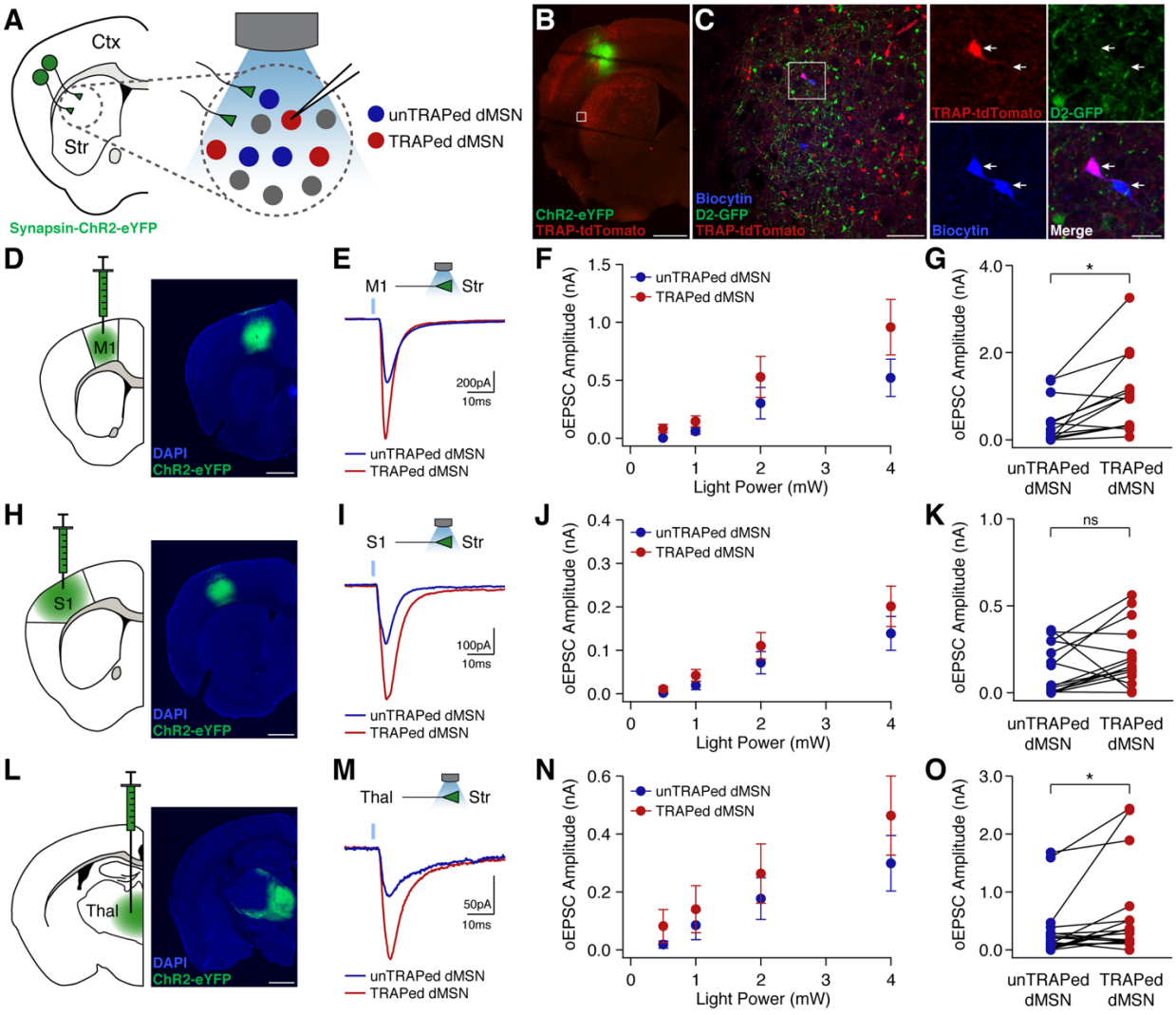
A
Ctx
Str
Synapsin-ChR2-eYFP
unTRAPed dMSN
TRAPed dMSN
B
ChR2-eYFP
TRAP-tdTomato
C
Biocytin
D2-GFP
TRAP-tdTomato
TRAP-tdTomato
D2-GFP
Biocytin
Merge
D
M1
DAPI
ChR2-eYFP
E
M1
Str
200pA
10ms
unTRAPed dMSN
TRAPed dMSN
F
unTRAPed dMSN
TRAPed dMSN
oEPSC Amplitude (nA)
Light Power (mW)
G
*
oEPSC Amplitude (nA)
unTRAPed dMSN
TRAPed dMSN
H
S1
DAPI
ChR2-eYFP
I
S1
Str
100pA
10ms
unTRAPed dMSN
TRAPed dMSN
J
unTRAPed dMSN
TRAPed dMSN
oEPSC Amplitude (nA)
Light Power (mW)
K
ns
oEPSC Amplitude (nA)
unTRAPed dMSN
TRAPed dMSN
L
Thal
DAPI
ChR2-eYFP
M
Thal
Str
50pA
10ms
unTRAPed dMSN
TRAPed dMSN
N
unTRAPed dMSN
TRAPed dMSN
oEPSC Amplitude (nA)
Light Power (mW)
O
*
oEPSC Amplitude (nA)
unTRAPed dMSN
TRAPed dMSN

3.5 Figure 5. Strengthened Motor Cortical and Thalamic Inputs onto TRAPed dMSNs
(A) Coronal schematic depicting expression of Synapsin-ChR2-eYFP in a given input region and recording optically-evoked currents from unTRAPed dMSNs (blue), and TRAPed dMSNs (red) in the dorsolateral striatum of FosTRAPxAi14xD2-GFP (FAD) mice.
(B) Low magnification of coronal section with Synapsin-ChR2-eYFP expression in primary motor cortex (green) and TRAPed neurons (red). Scale bar = 1mm.
(C) Left: high magnification of dorsolateral striatum, showing TRAPed neurons (red), D2R-expressing neurons (green), and a pair of biocytin-filled neurons (blue). Scale bar = 100 μm Right: higher magnification showing a sequentially recorded TRAPed and unTRAPed dMSN pair. Scale bar = 25 μm.
(D-G) Optical activation of primary motor cortical inputs (M1, n=19, N=4).
(H-K) Optical activation of primary somatosensory cortical inputs (S1, n=13, N=7).
(L-O) Optical activation of thalamic inputs (Thal, n=15, N=5).
(D,H,L) Coronal schematic (left) and histological section (right) of viral expression of Synapsin-ChR2-eYFP. Scale bar = 1 mm.
(E,I,M) Schameitc (top) and representative examples of optically-evoked EPSCs (oEPSCs) for a unTRAPed (blue) and TRAPed (red) dMSNs (bottom).
(F,J,N) Average oEPSC amplitude versus light power for unTRAPed (blue) and TRAPed (red) dMSNs.
(G,K,O) Average oEPSC amplitude at 4mW for unTRAPed (blue) and TRAPed (red) dMSNs.
n=pairs, N=mice. Data presented as mean ± SEM.

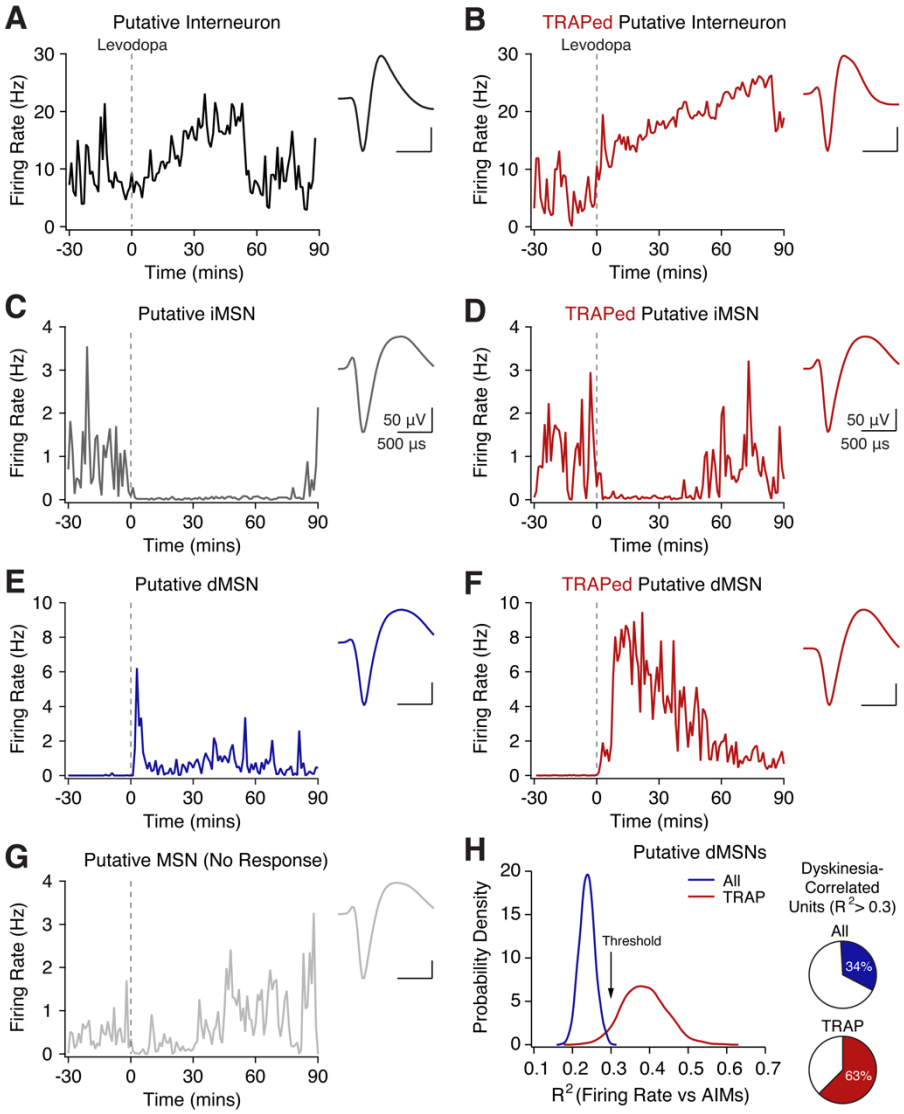

3.6 Figure S1. Optically Labeled TRAPed Putative dMSNs Show Altered Responses to Levodopa In Vivo. Related to Figure 1.

(A-G) Representative single units from parkinsonian mice treated with levodopa. Left: single unit firing rates, aligned to levodopa administration at t=0. Right: average waveform.

(A-B) Putative interneuron (A) and optogenetically labeled TRAPed putative interneuron (B).

(C-D) Putative iMSN (C) and optogenetically labeleld TRAPed putative iMSN (D).

(E-F) Putative dMSN (E) and optogenetically labeled TRAPed putative dMSN (F).

(G) Putative MSN with no response to levodopa

(H) Left: Probability density plot of average correlation (R^2) obtained from bootstrapping all putative dMSN (blue) and optogenetically labeled TRAPed putative dMSN data (red). Right: Proportion of all (n=117, N=14) and TRAPed (n=8, N=6) putative dMSNs with a significant correlation ($R^2 > 0.3$) between firing rate and dyskinesia score.

n=single units, N=mice.

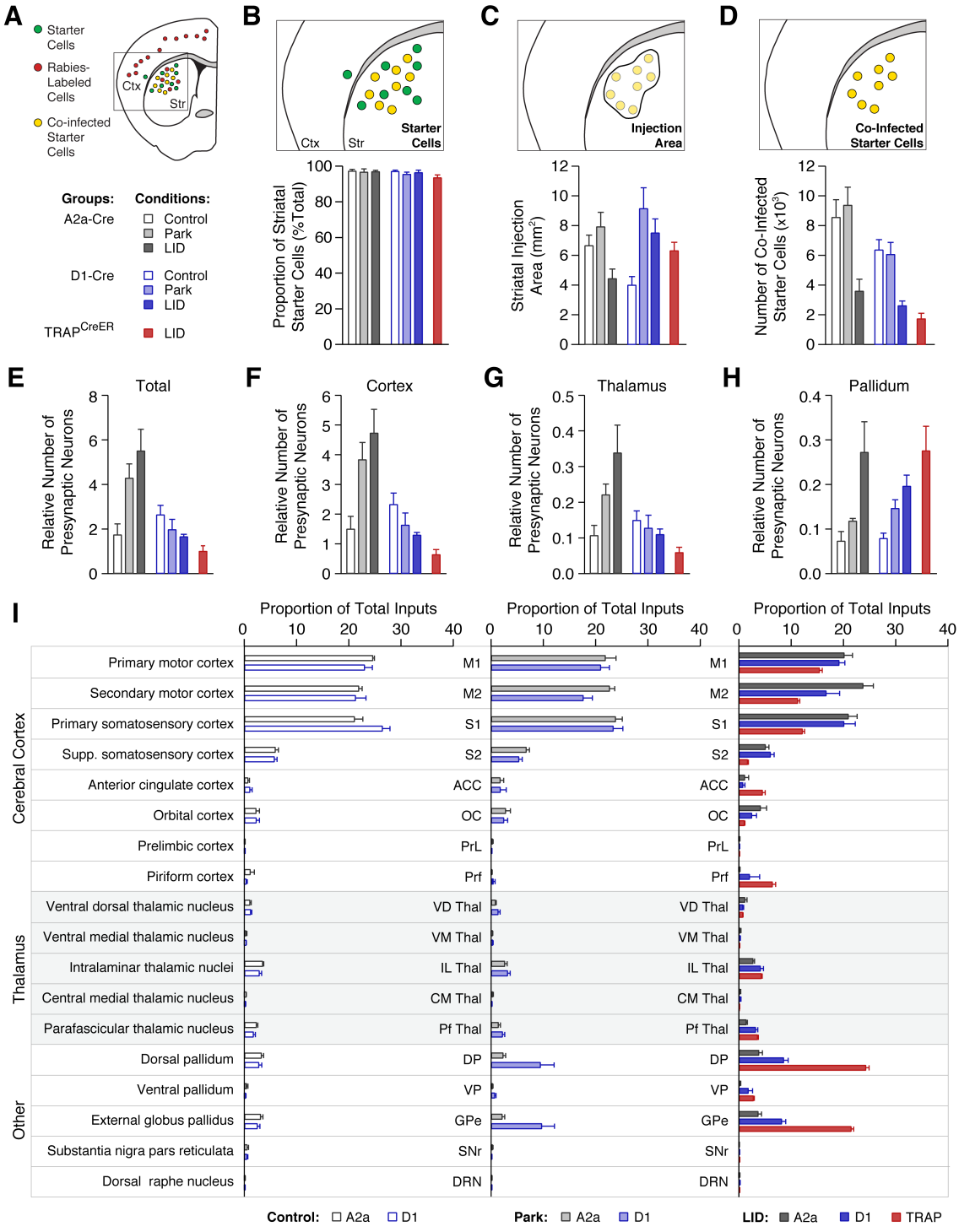
A
Starter Cells
Rabies-Labeled Cells
Co-infected Starter Cells
Ctx
Str
Groups:
Conditions:
A2a-Cre
Control
Park
LID
D1-Cre
Control
Park
LID
TRAPCreER
LID
B
Starter Cells
Proportion of Striatal Starter Cells (%Total)
C
Injection Area
Striatal Injection Area (mm2)
D
Co-Infected Starter Cells
Number of Co-Infected Starter Cells (x10³)
E
Total
F
Cortex
G
Thalamus
H
Pallidum
Relative Number of Presynaptic Neurons
I
Proportion of Total Inputs
Primary motor cortex
Secondary motor cortex
Primary somatosensory cortex
Supp. somatosensory cortex
Anterior cingulate cortex
Orbital cortex
Prelimbic cortex
Piriform cortex
Ventral dorsal thalamic nucleus
Ventral medial thalamic nucleus
Intralaminar thalamic nuclei
Central medial thalamic nucleus
Parafascicular thalamic nucleus
Dorsal pallidum
Ventral pallidum
External globus pallidus
Substantia nigra pars reticulata
Dorsal raphe nucleus
M1
M2
S1
S2
ACC
OC
PrL
Prf
VD Thal
VM Thal
IL Thal
CM Thal
Pf Thal
DP
VP
GPe
SNr
DRN
Cerebral Cortex
Thalamus
Other
Control: A2a D1
Park: A2a D1
LID: A2a D1 TRAP

3.7 Figure S2. Monosynaptic Rabies Tracing onto Indirect Pathway, Direct Pathway, and TRAPed Striatal Neurons. Related to Figure 3.

(A) Top: Coronal schematic of starter (green), rabies-labeled (red), and co-infected starter (yellow) cells. Bottom: Description of the groups and treatment conditions.

(B-D) Top: coronal schematic showing quantification approach. Bottom: quantification of injection site. (B) The proportion of striatal starter cells (sTpEpB positive) compared to all brain-wide starter cells. (C) Striatal injection area, quantified by the extent of co-infected cells in the striatum. (D) The total number of co-infected striatal neurons.

(E-H) The relative number of presynaptic neurons, calculated as the number of extra-striatal labeled neurons relative to the number of co-infected striatal neurons for all extra-striatal brain regions (E), cortex (F), thalamus (G), and globus pallidus (H).

(I) Summary quantification of the proportion of extra-striatal rabies labeled cells from a given brain region. A2a: Control, N=6, Park, N=4, LID, N=4; D1: Control, N=9, Park, N=10, LID, N=6; TRAP: LID, N=6. Data presented as mean ± SEM. N= animals.

3.8 Tables

Table 1. Baseline Passive and Active Membrane Properties of MSNs. Related to Figure 2.
Passive (input resistance and resting membrane potential) and active properties (action potential threshold, after-hyperpolarization amplitude, spike width, and rheobase) of excitability in the absence of dopamine receptor stimulation. Data presented as mean ± SEM.

	unTRAPed iMSNs	unTRAPed dMSNs	TRAPed dMSNs	p-value
Input Resistance (MOhm)	79.1 ± 9.5	81.1 ± 5.8	82.3 ± 7.1	0.503
Resting Membrane Potential (mV)	-88.3 ± 1.0	-89.2 ± 0.9	-89.4 ± 0.8	0.542
Action Potential Threshold (mV)	-39.8 ± 2.7	-38.9 ± 1.5	-38.9 ± 1.8	0.834
AHP Amplitude (mV)	15.6 ± 1.1	13.8 ± 1.1	14.7 ± 1.0	0.238
Spike Width (ms)	1.8 ± 0.1	2.0 ± 0.1	2.1 ± 0.1	0.159
Rheobase (pA)	406.1 ± 39.6	341.2 ± 25.1	384.2 ± 7.1	0.447

Table 2. Passive and Active Membrane Properties of MSNs in Response to the D1-receptor specific agonist, SKF-81297. Related to Figure 2.
Passive (input resistance and resting membrane potential) and active properties (action potential threshold, after-hyperpolarization amplitude, spike width, and rheobase) of excitability before (Control) and 10-15 minutes after bath application of a D1-specific agonist (SKF-81297). Bolded values represent significant p-values, following Bonferroni correction for multiple comparisons. Data presented as mean ± SEM.

	unTRAPed iMSNs			unTRAPed dMSNs			TRAPed dMSNs		
	Control	SKF-81297	p-value	Control	SKF-81297	p-value	Control	SKF-81297	p-value
Input Resistance (MOhm)	79.8 ± 13.8	91.8 ± 14.5	0.383	82.0 ± 7.8	99.9 ± 13.4	0.032	89.4 ± 8.7	90.4 ± 8.3	0.925
Resting Membrane Potential (mV)	-89.8 ± 0.8	-86.8 ± 3.1	0.469	-90.5 ± 1.1	-89.0 ± 1.3	0.320	-90.3 ± 1.0	-90.0 ± 1.6	0.791
Action Potential Threshold (mV)	-39.5 ± 3.5	-38.5 ± 3.0	0.313	-37.5 ± 1.9	-35.9 ± 1.6	0.910	-38.9 ± 2.3	-38.7 ± 2.8	0.910
AHP Amplitude (mV)	21.4 ± 3.2	20.8 ± 3.3	0.148	28.8 ± 3.3	22.8 ± 2.5	0.700	27.1 ± 2.3	22.9 ± 3.9	0.204
Spike Width (ms)	1.8 ± 0.2	2.2 ± 0.7	0.313	2.0 ± 0.1	2.1 ± 0.1	0.049	2.1 ± 0.6	2.2 ± 0.7	0.233
Rheobase (pA)	440.0 ± 51.5	405 ± 51.9	0.250	345.8 ± 29.2	312.5 ± 28.3	0.125	**371.4 ± 29.0**	**321.4 ± 31.8**	**0.0078**

3.9 References

Ahlskog, J.E., and Muenter, M.D. (2001). Frequency of levodopa-related dyskinesias and motor fluctuations as estimated from the cumulative literature. Mov. Disord. *16*, 448–458.

Albin, R.L., Young, A.B., and Penney, J.B. (1989). The functional anatomy of basal ganglia disorders. Trends Neurosci. *12*, 366–375.

Alcacer, C., Andreoli, L., Sebastianutto, I., Jakobsson, J., Fieblinger, T., and Cenci, M.A. (2017). Chemogenetic stimulation of striatal projection neurons modulates responses to Parkinson's disease therapy. Journal of Clinical Investigation *127*, 720–734.

Alexander, G.E., and Crutcher, M.D. (1990). Functional architecture of basal ganglia circuits: neural substrates of parallel processing. Trends Neurosci. *13*, 266–271.

Andersson, M., Hilbertson, A., and Cenci, M.A. (1999). Striatal fosB expression is causally linked with l-DOPA-induced abnormal involuntary movements and the associated upregulation of striatal prodynorphin mRNA in a rat model of Parkinson's disease. Neurobiol. Dis. *6*, 461–474.

Aquino, C.C., and Fox, S.H. (2015). Clinical spectrum of levodopa-induced complications. Mov. Disord. *30*, 80–89.

Aubert, I., Guigoni, C., Håkansson, K., Li, Q., Dovero, S., Barthe, N., Bioulac, B.H., Gross, C.E., Fisone, G., Bloch, B., et al. (2005). Increased D1 dopamine receptor signaling in levodopa-induced dyskinesia. Ann. Neurol. *57*, 17–26.

Bagetta, V., Sgobio, C., Pendolino, V., Del Papa, G., Tozzi, A., Ghiglieri, V., Giampà, C., Zianni, E., Gardoni, F., Calabresi, P., et al. (2012). Rebalance of striatal NMDA/AMPA receptor ratio

underlies the reduced emergence of dyskinesia during D2-like dopamine agonist treatment in experimental Parkinson's disease. J. Neurosci. *32*, 17921–17931.

Barbera, G., Liang, B., Zhang, L., Gerfen, C.R., Culurciello, E., Chen, R., Li, Y., and Lin, D.-T. (2016). Spatially Compact Neural Clusters in the Dorsal Striatum Encode Locomotion Relevant Information. Neuron *92*, 202–213.

Barnes, T.D., Kubota, Y., Hu, D., Jin, D.Z., and Graybiel, A.M. (2005). Activity of striatal neurons reflects dynamic encoding and recoding of procedural memories. Nature *437*, 1158–1161.

Bateup, H.S., Santini, E., Shen, W., Birnbaum, S., Valjent, E., Surmeier, D.J., Fisone, G., Nestler, E.J., and Greengard, P. (2010). Distinct subclasses of medium spiny neurons differentially regulate striatal motor behaviors. Proc. Natl. Acad. Sci. U.S.A. *107*, 14845–14850.

Beckstead, R.M., Domesick, V.B., and Nauta, W.J. (1979). Efferent connections of the substantia nigra and ventral tegmental area in the rat. Brain Res. *175*, 191–217.

Beier, K.T., Kim, C.K., Hoerbelt, P., Hung, L.W., Heifets, B.D., DeLoach, K.E., Mosca, T.J., Neuner, S., Deisseroth, K., Luo, L., et al. (2017). Rabies screen reveals GPe control of cocaine-triggered plasticity. Nature *549*, 345–350.

Beitz, J.M. (2014). Parkinson's disease: a review. Front Biosci (Schol Ed) *6*, 65–74.

Benazzouz, A., Breit, S., Koudsie, A., Pollak, P., Krack, P., and Benabid, A.-L. (2002). Intraoperative microrecordings of the subthalamic nucleus in Parkinson's disease. Mov. Disord. *17 Suppl 3*, S145-149.

Bergman, H., Wichmann, T., Karmon, B., and DeLong, M.R. (1994). The primate subthalamic nucleus. II. Neuronal activity in the MPTP model of parkinsonism. J. Neurophysiol. *72*, 507–520.

Berke, J.D., Okatan, M., Skurski, J., and Eichenbaum, H.B. (2004). Oscillatory entrainment of striatal neurons in freely moving rats. Neuron *43*, 883–896.

Bezard, E., Gross, C.E., Qin, L., Gurevich, V.V., Benovic, J.L., and Gurevich, E.V. (2005). l-DOPA reverses the MPTP-induced elevation of the arrestin2 and GRK6 expression and enhanced ERK activation in monkey brain. Neurobiology of Disease *18*, 323–335.

Bhidayasiri, R., and Truong, D.D. (2008). Motor complications in Parkinson disease: clinical manifestations and management. J. Neurol. Sci. *266*, 204–215.

Boraud, T., Bezard, E., Guehl, D., Bioulac, B., and Gross, C. (1998). Effects of L-DOPA on neuronal activity of the globus pallidus externalis (GPe) and globus pallidus internalis (GPi) in the MPTP-treated monkey. Brain Res. *787*, 157–160.

Borgkvist, A., Avegno, E.M., Wong, M.Y., Kheirbek, M.A., Sonders, M.S., Hen, R., and Sulzer, D. (2015). Loss of Striatonigral GABAergic Presynaptic Inhibition Enables Motor Sensitization in Parkinsonian Mice. Neuron *87*, 976–988.

Brimblecombe, K.R., and Cragg, S.J. (2017). The Striosome and Matrix Compartments of the Striatum: A Path through the Labyrinth from Neurochemistry toward Function. ACS Chem Neurosci *8*, 235–242.

Calabresi, P., Saiardi, A., Pisani, A., Baik, J.H., Centonze, D., Mercuri, N.B., Bernardi, G., and Borrelli, E. (1997). Abnormal synaptic plasticity in the striatum of mice lacking dopamine D2 receptors. J. Neurosci. *17*, 4536–4544.

Caroff, S.N., Ungvari, G.S., and Cunningham Owens, D.G. (2018). Historical perspectives on tardive dyskinesia. J. Neurol. Sci. *389*, 4–9.

Carta, M., Lindgren, H.S., Lundblad, M., Stancampiano, R., Fadda, F., and Cenci, M.A. (2006). Role of striatal L-DOPA in the production of dyskinesia in 6-hydroxydopamine lesioned rats. J. Neurochem. *96*, 1718–1727.

Cenci, M.A., and Konradi, C. (2010). Maladaptive striatal plasticity in L-DOPA-induced dyskinesia. Prog. Brain Res. *183*, 209–233.

Cenci, M.A., and Lundblad, M. (2007). Ratings of L-DOPA-induced dyskinesia in the unilateral 6-OHDA lesion model of Parkinson's disease in rats and mice. Curr Protoc Neurosci *Chapter 9*, Unit 9.25.

Chang, H.T., Wilson, C.J., and Kitai, S.T. (1982). A Golgi study of rat neostriatal neurons: light microscopic analysis. J. Comp. Neurol. *208*, 107–126.

Chen, M.-T., Morales, M., Woodward, D.J., Hoffer, B.J., and Janak, P.H. (2001). In Vivo Extracellular Recording of Striatal Neurons in the Awake Rat Following Unilateral 6-Hydroxydopamine Lesions. Experimental Neurology *171*, 72–83.

Choi, K., Holly, E., Davatolhagh, M.F., Beier, K.T., and Fuccillo, M.V. (2019). Integrated anatomical and physiological mapping of striatal afferent projections. Eur J Neurosci *49*, 623–636.

Ciriachi, C., Svane-Petersen, D., and Rickhag, M. (2019). Genetic tools to study complexity of striatal function. J. Neurosci. Res. *97*, 1181–1193.

Costa, R.M., Lin, S.-C., Sotnikova, T.D., Cyr, M., Gainetdinov, R.R., Caron, M.G., and Nicolelis, M.A.L. (2006). Rapid alterations in corticostriatal ensemble coordination during acute dopamine-dependent motor dysfunction. Neuron *52*, 359–369.

Cui, G., Jun, S.B., Jin, X., Pham, M.D., Vogel, S.S., Lovinger, D.M., and Costa, R.M. (2013). Concurrent activation of striatal direct and indirect pathways during action initiation. Nature *494*, 238–242.

Dautan, D., Huerta-Ocampo, I., Witten, I.B., Deisseroth, K., Bolam, J.P., Gerdjikov, T., and Mena-Segovia, J. (2014). A major external source of cholinergic innervation of the striatum and nucleus accumbens originates in the brainstem. J. Neurosci. *34*, 4509–4518.

Day, M., Wang, Z., Ding, J., An, X., Ingham, C.A., Shering, A.F., Wokosin, D., Ilijic, E., Sun, Z., Sampson, A.R., et al. (2006). Selective elimination of glutamatergic synapses on striatopallidal neurons in Parkinson disease models. Nat. Neurosci. *9*, 251–259.

Deffains, M., and Bergman, H. (2015). Striatal cholinergic interneurons and cortico-striatal synaptic plasticity in health and disease. Mov. Disord. *30*, 1014–1025.

Deffains, M., Iskhakova, L., Katabi, S., Haber, S.N., Israel, Z., and Bergman, H. (2016). Subthalamic, not striatal, activity correlates with basal ganglia downstream activity in normal and parkinsonian monkeys. Elife *5*.

DeLong, M.R. (1990). Primate models of movement disorders of basal ganglia origin. Trends Neurosci. *13*, 281–285.

Ding, J., Peterson, J.D., and Surmeier, D.J. (2008). Corticostriatal and Thalamostriatal Synapses Have Distinctive Properties. Journal of Neuroscience *28*, 6483–6492.

Eastwood, B.S., Hooks, B.M., Paletzki, R.F., O'Connor, N.J., Glaser, J.R., and Gerfen, C.R. (2019). Whole mouse brain reconstruction and registration to a reference atlas with standard histochemical processing of coronal sections. Journal of Comparative Neurology *527*, 2170–2178.

Fieblinger, T., Graves, S.M., Sebel, L.E., Alcacer, C., Plotkin, J.L., Gertler, T.S., Chan, C.S., Heiman, M., Greengard, P., Cenci, M.A., et al. (2014). Cell type-specific plasticity of striatal projection neurons in parkinsonism and L-DOPA-induced dyskinesia. Nat Commun *5*, 5316.

Fieblinger, T., Zanetti, L., Sebastianutto, I., Breger, L.S., Quintino, L., Lockowandt, M., Lundberg, C., and Cenci, M.A. (2018). Striatonigral neurons divide into two distinct morphological-physiological phenotypes after chronic L-DOPA treatment in parkinsonian rats. Sci Rep *8*, 10068.

Filion, M., and Tremblay, L. (1991). Abnormal spontaneous activity of globus pallidus neurons in monkeys with MPTP-induced parkinsonism. Brain Res. *547*, 142–151.

Flaherty, A.W., and Graybiel, A.M. (1991). Corticostriatal transformations in the primate somatosensory system. Projections from physiologically mapped body-part representations. J. Neurophysiol. *66*, 1249–1263.

Francardo, V., Recchia, A., Popovic, N., Andersson, D., Nissbrandt, H., and Cenci, M.A. (2011). Impact of the lesion procedure on the profiles of motor impairment and molecular responsiveness

to L-DOPA in the 6-hydroxydopamine mouse model of Parkinson's disease. Neurobiol. Dis. *42*, 327–340.

Freeze, B.S., Kravitz, A.V., Hammack, N., Berke, J.D., and Kreitzer, A.C. (2013). Control of basal ganglia output by direct and indirect pathway projection neurons. J. Neurosci. *33*, 18531–18539.

Gage, G.J., Stoetzner, C.R., Wiltschko, A.B., and Berke, J.D. (2010). Selective activation of striatal fast-spiking interneurons during choice execution. Neuron *67*, 466–479.

Galvan, A., Devergnas, A., and Wichmann, T. (2015). Alterations in neuronal activity in basal ganglia-thalamocortical circuits in the parkinsonian state. Front Neuroanat *9*, 5.

Gerfen, C.R., and Surmeier, D.J. (2011). Modulation of striatal projection systems by dopamine. Annu. Rev. Neurosci. *34*, 441–466.

Gerfen, C.R., Engber, T.M., Mahan, L.C., Susel, Z., Chase, T.N., Monsma, F.J., and Sibley, D.R. (1990). D1 and D2 dopamine receptor-regulated gene expression of striatonigral and striatopallidal neurons. Science *250*, 1429–1432.

Gerfen, C.R., Paletzki, R., and Heintz, N. (2013). GENSAT BAC cre-recombinase driver lines to study the functional organization of cerebral cortical and basal ganglia circuits. Neuron *80*, 1368–1383.

Girasole, A.E., Lum, M.Y., Nathaniel, D., Bair-Marshall, C.J., Guenthner, C.J., Luo, L., Kreitzer, A.C., and Nelson, A.B. (2018). A Subpopulation of Striatal Neurons Mediates Levodopa-Induced Dyskinesia. Neuron *97*, 787-795.e6.

Gokce, O., Stanley, G., Treutlein, B., Neff, N.F., Camp, G.J., Malenka, R.C., Rothwell, P.E., Fuccillo, M.V., Südhof, T.C., and Quake, S.R. (2016). Cellular Taxonomy of the Mouse Striatum as Revealed by Single-Cell RNA-Seq. Cell Rep *16*, 1126–1137.

Gong, S., Doughty, M., Harbaugh, C.R., Cummins, A., Hatten, M.E., Heintz, N., and Gerfen, C.R. (2007). Targeting Cre Recombinase to Specific Neuron Populations with Bacterial Artificial Chromosome Constructs. Journal of Neuroscience *27*, 9817–9823.

Graveland, G.A., and DiFiglia, M. (1985). The frequency and distribution of medium-sized neurons with indented nuclei in the primate and rodent neostriatum. Brain Res. *327*, 307–311.

Guenthner, C.J., Miyamichi, K., Yang, H.H., Heller, H.C., and Luo, L. (2013). Permanent Genetic Access to Transiently Active Neurons via TRAP: Targeted Recombination in Active Populations. Neuron *78*, 773–784.

Guigoni, C., Doudnikoff, E., Li, Q., Bloch, B., and Bezard, E. (2007). Altered D(1) dopamine receptor trafficking in parkinsonian and dyskinetic non-human primates. Neurobiol. Dis. *26*, 452–463.

Guo, Q., Wang, D., He, X., Feng, Q., Lin, R., Xu, F., Fu, L., and Luo, M. (2015). Whole-brain mapping of inputs to projection neurons and cholinergic interneurons in the dorsal striatum. PLoS ONE *10*, e0123381.

Haber, S.N., Fudge, J.L., and McFarland, N.R. (2000). Striatonigrostriatal pathways in primates form an ascending spiral from the shell to the dorsolateral striatum. J. Neurosci. *20*, 2369–2382.

Harris, K.D., Henze, D.A., Csicsvari, J., Hirase, H., and Buzsáki, G. (2000). Accuracy of tetrode spike separation as determined by simultaneous intracellular and extracellular measurements. J. Neurophysiol. *84*, 401–414.

Heiman, M., Heilbut, A., Francardo, V., Kulicke, R., Fenster, R.J., Kolaczyk, E.D., Mesirov, J.P., Surmeier, D.J., Cenci, M.A., and Greengard, P. (2014). Molecular adaptations of striatal spiny projection neurons during levodopa-induced dyskinesia. Proc. Natl. Acad. Sci. U.S.A. *111*, 4578–4583.

Hely, M.A., Reid, W.G.J., Adena, M.A., Halliday, G.M., and Morris, J.G.L. (2008). The Sydney multicenter study of Parkinson's disease: the inevitability of dementia at 20 years. Mov. Disord. *23*, 837–844.

Henderson, J.M., Carpenter, K., Cartwright, H., and Halliday, G.M. (2000). Degeneration of the centré median–parafascicular complex in Parkinson's disease. Ann Neurol. *47*, 345–352.

Hernandez, L.F., Kubota, Y., Hu, D., Howe, M.W., Lemaire, N., and Graybiel, A.M. (2013). Selective effects of dopamine depletion and L-DOPA therapy on learning-related firing dynamics of striatal neurons. J. Neurosci. *33*, 4782–4795.

Hernández-López, S., Bargas, J., Surmeier, D.J., Reyes, A., and Galarraga, E. (1997). D1 receptor activation enhances evoked discharge in neostriatal medium spiny neurons by modulating an L-type Ca2+ conductance. J. Neurosci. *17*, 3334–3342.

Hernandez-Lopez, S., Tkatch, T., Perez-Garci, E., Galarraga, E., Bargas, J., Hamm, H., and Surmeier, D.J. (2000). D2 dopamine receptors in striatal medium spiny neurons reduce L-type

Ca2+ currents and excitability via a novel PLC[beta]1-IP3-calcineurin-signaling cascade. J. Neurosci. *20*, 8987–8995.

Hornykiewicz, O. (2015). 50 years of levodopa. Mov. Disord. *30*, 1008.

Horstink, M.W., Zijlmans, J.C., Pasman, J.W., Berger, H.J., and van't Hof, M.A. (1990). Severity of Parkinson's disease is a risk factor for peak-dose dyskinesia. J. Neurol. Neurosurg. Psychiatr. *53*, 224–226.

Hutchinson, W.D., Lozano, A.M., Davis, K.D., Saint-Cyr, J.A., Lang, A.E., and Dostrovsky, J.O. (1994). Differential neuronal activity in segments of globus pallidus in Parkinson's disease patients. Neuroreport *5*, 1533–1537.

Ingham, C.A., Hood, S.H., and Arbuthnott, G.W. (1989). Spine density on neostriatal neurones changes with 6-hydroxydopamine lesions and with age. Brain Res. *503*, 334–338.

Jankovic, J. (2008). Parkinson's disease: clinical features and diagnosis. J. Neurol. Neurosurg. Psychiatr. *79*, 368–376.

Jenner, P. (2008). Molecular mechanisms of L-DOPA-induced dyskinesia. Nat. Rev. Neurosci. *9*, 665–677.

Jin, X., Tecuapetla, F., and Costa, R.M. (2014). Basal ganglia subcircuits distinctively encode the parsing and concatenation of action sequences. Nat Neurosci *17*, 423–430.

Johansson, Y., and Silberberg, G. (2020). The Functional Organization of Cortical and Thalamic Inputs onto Five Types of Striatal Neurons Is Determined by Source and Target Cell Identities. Cell Rep *30*, 1178-1194.e3.

Ketzef, M., Spigolon, G., Johansson, Y., Bonito-Oliva, A., Fisone, G., and Silberberg, G. (2017). Dopamine Depletion Impairs Bilateral Sensory Processing in the Striatum in a Pathway-Dependent Manner. Neuron *94*, 855-865.e5.

Kish, L.J., Palmer, M.R., and Gerhardt, G.A. (1999). Multiple single-unit recordings in the striatum of freely moving animals: effects of apomorphine and d-amphetamine in normal and unilateral 6-hydroxydopamine-lesioned rats. Brain Research *833*, 58–70.

Kravitz, A.V., Freeze, B.S., Parker, P.R.L., Kay, K., Thwin, M.T., Deisseroth, K., and Kreitzer, A.C. (2010). Regulation of parkinsonian motor behaviours by optogenetic control of basal ganglia circuitry. Nature *466*, 622–626.

Kravitz, A.V., Tye, L.D., and Kreitzer, A.C. (2012). Distinct roles for direct and indirect pathway striatal neurons in reinforcement. Nat Neurosci *15*, 816–818.

Kravitz, A.V., Owen, S.F., and Kreitzer, A.C. (2013). Optogenetic identification of striatal projection neuron subtypes during in vivo recordings. Brain Res. *1511*, 21–32.

Kreiss, D.S., Mastropietro, C.W., Rawji, S.S., and Walters, J.R. (1997). The response of subthalamic nucleus neurons to dopamine receptor stimulation in a rodent model of Parkinson's disease. J. Neurosci. *17*, 6807–6819.

Kreitzer, A.C., and Malenka, R.C. (2007). Endocannabinoid-mediated rescue of striatal LTD and motor deficits in Parkinson's disease models. Nature *445*, 643–647.

Lahiri, A.K., and Bevan, M.D. (2020). Dopaminergic Transmission Rapidly and Persistently Enhances Excitability of D1 Receptor-Expressing Striatal Projection Neurons. Neuron *106*, 277-290.e6.

Lenz, J.D., and Lobo, M.K. (2013). Optogenetic insights into striatal function and behavior. Behav. Brain Res. *255*, 44–54.

Levy, R., Dostrovsky, J.O., Lang, A.E., Sime, E., Hutchison, W.D., and Lozano, A.M. (2001). Effects of apomorphine on subthalamic nucleus and globus pallidus internus neurons in patients with Parkinson's disease. J. Neurophysiol. *86*, 249–260.

Liang, L., DeLong, M.R., and Papa, S.M. (2008). Inversion of dopamine responses in striatal medium spiny neurons and involuntary movements. J. Neurosci. *28*, 7537–7547.

Lozano, A.M., Lang, A.E., Levy, R., Hutchison, W., and Dostrovsky, J. (2000). Neuronal recordings in Parkinson's disease patients with dyskinesias induced by apomorphine. Ann. Neurol. *47*, S141-146.

Mallet, N., Ballion, B., Le Moine, C., and Gonon, F. (2006). Cortical inputs and GABA interneurons imbalance projection neurons in the striatum of parkinsonian rats. J. Neurosci. *26*, 3875–3884.

Mallet, N., Pogosyan, A., Sharott, A., Csicsvari, J., Bolam, J.P., Brown, P., and Magill, P.J. (2008). Disrupted dopamine transmission and the emergence of exaggerated beta oscillations in subthalamic nucleus and cerebral cortex. J. Neurosci. *28*, 4795–4806.

Mathur, B.N., and Lovinger, D.M. (2012). Serotonergic action on dorsal striatal function. Parkinsonism Relat. Disord. *18 Suppl 1*, S129-131.

McGeorge, A.J., and Faull, R.L. (1987). The organization and collateralization of corticostriate neurones in the motor and sensory cortex of the rat brain. Brain Res. *423*, 318–324.

McGregor, M.M., and Nelson, A.B. (2019). Circuit Mechanisms of Parkinson's Disease. Neuron *101*, 1042–1056.

McNeill, T.H., Brown, S.A., Rafols, J.A., and Shoulson, I. (1988). Atrophy of medium spiny I striatal dendrites in advanced Parkinson's disease. Brain Res. *455*, 148–152.

Mena-Segovia, J., Bolam, J.P., and Magill, P.J. (2004). Pedunculopontine nucleus and basal ganglia: distant relatives or part of the same family? Trends Neurosci. *27*, 585–588.

Mink, J.W. (1996). The basal ganglia: focused selection and inhibition of competing motor programs. Prog. Neurobiol. *50*, 381–425.

Mink, J.W. (2003). The Basal Ganglia and involuntary movements: impaired inhibition of competing motor patterns. Arch. Neurol. *60*, 1365–1368.

Nonomura, S., Nishizawa, K., Sakai, Y., Kawaguchi, Y., Kato, S., Uchigashima, M., Watanabe, M., Yamanaka, K., Enomoto, K., Chiken, S., et al. (2018). Monitoring and Updating of Action Selection for Goal-Directed Behavior through the Striatal Direct and Indirect Pathways. Neuron *99*, 1302-1314.e5.

Oye, C., Bouchard, R., Boucher, R., and Poirier, L.J. (1970). Spontaneous activity of the putamen after chronic interruption of the dopaminergic pathway: effect of L-dopa. J. Pharmacol. Exp. Ther. *175*, 700–708.

Pan, H.S., and Walters, J.R. (1988). Unilateral lesion of the nigrostriatal pathway decreases the firing rate and alters the firing pattern of globus pallidus neurons in the rat. Synapse *2*, 650–656.

Pan, W.X., Mao, T., and Dudman, J.T. (2010). Inputs to the dorsal striatum of the mouse reflect the parallel circuit architecture of the forebrain. Front Neuroanat *4*, 147.

Papa, S.M., Desimone, R., Fiorani, M., and Oldfield, E.H. (1999). Internal globus pallidus discharge is nearly suppressed during levodopa-induced dyskinesias. Ann. Neurol. *46*, 732–738.

Parker, J.G., Marshall, J.D., Ahanonu, B., Wu, Y.-W., Kim, T.H., Grewe, B.F., Zhang, Y., Li, J.Z., Ding, J.B., Ehlers, M.D., et al. (2018). Diametric neural ensemble dynamics in parkinsonian and dyskinetic states. Nature *557*, 177–182.

Perez, X.A., Zhang, D., Bordia, T., and Quik, M. (2017). Striatal D1 medium spiny neuron activation induces dyskinesias in parkinsonian mice. Mov. Disord.

Picconi, B., Centonze, D., Håkansson, K., Bernardi, G., Greengard, P., Fisone, G., Cenci, M.A., and Calabresi, P. (2003). Loss of bidirectional striatal synaptic plasticity in L-DOPA-induced dyskinesia. Nat. Neurosci. *6*, 501–506.

Planert, H., Berger, T.K., and Silberberg, G. (2013). Membrane properties of striatal direct and indirect pathway neurons in mouse and rat slices and their modulation by dopamine. PLoS ONE *8*, e57054.

Prager, E.M., and Plotkin, J.L. (2019). Compartmental function and modulation of the striatum. J. Neurosci. Res. *97*, 1503–1514.

Redgrave, P., Rodriguez, M., Smith, Y., Rodriguez-Oroz, M.C., Lehericy, S., Bergman, H., Agid, Y., DeLong, M.R., and Obeso, J.A. (2010). Goal-directed and habitual control in the basal ganglia: implications for Parkinson's disease. Nat. Rev. Neurosci. *11*, 760–772.

Rothwell, P.E., Hayton, S.J., Sun, G.L., Fuccillo, M.V., Lim, B.K., and Malenka, R.C. (2015). Input- and Output-Specific Regulation of Serial Order Performance by Corticostriatal Circuits. Neuron *88*, 345–356.

Ryan, M.B., Bair-Marshall, C., and Nelson, A.B. (2018). Aberrant Striatal Activity in Parkinsonism and Levodopa-Induced Dyskinesia. Cell Rep *23*, 3438-3446.e5.

Sagot, B., Li, L., and Zhou, F.-M. (2018). Hyperactive Response of Direct Pathway Striatal Projection Neurons to L-dopa and D1 Agonism in Freely Moving Parkinsonian Mice. Front Neural Circuits *12*, 57.

Schultz, W. (2016). Reward functions of the basal ganglia. J Neural Transm (Vienna) *123*, 679–693.

Shen, W., Flajolet, M., Greengard, P., and Surmeier, D.J. (2008). Dichotomous dopaminergic control of striatal synaptic plasticity. Science *321*, 848–851.

Shen, W., Plotkin, J.L., Francardo, V., Ko, W.K.D., Xie, Z., Li, Q., Fieblinger, T., Wess, J., Neubig, R.R., Lindsley, C.W., et al. (2015). M4 Muscarinic Receptor Signaling Ameliorates Striatal Plasticity Deficits in Models of L-DOPA-Induced Dyskinesia. Neuron *88*, 762–773.

Shin, J.H., Kim, D., and Jung, M.W. (2018). Differential coding of reward and movement information in the dorsomedial striatal direct and indirect pathways. Nat Commun *9*, 404.

Soares, J., Kliem, M.A., Betarbet, R., Greenamyre, J.T., Yamamoto, B., and Wichmann, T. (2004). Role of external pallidal segment in primate parkinsonism: comparison of the effects of 1-methyl-4-phenyl-1,2,3,6-tetrahydropyridine-induced parkinsonism and lesions of the external pallidal segment. J. Neurosci. *24*, 6417–6426.

Suárez, L.M., Solís, O., Caramés, J.M., Taravini, I.R., Solís, J.M., Murer, M.G., and Moratalla, R. (2014). L-DOPA Treatment Selectively Restores Spine Density in Dopamine Receptor D2–Expressing Projection Neurons in Dyskinetic Mice. Biological Psychiatry *75*, 711–722.

Suarez, L.M., Solis, O., Aguado, C., Lujan, R., and Moratalla, R. (2016). L-DOPA Oppositely Regulates Synaptic Strength and Spine Morphology in D1 and D2 Striatal Projection Neurons in Dyskinesia. Cereb. Cortex *26*, 4253–4264.

Suarez, L.M., Alberquilla, S., García-Montes, J.R., and Moratalla, R. (2018). Differential Synaptic Remodeling by Dopamine in Direct and Indirect Striatal Projection Neurons in Pitx3 $^{-/-}$ Mice, a Genetic Model of Parkinson's Disease. J. Neurosci. *38*, 3619–3630.

Surmeier, D.J., Song, W.J., and Yan, Z. (1996). Coordinated expression of dopamine receptors in neostriatal medium spiny neurons. J. Neurosci. *16*, 6579–6591.

Surmeier, D.J., Ding, J., Day, M., Wang, Z., and Shen, W. (2007). D1 and D2 dopamine-receptor modulation of striatal glutamatergic signaling in striatal medium spiny neurons. Trends Neurosci. *30*, 228–235.

Tepper, J.M., Tecuapetla, F., Koós, T., and Ibáñez-Sandoval, O. (2010). Heterogeneity and diversity of striatal GABAergic interneurons. Front Neuroanat *4*, 150.

Vijayakumar, D., and Jankovic, J. (2016). Drug-Induced Dyskinesia, Part 1: Treatment of Levodopa-Induced Dyskinesia. Drugs *76*, 759–777.

Villalba, R.M., and Smith, Y. (2018). Loss and remodeling of striatal dendritic spines in Parkinson's disease: from homeostasis to maladaptive plasticity? J Neural Transm (Vienna) *125*, 431–447.

Villalba, R.M., Lee, H., and Smith, Y. (2009). Dopaminergic denervation and spine loss in the striatum of MPTP-treated monkeys. Exp. Neurol. *215*, 220–227.

Villalba, R.M., Wichmann, T., and Smith, Y. (2014). Neuronal loss in the caudal intralaminar thalamic nuclei in a primate model of Parkinson's disease. Brain Struct Funct *219*, 381–394.

Wall, N.R., De La Parra, M., Callaway, E.M., and Kreitzer, A.C. (2013). Differential innervation of direct- and indirect-pathway striatal projection neurons. Neuron *79*, 347–360.

Wickens, J.R., and Wilson, C.J. (1998). Regulation of action-potential firing in spiny neurons of the rat neostriatum in vivo. J. Neurophysiol. *79*, 2358–2364.

Xuereb, J.H., Perry, R.H., Candy, J.M., Perry, E.K., Marshall, E., and Bonham, J.R. (1991). Nerve cell loss in the thalamus in Alzheimer's disease and Parkinson's disease. Brain *114 (Pt 3)*, 1363–1379.

Yoshida, M. (1991). The neuronal mechanism underlying parkinsonism and dyskinesia: differential roles of the putamen and caudate nucleus. Neurosci. Res. *12*, 31–40.

Zhai, S., Shen, W., Graves, S.M., and Surmeier, D.J. (2019). Dopaminergic modulation of striatal function and Parkinson's disease. J Neural Transm (Vienna) *126*, 411–422.

Chapter 4: Conclusion

4.1 Summary

The work presented in this dissertation provides insights into the precise cellular and circuit dysfunction that arise from chronic changes in dopamine, as occur in Parkinson's disease (PD). Here, we have demonstrated that an imbalance in striatal activity, due to a loss of activity in the movement-facilitating direct pathway, results from chronic dopamine loss. In response to dopamine replacement therapy with levodopa, we found bidirectional modulation of direct and indirect pathway activity, resulting in excessive direct pathway activity in levodopa-induced dyskinesia (LID). However, most interestingly, we identified a distinct subset of direct pathway neurons that showed this aberrant excitation in response to levodopa, whereas levodopa helped to restore normal firing rates in other direct pathway neurons (Chapter 2). These results suggest that subsets of direct pathway neurons may underlie the therapeutic and dyskinetic effects of levodopa, with aberrant excitation in a subset of direct pathway neurons underlying the pathological, and restored activity in a different subset underlying the therapeutic effects of levodopa. We investigated the potential cellular and synaptic mechanisms that shape these differential responses to levodopa using FosTRAP to selectively identify LID-associated striatal neurons (Chapter 3). Using this approach, we identified selective dopamine-dependent increases in intrinsic excitability and greater excitatory synaptic input onto TRAPed dMSNs, compared to unTRAPed dMSNs. Together, these findings integrate how cellular and synaptic differences in direct pathway neurons shape their responses to levodopa in vivo, leading to aberrant excitation in a distinct subset of striatal neurons involved in LID.

In the future, combining this approach with other techniques may help answer questions raised by these findings. For instance, how might a subset of direct pathway neurons develop such

aberrant responses to levodopa? Might these cellular and synaptic properties arise in response to chronic parkinsonism and levodopa treatment or do they exist in the intact circuit and are simply exploited by dopamine replacement therapy? Using FosTRAP in combination with genetic sequencing may provide some answers. Creating a genetic profile of TRAPed, LID-associated neurons may identify fixed markers, which would allow this subpopulation to be studied prior to the chronic manipulations in dopamine that are necessary for the expression of LID. Alternatively, they might identify maladaptive changes in gene expression that are specific to LID, and not shared by other direct pathway neurons whose activity is normalized by levodopa, allowing for the development of more targeted pharmacological interventions. As the studies outlined here also only investigate changes in excitatory neurotransmission, it also remains to be seen how inhibitory inputs, such as extrastriatal inputs from the external globus pallidus or intrastriatal inputs from striatal interneurons or other MSNs shape the responses of LID-associated neurons in parkinsonism and LID. Finally, changes in the release of GABA from direct pathway terminals in the SNr is potentiated in parkinsonian mice, mediated by a loss of presynaptic $GABA_B$ receptors (Borgkvist et al., 2015). Might this loss of presynaptic inhibition be differentially regulated between TRAPed and unTRAPed dMSNs? If so, such a change would facilitate the inhibition nof basal ganglia output by TRAPed dMSNs, which could contribute to the ability of TRAPed striatal neurons to elicit dyskinesia.

While major predictions of the rate model for striatal firing in PD and LID were confirmed at the broadest population level, our findings indicate there is substantial heterogeneity amongst neurons. These aberrant levodopa-evoked changes in intrinsic properties and synaptic inputs appear to preferentially affect those direct pathway neurons functionally involved in LID. Therefore, understanding this striatal heterogeneity will likely be critical in developing novel

therapies for Parkinson's disease, whereby treatment can harness therapeutic effects of levodopa while avoiding dyskinesia by differentially activating striatal direct pathway neurons. It is likely that similar heterogeneity is present in the healthy striatum, and that this diversity may contribute to the many functions of the striatum, whereby functional specialization may underlie the diverse behaviors mediated by the striatum. For example, there is evidence for heterogeneity in the responses of direct pathway neurons during normal movement (Barbera et al., 2016) and reinforcement learning (Nonomura et al., 2018; Shin et al., 2018). To further our understanding of normal striatal function, it will therefore be necessary to link the distinct cellular and synaptic properties of striatal neurons to their functional role in action selection.

4.2 References

Barbera, G., Liang, B., Zhang, L., Gerfen, C.R., Culurciello, E., Chen, R., Li, Y., and Lin, D.-T. (2016). Spatially Compact Neural Clusters in the Dorsal Striatum Encode Locomotion Relevant Information. Neuron *92*, 202–213.

Nonomura, S., Nishizawa, K., Sakai, Y., Kawaguchi, Y., Kato, S., Uchigashima, M., Watanabe, M., Yamanaka, K., Enomoto, K., Chiken, S., et al. (2018). Monitoring and Updating of Action Selection for Goal-Directed Behavior through the Striatal Direct and Indirect Pathways. Neuron *99*, 1302-1314.e5.

Shin, J.H., Kim, D., and Jung, M.W. (2018). Differential coding of reward and movement information in the dorsomedial striatal direct and indirect pathways. Nat Commun *9*, 404.

Publishing Agreement

It is the policy of the University to encourage open access and broad distribution of all theses, dissertations, and manuscripts. The Graduate Division will facilitate the distribution of UCSF theses, dissertations, and manuscripts to the UCSF Library for open access and distribution. UCSF will make such theses, dissertations, and manuscripts accessible to the public and will take reasonable steps to preserve these works in perpetuity.

I hereby grant the non-exclusive, perpetual right to The Regents of the University of California to reproduce, publicly display, distribute, preserve, and publish copies of my thesis, dissertation, or manuscript in any form or media, now existing or later derived, including access online for teaching, research, and public service purposes.

DocuSigned by:
Michael Ryan
823C9CF0CF9F47E...
Author Signature

9/3/2020
Date